



TAMPEREEN TEKNILLINEN YLIOPISTO
TAMPERE UNIVERSITY OF TECHNOLOGY
Julkaisu 532 • Publication 532

Sassan Iraji

Novel Signal Processing Techniques for Advanced Wireless Communications



Tampereen teknillinen yliopisto. Julkaisu 532
Tampere University of Technology. Publication 532

Sassan Iraj

Novel Signal Processing Techniques for Advanced Wireless Communications

Thesis for the degree of Doctor of Technology to be presented with due permission for public examination and criticism in Tietotalo Building, Auditorium TB109, at Tampere University of Technology, on the 6th of May 2005, at 12 noon.

Tampereen teknillinen yliopisto - Tampere University of Technology
Tampere 2005

ISBN 952-15-1349-7 (printed)
ISBN 952-15-1822-7 (PDF)
ISSN 1459-2045

TAMPERE UNIVERSITY OF TECHNOLOGY

Date: **April 2005**

Author: **Sassan Iraji**

Title: **Novel Signal Processing Techniques for Advanced
Wireless Communications**

Department: **Department of Information Technology**

Degree: **DTech** Convocation: **May** Year: **2005**

Permission is herewith granted to Tampere University of Technology to circulate and to have copied for non-commercial purposes, at its discretion, the above title upon the request of individuals or institutions.

Sassan Iraji

THE AUTHOR RESERVES OTHER PUBLICATION RIGHTS, AND NEITHER THE THESIS NOR EXTENSIVE EXTRACTS FROM IT MAY BE PRINTED OR OTHERWISE REPRODUCED WITHOUT THE AUTHOR'S WRITTEN PERMISSION.

© Copyright by Sassan Iraji, 2005

*To Hanna and Darius with all my love
and to the memory of my parents*

Abstract

There is a high demand to increase the data rate and quality of current wireless communication systems. Therefore, techniques that can increase the data rate, improve the spectral efficiency and enhance the performance of wireless communication systems are of great interest. One way to meet the above challenges is to exploit multiple transmit and receive antennas and in particular space-time processing techniques. These concepts have been recently proposed and extensively investigated. Nevertheless, designing space-time codes for multiple fading channels remains a big challenge. The first part of this thesis deals briefly with the multiple-antenna concept, in general, and the space-time processing techniques, in particular. Specifically, we focus on the design of space-time block codes for a multipath fading channel. Previous work has concentrated on the design of orthogonal space-time block codes. We propose a non-orthogonal space-time block code for multipath fading channels. Our design is based upon the upper bounds of the average pairwise error probability. It is shown that this non-orthogonal space-time block code takes advantage of the diversity provided by a multipath channel.

Another way to increase the performance of a cellular wireless communication system is to implement multiuser detection. In the second part of this work, we have designed an interference canceller. This is based on the expectation-maximization (EM) algorithm for the space-time block coded WCDMA system, which is the air-interface of the currently being deployed 3G system, over a multipath fading channel.

The EM algorithm iteratively seeks the maximum likelihood solution when a direct solution is not feasible. We assess the performance of the algorithm in an HSDPA system, an extension to WCDMA. It is shown that the parallel-interference cancellation (PIC) and the conventional matched filter are special cases of our proposed EM algorithm. Performance of the receiver is significantly improved by using the EM algorithm.

As it is well known, one of the main impediments of wireless communications systems is signal fading caused by a multipath channel. Multicarrier techniques such as OFDM and a combination of the OFDM and CDMA (MC-CDMA) can overcome the above challenge. OFDM and MC-CDMA convert a frequency-selective channel into a parallel collection of flat frequency subchannels. In the third part of this thesis, we have proposed MC-CDMA as an advanced method for a future wireless communication system. For such a system, we have studied different receiver algorithms and a channel estimation algorithm. We have studied the performance of different receivers based on the EM, MMSE, PIC and MRC algorithms. Our results show that in a SISO MC-CDMA system, the MMSE receiver provides high performance gain compared to the MRC receiver. The PIC and the EM algorithm based receivers can further improve the performance of the MMSE receiver if we take the output of the MMSE receiver to be used as initial values for them. The complexity analysis of the different parts of a SISO MC-CDMA receiver is presented. Due to the simplicity of the space-time block coding technique, we have investigated the performance of the above receiver algorithms in a space-time block coded MC-CDMA system. It is shown that by increasing the number of antennas we achieve greater improvements in the performance of the system. In the proposed STBC MC-CDMA system, we show that our PIC and EM-based algorithms can improve the MRC performance if we take the MRC output to be used as initial values for those algorithms.

Preface

This research work has been carried out partly in the Nokia Technology Platform organization (at the time, Nokia Mobile Phones) and partly in the Nokia Research Center since 2001. The period of my graduate studies has been the most challenging and exciting time in my life due to the fact that I have been working for this company on different tasks and topics while trying to focus on my graduate studies. Even though my studies have almost ended, future challenges and especially learning will continue. There are many people that I would like to thank that helped me along this path. First and foremost, I would like to sincerely thank my adviser Professor Moncef Gabbouj. I am highly indebted to Moncef for his unwavering support in the final stages of this thesis especially for reviewing and revising its many versions. I also appreciate his tremendous help and generous support in many academic and non-academic occasions during my entire graduate studies.

I would like to thank Dr. Jorma Lilleberg for his great support, for giving me the opportunity to start this work in his research group and for the valuable discussions we have had during the past few years. I would like to express my deepest gratitude to Professor Kaveh Pahlavan for his brilliant mentorship, for his kind attention and support, for being a great academic inspiration and for the fruitful discussions we have had on different academic and non-academic topics especially on spiritual subjects. For me, Kaveh has been a great example of academic excellence and a source of inspiration.

I am very grateful to my colleague, Dr. Olav Tirkkonen, for his superb collaboration on the multi-antenna research work. My special thanks go to my former colleague and my friend, Teemu Sipilä, for his great cooperation on the MC-CDMA development work

I have had the honor to have Professor Khaled Ben Letaief from the Department of Electrical and Electronic Engineering, The Hong Kong University of Science & Technology (HKUST), Hong Kong and Professor Behnaam Aazhang from the Department of Electrical and Computer Engineering, Rice University, Houston, Texas, USA, to serve as reviewers and examiners of my thesis. I am deeply grateful to both of them for their time spent examining the manuscript and for their valuable comments and feedback.

I would like to thank my friend and my colleague, Dr. Massimo Bertinelli, for spending his valuable time reading carefully the very early draft of this manuscript and providing me with very good suggestions. I am also grateful to my colleague Thomas Luby for his careful proofreading of this thesis. I would like to thank my manager at the Nokia Research Center, Antti Lappeteläinen, for his cooperation, help, facilitation and support.

My gratitude to my dear Persian friend, Peyman Arian, for his great friendship and support since the day one I came to this country. My warmest thanks to my father-in-law, Rauno Paajanen, for being such a fantastic support and being a role model of hard work and success, and to my mother-in-law, Tea Paajanen, for her encouragement and support. I am very grateful to this country and its friendly people for giving me all these opportunities. I praise and appreciate this country for its peacefulness and beautiful nature with vast forests, a unique archipelago, and thousands of lakes.

I would like to acknowledge my beloved parents, whose lives were sadly short-lived. I am indebted to my father for teaching me the importance of determination and for being a great teacher and to my mother for being a source of unlimited kindness and

passion and for teaching me the importance of hard work. I am also indebted to my three sisters, Rokhsareh, Raziye and Zohreh, and my brother, Ehsan, for their continuous love and support. As the youngest member of the family I have always enjoyed their innumerable support. My loving thanks to them.

And last but certainly not least, I would like to express my boundless thanks to my wife, Hanna, for her love and understanding during all these years and never ending support particularly during the final stage of this thesis. I would like to extend my loving thanks to our little son, Darius, for bringing lots of joy to our family since his birth in March 2004. Words are insufficient to express the depth of my love for them. Hanna and Darius made immeasurable sacrifices during the completion of this thesis. Without their sacrifices and encouragement, this work would never have been finished. I truly dedicate this work to them.

Helsinki, April 7, 2005

Sassan Iraji

Contents

Abstract	vii
Preface	ix
List of Figures	xvi
List of Tables	xix
Abbreviations	xxi
1 Introduction	1
1.1 Background	1
1.2 Author's Contributions	5
1.3 Thesis Outline	7
2 Multi-Antenna Wireless Communications	9
2.1 Introduction	9
2.2 Fading Channel Models	11
2.2.1 Rayleigh Fading	11
2.2.2 Rician Fading	13
2.3 Information Theoretic Aspects	15
2.3.1 Channel State Information	17
2.4 Space-Time Coding	18

2.4.1	Orthogonal Space-Time Block Code	20
2.4.2	Non-Orthogonal Space-Time Block Code	21
2.4.3	Orthogonal Space-Time Block Code in Multipath Channels	22
2.4.4	Non-Orthogonal Space-Time Block Code in Multipath Channels	24
2.4.5	Simulation Results	30
2.5	Summary	35
3	EM Algorithm Based Receivers	37
3.1	Introduction	37
3.2	EM Algorithm	38
3.2.1	Background	38
3.2.2	Formulation of the EM Algorithm	40
3.2.3	EM Solution to MLE in Gaussian Linear Systems	42
3.3	WCDMA Systems and its Extension (HSDPA)	44
3.4	Conventional Receivers for WCDMA System	47
3.4.1	Single Antenna	47
3.4.2	Space-Time Block Coded WCDMA	49
3.5	EM Algorithm Based Receiver for WCDMA System	52
3.5.1	Single Antenna	52
3.5.2	Space-Time Block Coded WCDMA	53
3.6	Simulation Results	55
3.7	Summary	59
4	Multi-Carrier CDMA	61
4.1	Introduction	61
4.2	OFDM	62
4.2.1	Cyclic Prefix	64
4.2.2	Zero Padding	65
4.3	SISO MC-CDMA System Model	66

4.4	Channel Estimation	68
4.5	Multiuser Detection for SISO MC-CDMA	69
4.5.1	Maximum Ratio Combining (MRC)	69
4.5.2	Minimum Mean Square Error (MMSE)	69
4.5.3	EM-based Detection and PIC	70
4.6	Simulation Results for SISO MC-CDMA System	71
4.7	Doppler Effects	74
4.8	Complexity Analysis for the SISO MC-CDMA	76
4.8.1	Background and Assumptions	76
4.8.2	Complexity of LS Channel Estimation	77
4.8.3	Complexity of Common Parts	77
4.8.4	Complexity of MRC	79
4.8.5	Complexity of MMSE	80
4.8.6	Complexity of PIC	80
4.8.7	Complexity of EM	82
4.9	Space-Time Block-Coded MC-CDMA System Model	83
4.10	Simulation Results for STBC MC-CDMA System	85
4.11	Effects of Frequency Interleaving	88
4.12	Summary	89
5	Conclusions and Future Research	93
5.1	Conclusions	93
5.2	Future Research	95
	Bibliography	97

List of Figures

2.1	Block diagram of a MIMO system	10
2.2	The pdf of a normalized Rayleigh distribution	13
2.3	Normalized Rician distributions with various K values	15
2.4	A wireless communication system using space-time coding	19
2.5	Performance of 2-tap ABBA with different permutations	29
2.6	Performance of the time-reversed space-time block code, single receive antenna	31
2.7	Performance of the time-reversed space-time block code with multiple receive antennas	32
2.8	Performance of the novel non-orthogonal code vs. ABBA code	34
2.9	Performance of ABBA code and the new non-orthogonal code with multiple receive antennas	35
3.1	Multiple access schemes	45
3.2	QPSK and 16-QAM constellations in the HSDPA system.	47
3.3	Block diagram of the downlink of a STBC-WCDMA system.	50
3.4	BER versus SNR in Veh. A channel, 2-Tx and 1-Rx antennas.	56
3.5	BER versus SNR in Veh. A channel, 2-Tx and 1-Rx antennas.	57
3.6	BER versus SNR in Ped. B channel (3 km/h).	58
3.7	BER versus SNR in Ped. B channel (3 km/h).	59

4.1	Basic OFDM System.	64
4.2	OFDM System Implemented using IFFT/FFT.	65
4.3	Baseband model for the MC-CDMA system.	67
4.4	BER versus SNR, Ped. B channels.	72
4.5	BER versus SNR, Veh. A channel.	73
4.6	Doppler effects, Veh. A channels.	75
4.7	Linear interpolation for channel estimation.	79
4.8	Transmitter and receiver structure for an STBC MC-CDMA system.	84
4.9	Raw BER vs. SNR in Vehicular A channel.	86
4.10	Raw BER vs. SNR in Pedestrian B channel	87
4.11	Effects of frequency interleaving in a MC-CDMA system.	88
4.12	Effects of frequency interleaving in an STBC MC-CDMA system.	89

List of Tables

2.1	Self-interference measures for different permutation	28
2.2	Power profile of the assumed 5-tap channel	31
3.1	Delay and power profile of the ITU pedestrian B channel	55
3.2	Delay and power profile of the ITU vehicular A channel	55
4.1	The used mapping from higher-level operations to the two used complexity measures	77
4.2	System Parameters	78
4.3	The operation counts for the LS channel estimation	78
4.4	The operation counts for the Decimation-In-Frequency (DIF) FFT	78
4.5	The operation counts for the de-scrambling operation	79
4.6	The operation counts for the de-spreading operation	80
4.7	The operation counts for the MRC	80
4.8	The operation counts for the MMSE	81
4.9	The operation counts for the PIC with 2 iterations	82
4.10	The operation counts for the EM with 2 iterations	83

Abbreviations

3G	Third Generation
4G	Fourth Generation
AWGN	Additive White Gaussian Noise
B3G	Beyond Third Generation
BER	Bit Error Rate
CDMA	Code Division Multiple Access
CP	Cyclic Prefix
CSI	Channel State Information
DFT	Discrete Fourier Transform
DS-CDMA	Direct-Sequence CDMA
EM	Expectation-Maximization
FFT	Fast Fourier Transform
HSDPA	High Speed Downlink Packet Access
ICI	Inter-Carrier Interference
IDFT	Inverse Discrete Fourier Transform
IFFT	Inverse Fast Fourier Transform
ISI	Inter-Symbol Interference
LOS	Line-Of-Sight
LS	Least Squares

MAI	M ultiple A ccess I nterference
MC-CDMA	M ulti- C arrier C DMA
MIMO	M ultiple- I nput M ultiple- O utput
MLE	M aximum- L ikelihood E stimator
MMSE	M inimum M ean S quare E rror
MRC	M aximum R atio C ombining
MUI	M ulti- U ser I nterference
OFDM	O rthogonal F requency D ivision M ultiplexing
PIC	P arallel I nterference C ancellation
QAM	Q uadrature A mplitude M odulation
QPSK	Q uadrature P hase S hift K eying
SF	S preading F actor
SIMO	S ingle- I nput M ultiple- O utput
SISO	S ingle- I nput S ingle- O utput
SNR	S ignal-to- N oise R atio
STB	S pace- T ime B lock
STBC	S pace- T ime B lock- C oded
STC	S pace- T ime C oding
V-BLAST	V ertical- B ell Labs L Ayered S pace- T ime
WCDMA	W ideband C DMA
ZP	Z ero P adding

Chapter 1

Introduction

1.1 Background

Since the early 90's, the field of wireless communications has experienced a tremendous growth. Research in this field has been expanding at an explosive rate, stimulated by a host of important emerging technologies and applications such as 2G (e.g., GSM), 2.5G (e.g., EDGE), 3G (WCDMA, CDMA2000), beyond 3G (e.g., HSDPA), Wireless LANs, RFID, and Ultrawideband. The ultimate goal of wireless communications is to make it possible for people to communicate reliably in any form, at any time, and at any place. These systems are expected to support very high data rates, with many number of users (higher capacity), better performance and under difficult propagation conditions. The projections of rapidly expanding demand for future wireless communications creates numerous challenges for system designers, and meeting these challenges will require sustained technical innovation at many fronts. Many of the main technical challenges stem from a complex multipath and time-varying propagation environment and limited radio spectrum.

Any wireless communication system is limited in performance and capacity by three main impediments [77]. The first of these is signal fading caused by multipath

fading. The signals from different multipaths add with different amplitudes and phases resulting in a received signal that varies with time and location. This increases the required received signal power for a given Bit Error Rate (BER). The second impairment is Inter-Symbol Interference (ISI) caused by the delay spread, which is the difference in propagation delays among multiple paths. ISI can limit the maximum data rate. The third impediment is known as Multiple Access Interference (MAI) (also known as co-channel interference), which is caused by users sharing the same frequency bands. MAI can limit the maximum data rate.

In addressing these challenges in wireless communications, many techniques have been introduced. One of the most important techniques is to use wireless links using multiple antennas, which is called a MIMO (Multiple-Input Multiple-Output) system ([22] and references therein). These systems can be viewed as an extension of the so-called “Smart Antennas” [56]. Traditional smart antenna systems employ multiple antennas at the receiver end, whereas in a general MIMO system multiple antennas are employed at both the transmitter and receiver ends. The addition of multiple antennas at the transmitter side combined with advanced signal processing algorithms at the transmitter and the receiver ends yields significant advantage over traditional smart antenna systems both in terms of capacity and diversity advantage. Exploiting the space-time processing techniques in the underlying MIMO environment is shown to provide an enormous improvement in performance including higher data rates, capacity enhancements, and better BER performance.

As is well known, there are several different ways to allow access to a channel in a cellular system. Three main multiple access techniques are frequency division multiple-access (FDMA), time division multiple-access (TDMA) and code division multiple-access (CDMA). While 2G and 2.5G cellular systems have adopted TDMA as their multiple access techniques, the emerging 3G system is using the Wideband Code Division Multiple Access (WCDMA) technique because of its robustness to fading, its anti-interference property, and its capabilities to provide higher capacity

compared to previous generations of mobile communication systems [23, 73]. The use of direct sequence spread spectrum and CDMA to combat potential sources of degradation, such as multipath fading, is a technique that has been known for decades ([51] and references therein). In a WCDMA system, a data symbol of each user is modulated with a noise-like wideband signal called a pseudo-noise (PN) sequence, which is user-specific. The process of modulating each user's symbol with its specific PN sequence is so called "spreading". The capacity of a WCDMA system is limited by the available bandwidth and the PN sequence properties. Two major factors that limit the performance of WCDMA systems are MAI and the multipath fading channel. To improve the performance and increase the capacity of WCDMA systems, multiuser detection [72] and multiple antenna concepts can be implemented simultaneously.

3G systems provide a high data rate up to 2 Mb/s and with its extension (HSDPA) the data rate can reach 7 Mb/s. However, in wireless research communities, there is an increasing demand to improve the performance of wireless systems beyond what 3G systems can provide. These wireless systems promise to deliver a much higher data rate and more diverse services than 3G systems currently do. Some researchers have given the name of "4G" for the coming wireless communication systems and some simply call it "Beyond 3G" (B3G) systems. The dominant load in B3G wireless channels will be high-speed burst-type traffic. Therefore, the air interface of the future wireless systems has to support high amount of packet transmissions. Recently, most standards developed for wireless high transmission rates such as Wireless LAN (IEEE 802.11a) [34], Digital Video Broadcasting (DVB-T) [15], MB-OFDM Ultrawideband (IEEE 802.15.3a) [34, 49], and Broadband Wireless Access Technology (WiMAX or IEEE 802.16) [34, 76] are based on Multicarrier Modulation (MCM) specifically the Orthogonal Frequency Division Multiplexing (OFDM) technique. OFDM is a special form of multicarrier transmission where a single high-speed data stream is transmitted over a number of lower-rate subcarriers [9]. It supports high data transmission

rates, it is robust to multipath delays, has high spectral efficiency due to a nearly rectangular frequency spectrum and can be implemented with effectively low complexity. Therefore, OFDM has been considered as one of the potential candidates for air interface of B3G or 4G systems. In order to have the benefit of both OFDM and CDMA systems and improve the shortcomings of CDMA in 3G systems, these two systems are combined and result in a system known as “MC-CDMA” [7, 12, 16, 26, 70, 75, 80]. Although OFDM and/or MC-CDMA will be the potential transmission schemes for the B3G or 4G wireless communication systems, there are still several challenges ahead. Some of the challenges are due to impediments such as frequency offset and the interferences caused by MAI and Doppler shifts, which result in intercarrier interference (ICI).

Allocating additional licensed frequency bands alone will not be sufficient to meet the high demands of future wireless systems. Besides, frequency spectrum is a significant capital investment (e.g., the 3G spectrum auctions in Europe). Therefore, for wireless service providers, increasing the capacity of the cellular system is a prime motive for their investments in future wireless systems. One solution to increase the capacity is cell-splitting but its drawback is to have additional basestations. Another solution is to use MIMO and space-time processing techniques. Therefore, the physical layer of the future wireless communications system (B3G or 4G) will employ both multicarrier techniques (e.g., MC-CDMA) and MIMO concepts.

In meeting all the above challenges, signal processing has a central role. In fact, the increasing trend is that many key problems in the design of wireless communication system have been solved using signal processing algorithms. Thus, there has been increasing mutual interests between signal processing and wireless communication communities. On one hand, there is a significant growth of interest within the signal processing community in wireless communication applications and on the other hand, the wireless communication community has increasing interests in signal processing algorithms.

1.2 Author's Contributions

The focus of this thesis is to develop efficient signal processing algorithms and techniques to increase the capacity of the current wireless communications systems and improve their performance, e.g., by overcoming one of their major impairments namely MAI. The author's contributions can be divided into three main categories as follows:

1. In spite of the fact that wireless communication channels, in most of the original research on space-time coding and MIMO systems, are considered flat fading, this is not the case most of the time. On the other hand, space-time block coding has been adopted in many standards including 3GPP due to the simplicity of its decoding. Tarokh et al [63] proved that there exists no space-time block code based on the complex orthogonal design providing full diversity gain and transmission rate one for more than two transmit antennas. Thus, the concept of non-orthogonal or semi-orthogonal space-time block coding was introduced [42, 68]. In non-orthogonal space-time block codes in multipath channels there are two main sources causing interferences: one is due to the multipath fading and the other is due to the non-orthogonality of the code. The main contribution of this thesis in this part is to introduce a novel non-orthogonal space-time block code which offers robustness in multipath fading channels [40, 41].

2. As mentioned earlier, space-time block coding has been adopted as part of 3G standards (3GPP). It is also known that MAI is a major problem in WCDMA systems. The MAI arises due to the non-orthogonality of the spreading code sequences employed by users and the fact that all users in a CDMA system share the same frequency spectrum for transmission at any given time. Even if the spreading code sequences are orthogonal to each other (Walsh-Hadamard codes [32]), in practice, the orthogonality of the spreading sequences cannot be maintained after they are transmitted through the multipath fading channels. Hence the MAI is always present. Combining the WCDMA with space-time block (STB) coding in multipath fading

channels will further increase the interference due to transmission from the additional transmit antenna. It has been shown in [35, 36, 38] that the performance of the space-time block coded WCDMA in a multipath fading channel is even worse than that in a single transmit antenna WCDMA system. Therefore, MAI can severely limit the performance of WCDMA systems and especially in an space-time block coded (STBC) WCDMA system if it is not properly exploited at the receiver. Multiuser detection (MUD) for downlink of the space-time block coded WCDMA in multipath fading channel has been addressed in [36, 38]. The presented MUD is based on the Expectation-Maximization (EM) algorithm. In order to use the EM algorithm there is a need to linearize the receive equations. This has been done by introducing some transformation matrices [36, 38]. The introduced EM algorithm can be easily transformed to Parallel Interference Cancellation (PIC) or a simple matched-filter receiver by adjusting a scalar parameter. The performance of the introduced EM algorithm has been compared to that of PIC and matched-filter receivers. We assess the performance of the proposed EM receiver in an HSDPA system [35, 38].

3. The third contribution in this thesis is in a MC-CDMA system. As mentioned earlier, the combination of an OFDM and a CDMA system gives birth to a MC-CDMA system. This is a potential air-interface candidate for B3G or 4G systems. In this thesis, first, a SISO MC-CDMA system is considered. A pilot-based channel estimation scheme as well as different receiver algorithms including Maximum Ratio Combining (MRC), Minimum Mean Square Error (MMSE), PIC and EM-based receiver have been implemented for such a system [39]. Another contribution in this part is the complexity analysis for such a system with different receiver algorithms. Since future wireless systems will be most likely equipped with multiple antennas and due to the simplicity of space-time block coding, the STBC MC-CDMA system in multipath fading channels has been studied [37]. In this thesis, we have implemented receivers based on the MRC, MMSE, PIC, and EM algorithms for a space-time block coded MC-CDMA system.

1.3 Thesis Outline

This dissertation is organized as follows. Chapter 2 first discusses multipath propagation and fading. Then information theoretic aspects of multiple antenna systems are described. Space-time coding with emphasis on the orthogonal and non-orthogonal space-time block coding are shortly reviewed in this chapter. The space-time block coding for multipath fading channels is introduced based on the time-reversal algorithm and finally, our novel non-orthogonal space-time block code in multipath fading channels is presented.

Chapter 3 focuses on the problem of multiuser detection in a space-time block coded WCDMA system in multipath fading channels. It starts by reviewing the EM algorithm, WCDMA and its extension (HSDPA). Then some conventional receivers are considered for both the single-antenna and STBC WCDMA system. These conventional receivers are based on maximum-likelihood estimation, matched filters, and parallel interference cancellation. The EM algorithm is introduced for an STBC WCDMA and its extension HSDPA. Finally, the numerical results are provided by computer simulations.

Chapter 4 considers the MC-CDMA system. Since MC-CDMA is a combination of an OFDM and CDMA system, this chapter, firstly, gives an overview of the OFDM system. Then the model for a SISO MC-CDMA system is given. Next, the pilot-based channel estimation algorithm and multiuser detection schemes are introduced. The multiuser detection algorithms are based on maximum ratio combining, MMSE, PIC and EM algorithms. Complexity analysis of all algorithms in a SISO MC-CDMA is given in this chapter. Then the STBC MC-CDMA in multipath fading channels is introduced and receiver algorithms for this system are studied. The performance of all algorithms are assessed by simulation. We also study the effects of Doppler shifts and frequency interleaving on the performance of the proposed receiver algorithms.

Finally, Chapter 5 gives the conclusions and possible future research directions.

Chapter 2

Multi-Antenna Wireless Communications

2.1 Introduction

Multi-antenna techniques have been extensively investigated in the wireless communication communities. A multi-antenna system forms a multiple-input multiple-output (MIMO) system. In a MIMO system, a high-rate data stream is divided into multiple lower-rate streams, each of which is modulated and transmitted through a different antenna at the same time. Wireless capacity theory derived in the mid-1990s extended Shannon's limit to the case of MIMO systems transmitting in multipath channels [19, 66]. This theoretical result proved that the data rate capacity and range of MIMO wireless systems can be increased virtually indefinitely, without using more frequency spectrum, by increasing the number of transmit and receive antennas to exploit multipaths. Many experimental measurements that support this theoretical work have since been widely reported.

The system block diagram of a MIMO system with arrays of n_T transmit and n_R receive antennas is shown in Figure 2.1. Generally speaking, MIMO systems may be

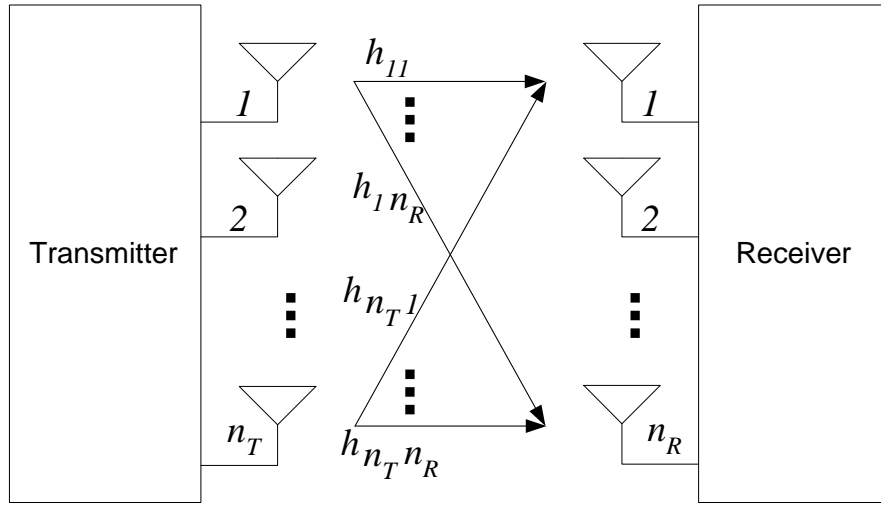


Figure 2.1: Block diagram of a MIMO system

implemented in a number of different ways to obtain either a diversity gain, to combat signal fading, or to obtain a capacity gain. Based on this, MIMO techniques can be categorized within three main groups [62]. The first one aims to improve the power efficiency by maximizing spatial diversity. Such techniques include delay diversity, space-time block codes [3, 63] and space-time trellis codes [65]. The second group uses a layered approach to increase capacity. An example of such a system is V-BLAST suggested in [79] where full spatial diversity is usually not achieved. Finally, the third type exploits the knowledge of the channel at the transmitter. It decomposes the channel coefficient matrix using singular value decomposition (SVD) and uses these decomposed unitary matrices as pre-filters and post-filters at the transmitter and the receiver to achieve near capacity [24].

After this brief introduction in this chapter, we give an overview of the multi-path fading models. Then we discuss the multi-antenna system's capacity which is the key advantage of implementing these systems. The space-time coding concept is presented next, followed by some more details on orthogonal and non-orthogonal

space-time block codes. Since in a real wireless scenario we are dealing with a multipath fading channel, orthogonal and novel non-orthogonal space-time block codes for such a channel are presented in this chapter. We examine the performance of the novel scheme by simulations.

2.2 Fading Channel Models

A central issue in a wireless communication system is the channel. In a wireless environment the received signal is usually a collection of reflected and scattered signals from stationary and moving objects such as surrounding buildings, hills, vehicles, and other obstructions. As a consequence, we observe multiple propagation paths arriving at the receiver at different delays. The received signals have random amplitude, phase, and angle of arrival. Enormous research has been carried out on characterizing and modeling the multipaths. For the most practical cases and over short distances, when there is no line-of-sight (LOS), the amplitude of the received signal is Rayleigh distributed, and when there is a LOS signal, the received signal is Rician distributed [43, 59]. The phase in both cases has uniform distribution over the interval $[0, 2\pi]$. Over long distances, the signal amplitude has a Log-Normal distribution [11, 43, 59]. In the sequel the mathematical models for the distributions of the most common fadings, Rayleigh and Rician fadings, are presented.

2.2.1 Rayleigh Fading

The baseband equivalent model of [59] is used. Each multipath gain can be depicted as a complex Gaussian random variable given by

$$h = h_{\text{Re}} + jh_{\text{Im}} \quad (2.1)$$

where h_{Re} and h_{Im} are Gaussian random variables with zero mean and variance σ^2 , i.e., $N(0, \sigma^2)$. Therefore, probability density functions for h_{Re} and h_{Im} are

$$p(h_{\text{Re}}) = \frac{1}{\sqrt{2\pi\sigma^2}} e^{-\frac{h_{\text{Re}}^2}{2\sigma^2}} \quad (2.2)$$

$$p(h_{\text{Im}}) = \frac{1}{\sqrt{2\pi\sigma^2}} e^{-\frac{h_{\text{Im}}^2}{2\sigma^2}} \quad (2.3)$$

The amplitude, r , and the phase, θ , of $h = re^{j\theta}$ are given by

$$\begin{aligned} r &= \|h\| = \sqrt{h_{\text{Re}}^2 + h_{\text{Im}}^2} \\ \theta &= \tan^{-1}\left(\frac{h_{\text{Im}}}{h_{\text{Re}}}\right) \end{aligned} \quad (2.4)$$

Then, the amplitude r will have the following Rayleigh probability density function

$$p(r) = \begin{cases} \frac{r}{\sigma^2} e^{-\frac{r^2}{2\sigma^2}}, & r \geq 0 \\ 0, & r < 0 \end{cases} \quad (2.5)$$

and the phase θ will have the following uniform distribution over the interval $[0, 2\pi]$

$$p(\theta) = \frac{1}{2\pi} \quad (2.6)$$

The mean and variance values of the Rayleigh distributed random variable denoted by m_r and σ_r^2 , respectively, are given by [74]

$$\begin{aligned} m_r &= \sqrt{\frac{\pi}{2}}\sigma = 1.25\sigma \\ \sigma_r^2 &= \left(2 - \frac{\pi}{2}\right)\sigma^2 = 0.43\sigma^2 \end{aligned} \quad (2.7)$$

If the probability density function (pdf) in (2.5) is normalized so that the average signal power, i.e., $E[r^2]$, is unity, then the normalized Rayleigh pdf is [74]

$$p(r) = \begin{cases} 2re^{-r^2}, & r \geq 0 \\ 0, & r < 0 \end{cases} \quad (2.8)$$

with mean and variance as

$$\begin{aligned} m_r &= 0.89 \\ \sigma_r^2 &= 0.21 \end{aligned} \quad (2.9)$$

The pdf of a normalized Rayleigh distribution is shown in Figure 2.2.

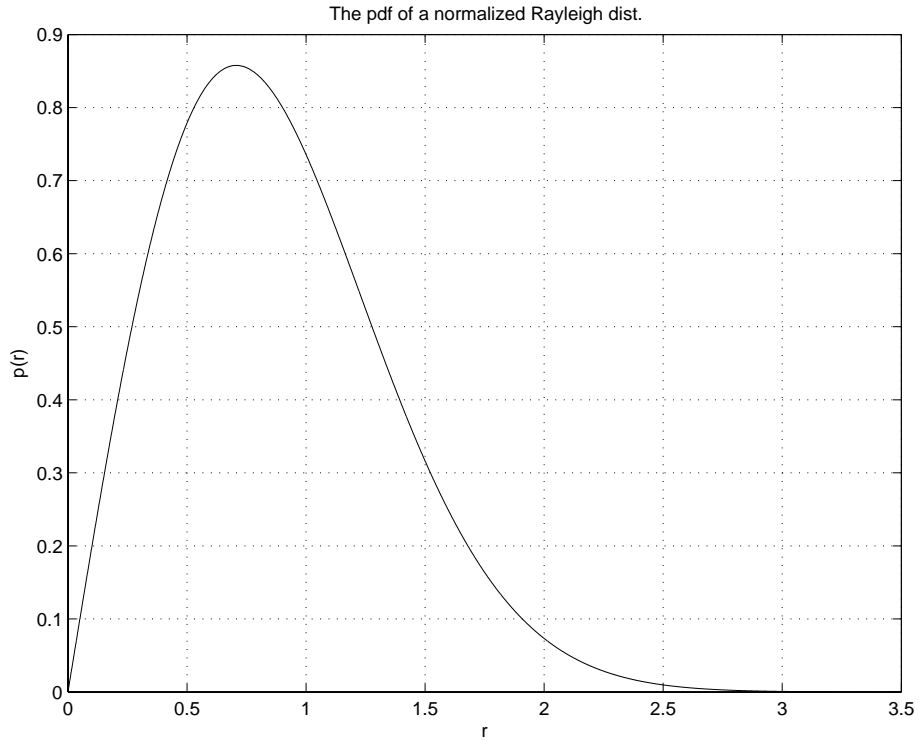


Figure 2.2: The pdf of a normalized Rayleigh distribution

2.2.2 Rician Fading

When there is a line-of-sight, the multipath fading is described by a Rician distribution. If the channel has a LOS component then h_{Re} and h_{Im} in (2.1) are not zero-mean. In this case the received signal equals the superposition of our Rayleigh fading multipath model and a LOS signal with slowly-varying amplitude and phase. If LOS component is assumed to be a real constant h_{LOS} then

$$h = h_{\text{LOS}} + h_{\text{Re}} + jh_{\text{Im}} \quad (2.10)$$

where h_{Re} and h_{Im} are Gaussian random variables with zero mean and variance σ^2 , i.e., $N(0, \sigma^2)$. They are zero mean since the mean values are denoted by h_{LOS} which is the LOS component.

The probability density functions of h_{Re} and h_{Im} are the same as in (2.2) and (2.3), respectively, and correspondingly the amplitude, r , and the phase, θ , of $h = re^{j\theta}$ are given by

$$\begin{aligned} r &= \|h\| = \sqrt{(h_{\text{LOS}} + h_{\text{Re}})^2 + h_{\text{Im}}^2} \\ \theta &= \tan^{-1} \left(\frac{h_{\text{Im}}}{h_{\text{LOS}} + h_{\text{Re}}} \right) \end{aligned} \quad (2.11)$$

Then the amplitude in this case can be shown to have a Rician distribution given by

$$p(r) = \begin{cases} \frac{r}{\sigma^2} e^{-\frac{(r^2 + h_{\text{LOS}}^2)}{2\sigma^2}} I_0 \left(\frac{rh_{\text{LOS}}}{\sigma^2} \right), & r \geq 0 \\ 0, & r < 0 \end{cases} \quad (2.12)$$

where function I_0 is the modified Bessel function of first kind and zero-order. The phase of h has a uniform distribution over $[0, 2\pi]$ as defined in (2.7).

The Rician distribution is often described in terms of a fading parameter K , defined by

$$K = \frac{h_{\text{LOS}}^2}{2\sigma^2}. \quad (2.13)$$

By defining K and assuming that the total average signal power is normalized to unity, the Rician distribution becomes [74]

$$p(r) = \begin{cases} 2r(K+1) e^{-(K+(K+1)r^2)} I_0 \left(2r\sqrt{K(K+1)} \right), & r \geq 0 \\ 0, & r < 0 \end{cases} \quad (2.14)$$

K is the ratio of the power in the LOS component to the power in the other (non-LOS) multipath components. For $K = 0$ we have Rayleigh fading, and for K approaching infinity, there is no fading at all resulting in an Additive White Gaussian Noise (AWGN) channel. The fading parameter K is therefore a measure of the severity of the fading, a small K implies severe fading and a large K implies a more benign channel. The Rician distributions with various K values are shown in Figure 2.3.

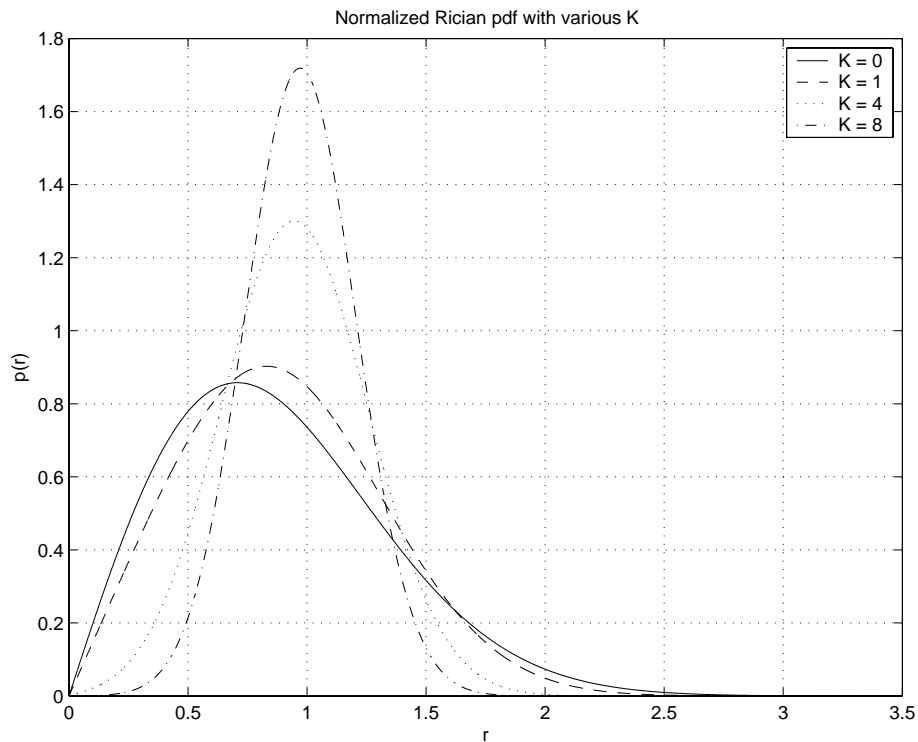


Figure 2.3: Normalized Rician distributions with various K values

2.3 Information Theoric Aspects

There are many techniques to consider when designing a communication system. One important measure of performance for any communication system is the rate at which the information is sent. Obviously, it would be advantageous to create a system which transmits data at a high rate. This would allow for signals to be sent faster, reducing the delay and permitting a higher quality of service. Unfortunately there is a limit on the rate at which information can be transmitted through a noisy channel. This upper bound is referred to as the capacity of the channel. Thus channel capacity is defined as the maximum rate of reliable information transmission through the channel and it is a good measure to analyze the potential gain of MIMO systems compared

to SISO systems. In this section the capacity aspects of SISO, SIMO and MIMO systems are presented and compared with each other.

The basic formula for the capacity of a single wireless channel corrupted by AWGN at an SNR level ρ is given by [10, 58, 61]

$$C = \log_2(1 + \rho) \quad \text{b/s/Hz} \quad (2.15)$$

Equation (2.15) can be interpreted in this way: an extra bit per second per Hertz requires 3 dB increase in SNR. In the practical case of a time-varying and randomly fading wireless channel, the capacity can be written as [66]

$$C = \log_2(1 + \rho |h|^2) \quad \text{b/s/Hz} \quad (2.16)$$

where h is the unit-power complex Gaussian amplitude of the channel. Therefore, the ergodic capacity grows logarithmically with the signal to noise ratio ρ .

Adding more receive antennas (SIMO) results in a roughly linear scaling of the SNR and thus leads to a logarithmic growth of channel capacity. In this case if the channel vector \mathbf{H} is $1 \times n_R$ the capacity is [66]

$$C = \log_2(1 + \rho \mathbf{H}\mathbf{H}^\dagger) \quad \text{b/s/Hz} \quad (2.17)$$

where the superscript \dagger is the complex conjugate transpose. The increase in capacity is due to the spatial diversity which reduces fading and improves SNR.

Additional degrees of freedom are available if antenna arrays are employed at both the transmitter and the receiver (MIMO). For the MIMO system with n_R receive and n_T transmit antennas, it is shown that the capacity is derived from

$$C = \log_2 \left[\det \left(\mathbf{I}_{n_R} + \frac{\rho}{n_T} \mathbf{H}\mathbf{H}^\dagger \right) \right] \quad \text{b/s/Hz} \quad (2.18)$$

where \mathbf{I}_{n_R} and \mathbf{H} are the $n_R \times n_R$ identity matrix and the $n_R \times n_T$ channel matrix, respectively. Foschini [19] and Telatar [66] showed that the capacity in (2.18) grows

linearly with $m = \min(n_R, n_T)$ rather than being logarithmic as in (2.17). While SISO systems gain 1 b/s/Hz in capacity every 3 dB, in MIMO the capacity growth rate is m times as high as that in SISO which is a remarkable improvement especially in high SNR.

2.3.1 Channel State Information

The achievable capacity depends on the channel state information (CSI) available for the transmitter and the receiver, respectively [25]. The three main scenarios are explained in here:

- CSI known at both the transmitter and the receiver

In this case the optimum transmit strategy is so called “waterfilling” [66] which can be interpreted as follows. The transmit power is poured like water into a vessel with the noise powers of the equivalent SISO channels representing the ground level. Thus, strong eigenmodes of the channel are allocated more power than weak ones.

- CSI not known at the transmitter but known at the receiver

In a slowly fading channel where the fading coefficients remain approximately constant for many symbol intervals, the transmitter can send training signals that allow the receiver to accurately estimate the fading coefficients; in this case, the capacity is given by (2.18). The ergodic channel capacity was derived by both Foschini [19] and Telatar [66]. However, this solution does not lend itself easy interpretation. Therefore, simpler upper and lower bounds as well as asymptotic expressions have been developed [8, 46, 55]. Note that in the high SNR regime the loss in capacity due to unknown channel parameters at the transmitter is negligible as long as $n_T \leq n_R$ because the waterfilling solution also tends to a uniform power allocation.

- CSI not known at both the transmitter and the receiver

In fast fading scenarios fading coefficients can change into new, almost independent values before being estimated by the receiver through training signals. In this case, the receiver has no a-priori channel knowledge. A noncoherent detection scheme, where the receiver detects the transmitted symbols without having any information about the current realization of the channel, is more suitable for these fast fading scenarios. The transmission scheme and capacity of the noncoherent systems have been studied in [29, 48]. This non-coherent transmission scheme is called “unitary space-time modulation”.

2.4 Space-Time Coding

Space-time coding (STC) is a coding technique used in the case of multiple transmit antenna. Figure 2.4 shows a wireless communication system using STC. Space-time codes introduce temporal and spatial correlation into signals transmitted from different antennas. In this way, they provide diversity and/or coding gain to the system. The first attempt to develop STC was presented by Seshadri and Winters in [60] which was inspired by the Wittneben [78] scheme based on delay diversity. Space-time trellis coding were developed by Tarokh et al. [65] which is considered as a major development in the STC concept. Delay diversity can be viewed as a special case of space-time trellis coding. The generalized approach combines trellis coded modulation (TCM) with transmit diversity techniques. Although, the decoding complexity for these codes grows exponentially with the number of antennas, they perform very well in slowly fading environments. The rank and determinant criteria emerged from this work and became a benchmark in space-time code design. Space-time trellis codes were shown to provide a diversity benefit equal to the number of transmit antennas in addition to a coding gain that depends on the complexity of the code without any loss in bandwidth efficiency. When the number of transmit antennas is

fixed, the decoding complexity of space-time trellis coding increases exponentially as a function of both the diversity level and the transmission rate.

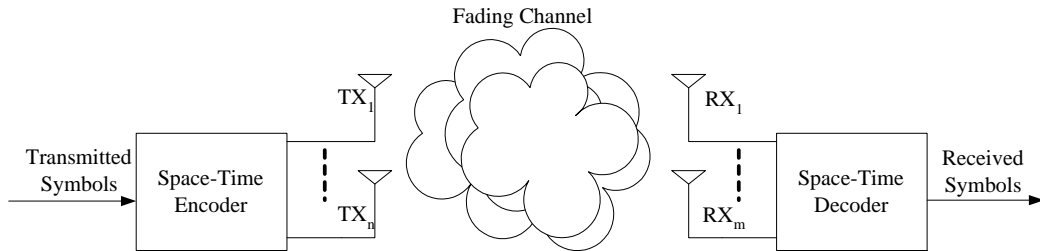


Figure 2.4: A wireless communication system using space-time coding

In addressing the issue of decoding complexity in space-time trellis coding, Alamouti [3] discovered a remarkable scheme for transmission with two transmit antennas in flat fading channels. This scheme is so called space-time block coding. In [63], the theory of orthogonal space-time block codes was considered. It was shown that for more than two transmit antennas, full diversity rate one codes do not exist. Subsequently, there have been many attempts to design non-orthogonal rate one space-time block codes for more than two transmit antennas (e.g., [42, 68]). When considering non-orthogonal space-time block codes in multipath channels, one experiences interference from both the multipath fading and the non-orthogonality of the code. Similarly to orthogonal codes, unitary space-time modulation [29] and differential unitary modulation [31] use a set of unitary code matrices to represent data. In general, the optimal receiver for a unitary modulation code is more complex than for an orthogonal design because the code matrix is not structured by symbols that can be decoupled for detection. These codes are typically non-square and designed for systems where channel state information (CSI) is unknown at the receiver. In the

following two subsequent sections, orthogonal and non-orthogonal space-time block codes are introduced.

2.4.1 Orthogonal Space-Time Block Code

In [3], Alamouti presented a transmit diversity scheme using a space-time block coding approach with two transmit antennas in frequency flat fading channels. This scheme supports a maximum likelihood detection algorithm with linear complexity at the receiver. Alamouti codes has been adopted by 3G standards [2]. In this scheme, at a given symbol period, two signals are transmitted from the two antennas. The signal transmitted from the first antenna is denoted s_1 and from the second antenna by s_2 . During the next symbol period signal $(-s_2^*)$ is transmitted from the first antenna, and signal (s_1^*) is transmitted from the second antenna, where $*$ denotes the complex conjugate operation. In matrix form, Alamouti codes are represented as

$$\mathbf{C}_{STBC} = \begin{bmatrix} s_1 & s_2 \\ -s_2^* & s_1^* \end{bmatrix}. \quad (2.19)$$

Space-time block coding using Alamouti scheme has diversity order of two and rate one since two symbols are transmitted in two time epochs.

Let us consider Alamouti codes in a communication system with two transmit antennas and one receive antenna in a flat fading channel. The original symbol sequence s is divided into two separate sequences s_1 and s_2 . Let us assume that the complex multiplicative distortion of the channels are h_1 for the first transmit antenna and h_2 for the second transmit antenna and they are constant across two consecutive symbols. The received signal (conjugated during the second symbol) is

$$\begin{aligned} \mathbf{r} &= \begin{bmatrix} h_1 & h_2 \\ -h_2^* & h_1^* \end{bmatrix} \begin{bmatrix} s_1 \\ s_2 \end{bmatrix} + \begin{bmatrix} n_1 \\ n_2 \end{bmatrix} \\ &= \mathbf{H}\mathbf{s} + \mathbf{n} \end{aligned} \quad (2.20)$$

As \mathbf{H} in (2.20) is an orthogonal matrix, it readily follows that

$$\mathbf{H}\mathbf{H}^\dagger = \mathbf{H}^\dagger\mathbf{H} = (|h_1|^2 + |h_2|^2) \mathbf{I}_2 \quad (2.21)$$

Therefore, the matched filter receiver which multiplies \mathbf{r} by \mathbf{H}^\dagger turns out to be the optimum receiver and the transmitted symbols are easily decoupled .

Orthogonal space-time block codes are designed from the theory of orthogonal designs presented in [63]. It was shown in the same article that square real orthogonal designs exist only if the number of the transmit antennas are 2, 4 and 8. Generalizing the concept of orthogonal designs to non-square matrices, real orthogonal designs exist that provide full diversity and full rate for any number of antennas [63]. For the case of complex orthogonal designs the Alamouti design for 2 transmit antennas is the only complex square orthogonal design. Relaxing the condition on the rate allows the construction of space-time block codes for more than two transmit antennas [63]. For 3 or 4 transmit antennas, several orthogonal codes have been discovered with full diversity and a rate of 3/4 [21, 30, 63, 64, 69].

2.4.2 Non-Orthogonal Space-Time Block Code

It was proved in [63] that no space-time block code based on the complex orthogonal design providing full diversity gain and transmission rate one exists for more than two transmit antennas. A formula for the maximum achievable data rate for square code matrices was given in [69]. Non-orthogonal or quasi-orthogonal space-time block codes for more than two transmit antennas were introduced in [20, 42, 47, 68]. These codes are able to provide higher symbol rates than their orthogonal counterparts.

As an example we consider the simplest rate one non-orthogonal code for 4 Tx antennas, discussed in [68]. This non-orthogonal code for transmitting four symbols through four transmit antennas and during four time epochs can be represented in

matrix form as

$$\mathbf{C}_{ABBA} = \begin{bmatrix} s_1 & -s_2^* & s_3 & -s_4^* \\ s_2 & s_1^* & s_4 & s_3^* \\ s_3 & -s_4^* & s_1 & -s_2^* \\ s_4 & s_3^* & s_2 & s_1^* \end{bmatrix} \quad (2.22)$$

It consists of two quasi-orthogonal layers constructed from Alamouti codes based on symbol pairs (s_1, s_2) and (s_3, s_4) . If we represent the Alamouti codes related to these symbol pairs with \mathbf{A} and \mathbf{B} , (2.22) becomes $\begin{bmatrix} \mathbf{A} & \mathbf{B} \\ \mathbf{B} & \mathbf{A} \end{bmatrix}$. Thus, the code is called “ABBA”. This is not an orthogonal space-time block code since

$$\mathbf{C}_{ABBA}^\dagger \mathbf{C}_{ABBA} = \left(\sum_{k=1}^4 |s_k|^2 \right) \mathbf{I}_4 + 2\text{Re}(s_1 s_3^* + s_2 s_4^*) \begin{bmatrix} 0 & 0 & 1 & 0 \\ 0 & 0 & 0 & 1 \\ 1 & 0 & 0 & 0 \\ 0 & 1 & 0 & 0 \end{bmatrix} \quad (2.23)$$

As it is seen from (2.23) the non-orthogonality between layers \mathbf{A} and \mathbf{B} induces interference among the symbols. The ABBA code provides transmission rate one but not full diversity gain. With symbol rotations, the loss in diversity gain may be recovered [67].

2.4.3 Orthogonal Space-Time Block Code in Multipath Channels

In [45], a method is introduced to enable the use of the space-time block coding scheme in multipath fading channels. We briefly explain this method by giving an example [14, 45, 54, 81].

We assume that data is transmitted during frames of size $2B$ symbols. Each frame is divided into two halves. Let us assume the input data frame is $s(k)$ with the size of

$2B$ symbols. We divide it to two frames $s_1(k)$ and $s_2(k)$ with the size of B symbols each. We define the time reversed and complex conjugated $s_1(k)$ and $s_2(k)$ as follows

$$\bar{s}_1(k) = s_1^*(B - k + 1) \quad k = 1, 2, \dots, B \quad (2.24)$$

$$\bar{s}_2(k) = s_2^*(B - k + 1) \quad k = 1, 2, \dots, B \quad (2.25)$$

As in Alamouti scheme during the first half of the frame, $s_1(k)$ is transmitted from antenna 1, and $s_2(k)$ from antenna 2. In the second half of the frame, $-\bar{s}_2(k)$ is transmitted from antenna 1, and $\bar{s}_1(k)$ from antenna 2. The transmitted code is given by

$$\begin{bmatrix} s_1(1) & s_1(2) & \cdots & s_1(B) & \text{Guard} & -s_2^*(B) & \cdots & -s_2^*(2) & -s_2^*(1) \\ s_2(1) & s_2(2) & \cdots & s_2(B) & \text{Guard} & s_1^*(B) & \cdots & s_1^*(2) & s_1^*(1) \end{bmatrix}. \quad (2.26)$$

In (2.26), a row is transmitted from a given antenna. The guard interval depends on the delay spread of the channel and the length of the guard interval should be at least equal to the delay spread.

For simplicity we consider two-tap channels from two transmit antennas to one receive antenna, and a transmission of a block of four symbols, $\mathbf{S} = [s_1 \ s_2 \ s_3 \ s_4]^T$. Hence, the following blocks are transmitted from antenna one and two

$$\begin{aligned} \text{ant.1} &\rightarrow s_1 \ s_2 \ 0 \ -s_4^* \ -s_3^* \ 0 \\ \text{ant.2} &\rightarrow s_3 \ s_4 \ 0 \ s_2^* \ s_1^* \ 0 \end{aligned} \quad (2.27)$$

where 0 represents the guard symbol.

The received signal (with the second half conjugated) is given by

$$\mathbf{r} = \begin{bmatrix} h_{11} & 0 & h_{21} & 0 \\ h_{12} & h_{11} & h_{22} & h_{21} \\ 0 & h_{12} & 0 & h_{22} \\ 0 & h_{21}^* & 0 & -h_{11}^* \\ h_{21}^* & h_{22}^* & -h_{11}^* & -h_{12}^* \\ h_{22}^* & 0 & -h_{12}^* & 0 \end{bmatrix} \mathbf{S} + \mathbf{n} \quad (2.28)$$

where h_{ij} is the j th tap of the channel from antenna i and \mathbf{n} is additive white Gaussian noise (AWGN). Equation (2.28) can be written concisely as

$$\mathbf{r} = \mathbf{H}\mathbf{S} + \mathbf{n} \quad (2.29)$$

It can be seen that $\mathbf{H}^\dagger\mathbf{H}$ is a block diagonal matrix with the largest absolute values on the main diagonal. Therefore, in multipath fading channels the symbols can be decoupled using the time-reversal algorithm.

2.4.4 Non-Orthogonal Space-Time Block Code in Multipath Channels

In this section we take the ABBA code introduced in section 2.4.2 as a benchmark for designing our novel non-orthogonal space-time block code in channels with multipath fading. In multipath environments, (2.22) has the same problem as the Alamouti code; complex conjugation cannot be represented as a linear operation over the complex field, and thus complex conjugated symbols cannot be treated by linear equalization. A basic idea in this case is similar to the time-reversal orthogonal STB code, that is, the symbol periods (i.e., columns in (2.22)) during which complex conjugated symbols are transmitted, may be moved to the other side of a guard period [40, 41]. If the guard period is longer than the delay spread, symbols and complex conjugates do not interfere with each other due to the multipath channel, and a complex-valued linear equalization may be used.

There are many alternatives when it comes to the ordering of time slots. To get insight into this, we consider a two-tap channel and the simplest block of a non-orthogonal space-time block code, which can be constructed from the columns of two ABBA blocks. For simplicity, we call the second block CDDC, and denote

$$\begin{aligned} \mathbf{s}_{AB} &= \begin{bmatrix} s_1 & s_2 & s_3 & s_4 \end{bmatrix}^T \\ \bar{\mathbf{s}}_{AB} &= \begin{bmatrix} -s_2^* & s_1^* & -s_4^* & s_3^* \end{bmatrix}^T \end{aligned}$$

$$\begin{aligned}
\mathbf{s}_{BA} &= \begin{bmatrix} s_3 & s_4 & s_1 & s_2 \end{bmatrix}^T \\
\bar{\mathbf{s}}_{BA} &= \begin{bmatrix} -s_4^* & s_3^* & -s_2^* & s_1^* \end{bmatrix}^T \\
\mathbf{s}_{CD} &= \begin{bmatrix} s_5 & s_6 & s_7 & s_8 \end{bmatrix}^T \\
\bar{\mathbf{s}}_{CD} &= \begin{bmatrix} -s_6^* & s_5^* & -s_8^* & s_7^* \end{bmatrix}^T \\
\mathbf{s}_{DC} &= \begin{bmatrix} s_7 & s_8 & s_5 & s_6 \end{bmatrix}^T \\
\bar{\mathbf{s}}_{DC} &= \begin{bmatrix} -s_8^* & s_7^* & -s_6^* & s_5^* \end{bmatrix}^T
\end{aligned}$$

Using this notation, (2.22) becomes

$$\mathbf{C}_{ABBA} = \begin{bmatrix} \mathbf{s}_{AB} & \bar{\mathbf{s}}_{AB} & \mathbf{s}_{BA} & \bar{\mathbf{s}}_{BA} \end{bmatrix} \quad (2.30)$$

The guard period is now one symbol, during which nothing is transmitted. If the complex conjugated symbols in the ABBA and CDDC blocks are transferred to the other side of the guard period, we get

$$\mathbf{C}_{ABCD} = [\mathbf{s}_{AB} \quad \mathbf{s}_{BA} \quad \mathbf{s}_{CD} \quad \mathbf{s}_{DC} \quad \mathbf{0} \quad \bar{\mathbf{s}}_{AB} \quad \bar{\mathbf{s}}_{BA} \quad \bar{\mathbf{s}}_{CD} \quad \bar{\mathbf{s}}_{DC} \quad \mathbf{0}] \quad (2.31)$$

Now three kinds of linear operations may be considered, which perform time reversal and interleaving on the time slots. These operations may be represented as 10×10 matrices, operating on (2.31).

- A time reversal

$$\Sigma_{TR} = \begin{bmatrix} \mathbf{I}_5 & \mathbf{0} & \mathbf{0} \\ \mathbf{0} & \mathbf{I}_2 \otimes \mathbf{\Pi} & \mathbf{0} \\ \mathbf{0} & \mathbf{0} & \mathbf{1} \end{bmatrix} \quad (2.32)$$

operates on the complex conjugates, by interchanging the two complex conjugate rows of a given ABBA-block. Here \mathbf{I}_n is the $n \times n$ identity matrix, $\mathbf{\Pi} = \begin{bmatrix} 0 & 1 \\ 1 & 0 \end{bmatrix}$ is the 2×2 permutation matrix, \otimes is the Kronecker product, and the zeros are interpreted as matrices or vectors of zeros, when appropriate.

- A block time reversal

$$\mathbf{\Sigma}_{BTR} = \begin{bmatrix} \mathbf{I}_5 & 0 & 0 \\ 0 & \mathbf{\Pi} \otimes \mathbf{I}_2 & 0 \\ 0 & 0 & 1 \end{bmatrix} \quad (2.33)$$

exchanges the order of the complex conjugated symbols of the AB and CD blocks.

- An interleaver

$$\mathbf{\Sigma}_{Int} = \begin{bmatrix} 1 & 0 & 0 & 0 & 0 \\ 0 & \mathbf{\Pi} & 0 & 0 & 0 \\ 0 & 0 & \mathbf{I}_3 & 0 & 0 \\ 0 & 0 & 0 & \mathbf{\Pi} & 0 \\ 0 & 0 & 0 & 0 & \mathbf{I}_2 \end{bmatrix} \quad (2.34)$$

interleaves the columns of the AB and CD blocks so that no two columns from the same block follow each other.

For concreteness, we may spell out the results of operating these matrices on the basic block of (2.31). Note that the first two matrix operations do not change the first half of the transmission. Therefore, we have

$$\begin{aligned} \mathbf{C}_{ABCD}\mathbf{\Sigma}_{TR} &= [\dots \quad \bar{\mathbf{s}}_{BA} \quad \bar{\mathbf{s}}_{AB} \quad \bar{\mathbf{s}}_{DC} \quad \bar{\mathbf{s}}_{CD} \quad \mathbf{0}] \\ \mathbf{C}_{ABCD}\mathbf{\Sigma}_{BTR} &= [\dots \quad \bar{\mathbf{s}}_{CD} \quad \bar{\mathbf{s}}_{DC} \quad \bar{\mathbf{s}}_{AB} \quad \bar{\mathbf{s}}_{BA} \quad \mathbf{0}] \\ \mathbf{C}_{ABCD}\mathbf{\Sigma}_{Int} &= [\mathbf{s}_{AB} \quad \mathbf{s}_{CD} \quad \mathbf{s}_{BA} \quad \mathbf{s}_{DC} \quad \mathbf{0} \\ &\quad \bar{\mathbf{s}}_{AB} \quad \bar{\mathbf{s}}_{CD} \quad \bar{\mathbf{s}}_{BA} \quad \bar{\mathbf{s}}_{DC} \quad \mathbf{0}] \end{aligned} \quad (2.35)$$

The combination of these three operations results in eight different schemes. We can use three bits in order to indicate that the given operation is performed or not. As

Σ_{Int} does not commute with the other two, one has to specify the order of operations to have an unique parameterization. We denote

$$\Sigma(t, b, i) = \Sigma_{TR}^t \Sigma_{BTR}^b \Sigma_{Int}^i \quad (2.36)$$

with t, b, i taking the values 0 and 1, indicating whether the given operation is performed or not.

A rough analytical tool may be developed to assess the merits of differently permuted schemes. First we note that the signal model in a multipath channel may be described as an equivalent signal model of the form

$$\mathbf{y} = \mathbf{H}\mathbf{S} + \text{noise} \quad (2.37)$$

In the example considered here, with a 10×4 matrix transmission in a two-tap channel with one receive antenna, \mathbf{y} is the received signal vector during the ten time slots the transmission extends over, with the last five complex conjugated. The equivalent channel \mathbf{H} is a 10×8 matrix operating on the 8×1 vector of symbols \mathbf{S} . The structure of \mathbf{H} depends on the space-time block code, and the permutation considered, and it is a function of the 4×2 channel coefficients. As an example, the equivalent channel for the permutation $\Sigma = \Sigma_{BTR}\Sigma_{Int}$ is

$$\mathbf{H} = \begin{bmatrix} \mathbf{h}_1 & \mathbf{h}_2 & \mathbf{P}\mathbf{h}_1 & \mathbf{P}\mathbf{h}_2 & 0 & & & \\ 0 & \mathbf{h}_1 & \mathbf{h}_2 & \mathbf{P}\mathbf{h}_1 & \mathbf{P}\mathbf{h}_2 & & & \dots \\ & & 0 & \bar{\mathbf{h}}_1 & \bar{\mathbf{h}}_2 & \mathbf{P}\bar{\mathbf{h}}_1 & \mathbf{P}\bar{\mathbf{h}}_2 & \\ & & \bar{\mathbf{h}}_1 & \bar{\mathbf{h}}_2 & \mathbf{P}\bar{\mathbf{h}}_1 & \mathbf{P}\bar{\mathbf{h}}_2 & 0 & \end{bmatrix}^T \quad (2.38)$$

where $\mathbf{h}_m = [h_{1m} \ h_{2m} \ h_{3m} \ h_{4m}]^T$ is the channel vector of tap m (one component for each transmit antenna), $\bar{\mathbf{h}}_m = [h_{2m}^* \ -h_{1m}^* \ h_{4m}^* \ -h_{3m}^*]^T$ is the corresponding vector with conjugate channels, and $\mathbf{P} = \mathbf{\Pi} \otimes \mathbf{I}_2$ interchanges the first two elements of a vector with the last two.

In general, the performance of any linear transmission scheme allowing an equivalent vector signal model (2.37) is characterized by the correlation matrix $\mathbf{H}^\dagger \mathbf{H}$, where \dagger means complex conjugate and transpose operation. In [27] it was shown that the average pairwise error probability, obtained by choosing Gaussian \mathbf{S} in (2.37) and averaging the pairwise error obtained between an independent \mathbf{S} and \mathbf{S}' has upper bound given by

$$P_e(\text{pairwise}) = E \{P_e(\text{pairwise}|\mathbf{H})\} \leq E \left\{ \frac{1}{2} \det \left(\mathbf{I} + \frac{\rho}{2n_T} \mathbf{H}^\dagger \mathbf{H} \right)^{-1/2} \right\} \quad (2.39)$$

where ρ is the SNR, \mathbf{I} is an identity matrix and n_T is the number of transmit antennas. This is the probability that a maximum-likelihood decoder mistakes \mathbf{S} for \mathbf{S}' , given that \mathbf{S} is transmitted, averaged over \mathbf{S} and \mathbf{S}' , and conditioned on \mathbf{H} [27]. For more realistic discrete modulation alphabets, the Gaussian result is indicative, with corrections coming from the discreteness of the alphabet.

Table 2.1: Self-interference measures for different permutation

t	b	i	$-\mu$ (dB)
0	0	0	1.0
0	0	1	1.2
0	1	0	0.9
1	0	0	1.0
1	1	0	0.9
1	0	1	1.2
0	1	1	0.8
1	1	1	0.8

Here we shall measure the self-interference of the transmission scheme. Let us denote the self-interference measure by μ . We define μ as follows

$$\mu = 10 \log_{10} \left\{ \frac{1}{\mathcal{N}} E \left\{ \det \left(\mathbf{H}^\dagger \mathbf{H} \right) \right\}^{1/n_T n_R n_D} \right\} \quad (dB) \quad (2.40)$$

where the expectation, $E \{ \cdot \}$, is over the channel realizations, and n_T , n_R , and n_D are the number of transmit antennas, receive antennas, and delay taps, respectively.

The normalization \mathcal{N} is chosen as the $n_T n_R n_D$ -th root of the $E \{ \det(\mathbf{H}^\dagger \mathbf{H}) \}$ of a matched filter bound, which nulls all off-diagonal correlation values in $\mathbf{H}^\dagger \mathbf{H}$. From (2.39) it follows that this measure correlates with high-SNR performance, at least for large constellation size. In the absence of self-interference, $\mu = 0$ dB.

For the eight candidate schemes, the self-interference measures are reported in Table 2.1. As a comparison, the self-interference of a transmission where two ABBA-blocks are simply separated by a guard period is $\mu = -1.98$ dB. From the table it is visible that time reversal Σ_{TR} of conjugate symbols within the same ABBA block has no effect on self-interference. In contrast, time reversal Σ_{BTR} of the blocks of conjugate symbols always diminishes the self-interference. Interleaving with Σ_{Int} has a mixed effect, but combined with Σ_{BTR} it gives the best self-interference.

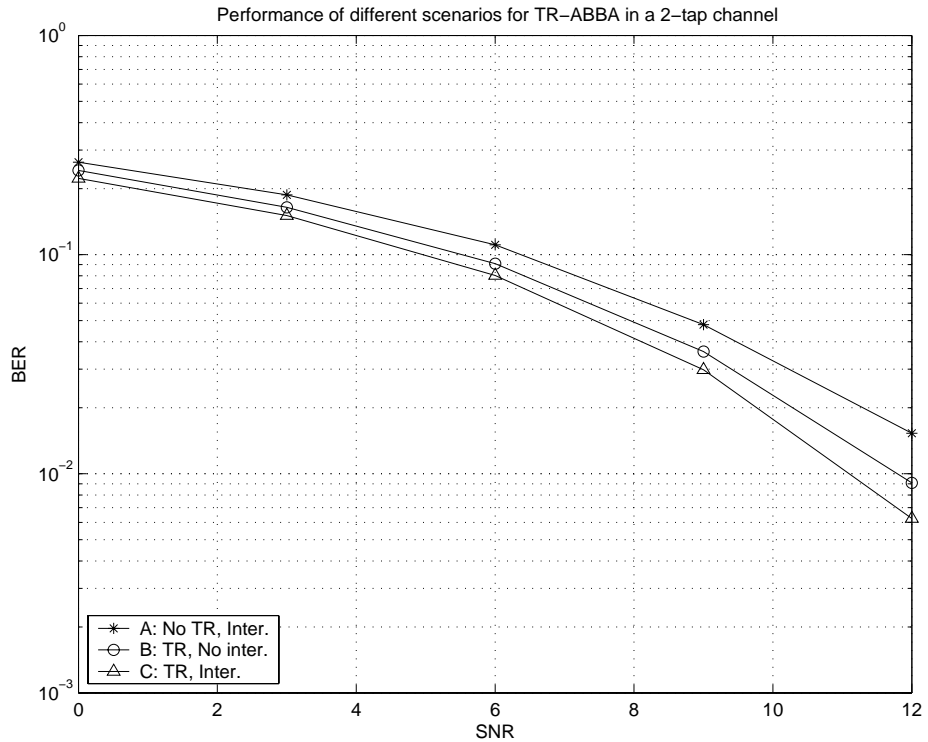


Figure 2.5: Performance of 2-tap ABBA with different permutations

In Figure 2.5, the 001, 010 and 011 schemes are compared, by simulating in a two-tap channel with relative tap power -1.92 dB for the second tap. Comparing the performance to Table 2.1 confirms the connection between self-interference and performance, even with discrete symbols.

Based on this, we propose this structure for a generic number $4B$ of symbols to be transmitted over a channel with a generic delay. The order of the blocks with complex conjugate symbols is reversed, and all blocks are interleaved, i.e. the 011 permutation is generalized to multiple blocks of symbols.

To be concrete the code can be represented explicitly as in (2.26). We divide the input data frame of $4B$ symbols to four frames $s_1(k)$, $s_2(k)$, $s_3(k)$ and $s_4(k)$ with B symbols each. The transmitted non-orthogonal code is then given by

$$\begin{bmatrix} s_1(1) & s_1(2) & \cdots & s_1(B) & s_3(1) & \cdots & s_3(B) & \text{Guard} & -s_2^*(B) & \cdots \\ s_2(1) & s_2(2) & \cdots & s_2(B) & s_4(1) & \cdots & s_4(B) & \text{Guard} & s_1^*(B) & \cdots \\ s_3(1) & s_3(2) & \cdots & s_3(B) & s_1(1) & \cdots & s_1(B) & \text{Guard} & -s_4^*(B) & \cdots \\ s_4(1) & s_4(2) & \cdots & s_4(B) & s_2(1) & \cdots & s_2(B) & \text{Guard} & s_3^*(B) & \cdots \\ -s_2^*(1) & -s_4^*(B) & \cdots & -s_4^*(2) & -s_4^*(1) & & & & & \\ s_1^*(1) & s_3^*(B) & \cdots & s_3^*(2) & s_3^*(1) & & & & & \\ -s_4^*(1) & -s_2^*(B) & \cdots & -s_2^*(2) & -s_2^*(1) & & & & & \\ s_3^*(1) & s_1^*(B) & \cdots & s_1^*(2) & s_1^*(1) & & & & & \end{bmatrix} \quad (2.41)$$

2.4.5 Simulation Results

In this section, we provide simulation results for the time-reversed (TR) orthogonal STB code (2.26) and the proposed non-orthogonal code (2.41). We compare their performance to those of (2.19) and (2.22) in both multipath and flat fading channels. In all simulations, QPSK modulation and a zero-forcing receiver are considered. It is assumed that the channel responses are perfectly known and fading is uncorrelated between the transmit–receive antenna pairs. Furthermore, the transmission

is normalized so that the total radiated power from four transmit antennas in the non-orthogonal scenario and two transmit antennas in the orthogonal case are equal to the power of a single antenna transmission.

We consider a five-tap fading channel, similar to the ITU vehicular A channel model. The relative power of taps is summarized in Table 2.2.

Table 2.2: Power profile of the assumed 5-tap channel

Tap	1	2	3	4	5
Power (dB)	0.0	-1.92	-7.31	-10.39	-10.89

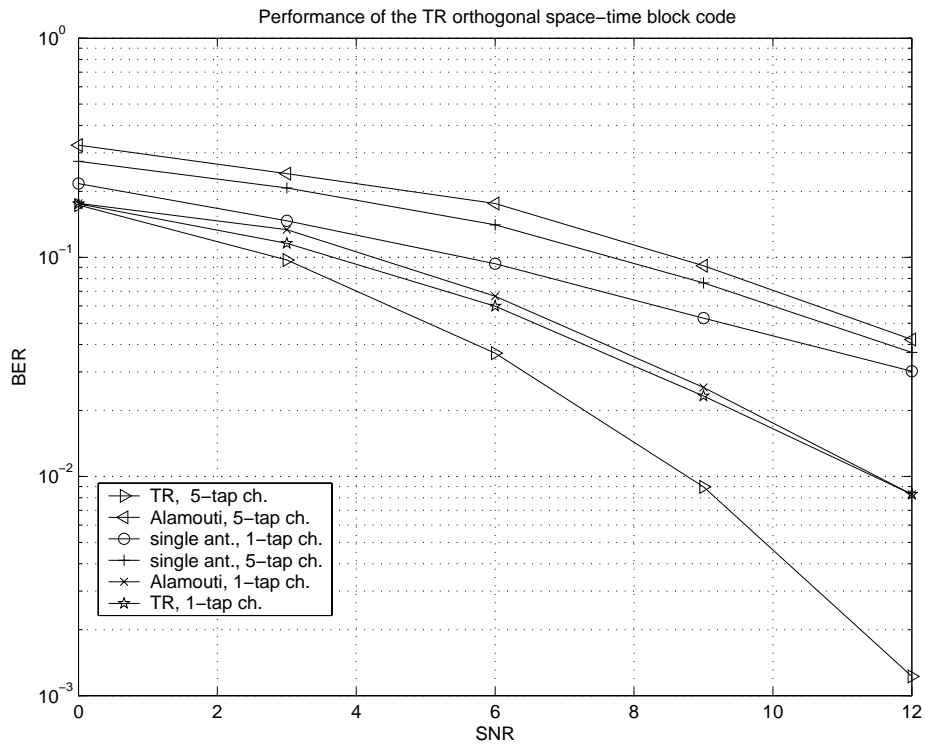


Figure 2.6: Performance of the time-reversed space-time block code, single receive antenna

Figure 2.6 presents the simulation results for a single transmit antenna scenario,

the Alamouti code and the TR orthogonal STB code. The single receive antenna case is considered. For flat fading channels the Alamouti code and its time-reversed version have the same performance, as it is expected. In a multipath fading channel, the Alamouti code faces severe inter-symbol-interference which explains the poor performance in such channels. The TR-STB code in (2.26) improves the performance of the orthogonal STB code in a multipath fading channel as is seen from Figure 2.6.

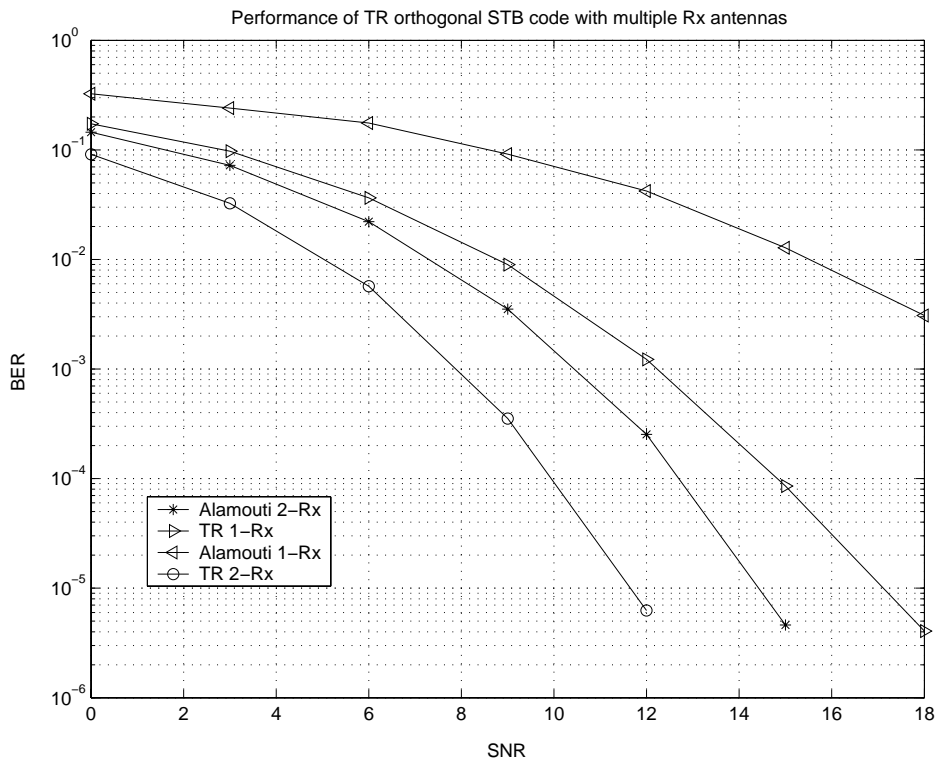


Figure 2.7: Performance of the time-reversed space-time block code with multiple receive antennas

Figure 2.7 shows the bit error rate performance of the Alamouti code and the TR-STB code against the signal-to-noise ratio (SNR) in the multiple receive antennas scenario. The channels between the transmit–receive antenna pairs are five-tap fading channels with the relative power of taps summarized in Table 2.2. Simulation results

show that with this channel the Alamouti code with two receive antennas can perform even better than the time-reversed scheme with one receive antenna. The diversity order in a Rayleigh (or Rician) fading environment can be defined as the asymptotic slope of the error probability curve on a logarithmic scale [58]. Therefore, if we calculate the slope of each curve in the figure for large SNR, we get the rough diversity order achieved in each scenario. For the Alamouti code with one receive antenna the diversity gain is 2.1. For a multipath channel with uncorrelated paths and uniform power profile and with an optimum receiver such as, maximum-likelihood estimator, the maximum achievable diversity order for the Alamouti code is equal to the number of taps times the number of transmit antennas times the number of receive antennas. In our scenario, the channel has a non-uniform power profile and the receiver is based on the zero-forcing algorithm, therefore, we lose some diversity gain. As soon as we use the second receive antenna, the diversity order is increased to 5.2. The diversity order for the case of the time-reversed orthogonal space-time block code with one receive antenna is 4.4. Therefore, compared to the scenario with the Alamouti code and one receive antenna, the time-reversed scheme increases the diversity gain, which is basically achieved from the multipath channel. In the last case, where there are two receive antennas and the time-reversed algorithm is in place, the diversity order is 6.

Figure 2.8 shows the simulation results for a single transmit antenna with the ABBA code and the new code. As expected, in flat fading channels, the ABBA code and the new code have the same performance, whereas the performance of the ABBA code in general is better than the single antenna transmission case. In a multipath fading channel, the ABBA code faces severe inter-symbol-interference which explains the poor performance in this scenario. With the proposed code in (2.41) we improve the performance of the ABBA code as is apparent from Figure 2.8.

Similar to Figure 2.7, the bit error rate performance of the ABBA code and the

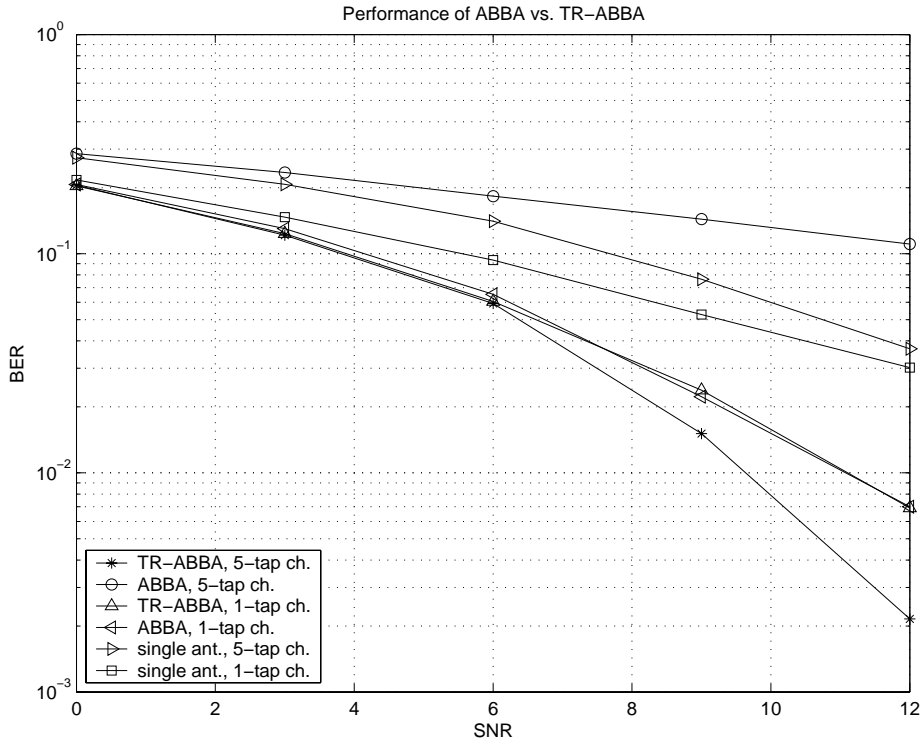


Figure 2.8: Performance of the novel non-orthogonal code vs. ABBA code

proposed code against the signal-to-noise ratio in the multiple-receive antenna scenario is presented in Figure 2.9. The channels between the transmit-receive antenna pairs are five-tap fading channels (Table 2.2). According to the simulation results, the performance of the system with the ABBA code in both one and two-receive antenna scenarios are poor. This is due to the non-orthogonality of the code and multipath fading channels. The diversity orders for the ABBA code with one and two receive antennas and in this type of channel are 0.3 and 1.8, respectively. Our proposed code provides higher performance than that of the ABBA code for both one and two-receive antenna cases. The diversity gain for the new code with one and two receive antennas are 3.1 and 5.8, respectively.

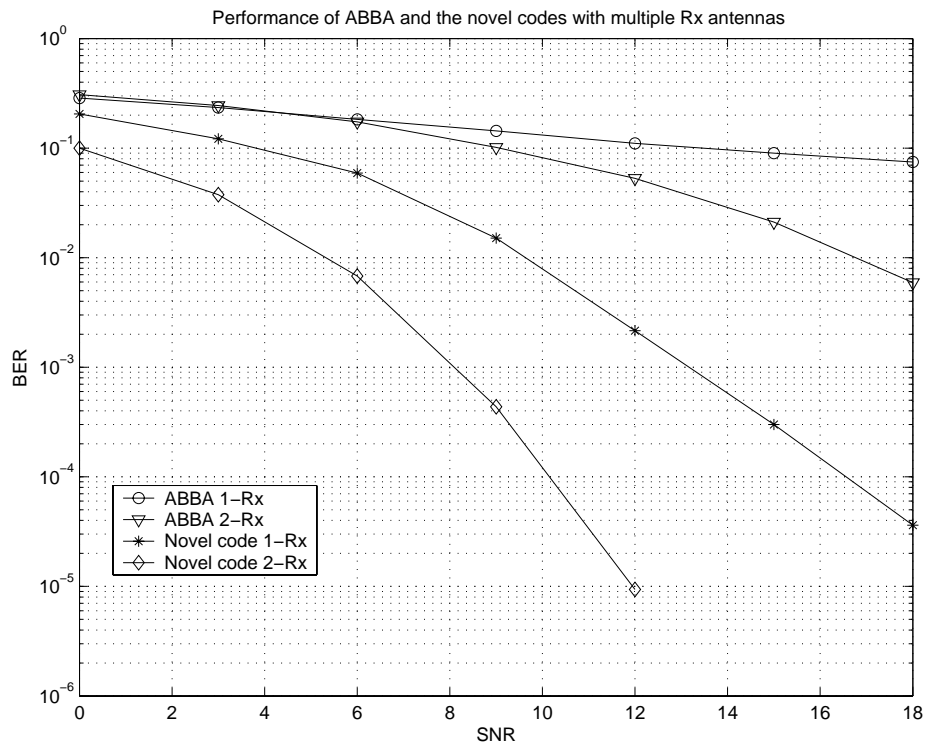


Figure 2.9: Performance of ABBA code and the new non-orthogonal code with multiple receive antennas

2.5 Summary

In this chapter we have presented the MIMO concept by giving an overview of its theory and advances. The information theoretic aspects of MIMO was also covered and the conclusion was that, while SISO systems gain 1 b/s/Hz in capacity every 3 dB, in MIMO the capacity growth rate is m times ($m = \min(n_R, n_T)$) higher, which gives a noticeable advantage for implementing MIMO especially in high SNR scenarios. The capacity generally depends on the channel state information available for the transmitter and the receiver. From this point of view, approaches to measure capacity for three main scenarios, CSI known at both the transmitter and the receiver,

CSI not known at the transmitter but known at the receiver, and CSI not known at both the transmitter and the receiver, were explained.

A central issue in a wireless communication system is the channel. The mathematical models for the distributions of the most common fading, Rayleigh and Rician, were presented. Then the concept of space-time coding was covered. Space-time codings are the techniques where appropriate coding schemes are employed to multiple transmit antennas. Our emphasis was on space-time block codings since they can be decoded with less complexity compared to other existing space-time coding schemes and they have been adopted in some practical cellular systems, e.g., 3G systems. We covered the orthogonal space-time block coding based on Alamouti codes. We addressed the problem of Alamouti codes in multipath fading channels and we explained how this problem can be fixed by implementing the time-reversal algorithm. The limitation of orthogonal STB coding for more than two transmit antennas and derivation from complex signals was addressed. This resulted in some non-orthogonal STB codes. Non-orthogonal STB codes in multipath channels suffer not only from the interference due to their non-orthogonality but also the interference caused by the channel. We proposed a novel scheme to improve the performance of a non-orthogonal space-time block code in multipath channels. Various permutations were investigated, and it was found that both the time reversal of complex symbols and the interleaving of time slots are required. For high SNR, the performance gain is high, as the overall diversity degree is changed. The resulting code enjoys both spatial diversity from the multi-antenna transmission, and diversity from properly equalized multipath channels.

Chapter 3

EM Algorithm Based Receivers

3.1 Introduction

Multiuser communication has been around among research communities for more than two decades. Its aim is to detect messages of several users who share a common communication channel. Many emerging wireless communication systems are incorporating considerable signal processing intelligence in order to meet the challenge of a multiuser system. These signal processing algorithms fall into the category of so called “multiuser detection” [72].

WCDMA is the air interface scheme of rapidly deploying 3G systems. It is based on DS-CDMA multiple access technique where users are multiplexed by distinct code waveforms. Two major factors that limit the performance of WCDMA systems are multipath fading and multiple access interference (MAI). As it was explained in Chapter 2, multipath fading is due to the channel dynamics created by the different scatterers involved in transmission. On the other hand, MAI is due to the fact that multiple users simultaneously use the same channel. Multiuser detection techniques for CDMA systems have been extensively studied in the literature (see e.g., [72] and the references therein).

In Chapter 2 we have seen that the use of MIMO techniques can greatly increase the information capacity of a wireless communication system. In the same chapter, we have seen that the very simple structure of the Alamouti coding scheme makes it a very attractive method, which is currently part of the WCDMA standard [2].

In this chapter we consider the nonlinear iterative detector derived from the EM algorithm. We, particularly, focus on the downlink of a space-time block coded (STBC) WCDMA system in the case of multipath fading channels. In multipath fading channels the decoding of Alamouti codes is no longer that simple. We introduce some transformation matrices in the process of the decoding of Alamouti codes to transform the received signal into a simpler form.

This chapter is organized as follows. We first give an overview of the EM algorithm. Then the WCDMA system and its extension, HSDPA, are briefly introduced. The system model for the downlink of an SISO and STBC WCDMA system are given. Then, we describe an EM-based receiver for both SISO and STBC WCDMA systems. Finally, Numerical results showing the performance of EM-based receivers are given.

3.2 EM Algorithm

3.2.1 Background

The Expectation-Maximization (EM) algorithm is an approach to the iterative computation of maximum likelihood (ML) estimates when direct maximization of the likelihood function may not be feasible [13, 17, 50, 52]. The main idea of the the EM algorithm is as follows. We have some observed data, but maximum likelihood-based parameter estimation of our model might be very complicated. According to the EM algorithm, some extra variables in an “augmented space” are defined, hoping that the maximum likelihood estimation in this “augmented space” would be much simplified. An important point is that the extra variables might be quite hypothetical. The real

data space is called “incomplete data space” and the augmented data space is called “complete data space”. Thus the basic idea of the EM algorithm is to associate with the given incomplete-data space, a complete-data space for which the ML estimation is computationally more tractable. The methodology of the EM algorithm then consists in reformulating the problem in terms of this more easily solved complete-data space, establishing a relationship between the likelihoods of these two spaces, and utilizing the simpler ML estimates computation of the complete-data problem in the M-step of the iterative computing algorithm.

The EM algorithm consists of two major steps. They are called the expectation step or the E-step, followed by a maximization step or the M-step. Thus the name EM algorithm. The name “EM algorithm” was originally given by Dempster, Laird and Rubin and the algorithm itself was initially formulated by them [13]. The expectation is with respect to the unknown underlying variables using the current estimate of the parameters and conditioned upon the observations. The maximization step provides a new estimate of the parameters. These two steps are iterated until convergence. The convergence rate of an EM algorithm is inversely related to the Fisher information of its complete-data space [13]. Fessler and Hero [18, 28] have shown that the less-informative complete data spaces lead to improved asymptotic convergence rates.

In certain scenarios, the convergence of the EM algorithm might be slow. For instance, a less informative complete data space can lead to an intractable maximization step due to simultaneous update employed by the EM algorithm [13]. To circumvent the trade off between convergence and complexity, modified versions and some extensions of the EM algorithm have been introduced. Going through different extensions of the algorithm is outside the scope of this thesis.

3.2.2 Formulation of the EM Algorithm

Let \mathbf{R} be a given realization with probability density $f_{\mathbf{R}}(\mathbf{r}; \mathbf{b})$ and a parameter $\mathbf{b} \in \Lambda$, Λ denotes the parameter space. The maximum-likelihood (ML) estimator of \mathbf{b} is defined as

$$\hat{\mathbf{b}}(\mathbf{r}) = \arg \max_{\mathbf{b} \in \Lambda} \log f_{\mathbf{R}}(\mathbf{r}; \mathbf{b}). \quad (3.1)$$

The EM algorithm is a broadly applicable algorithm that provides an iterative procedure for computing MLEs in situations where, but for the absence of some additional data, ML estimation would not be straightforward. Hence, in this context, the observed data \mathbf{R} is viewed as being the “incomplete data” and is regarded as an observable function of the so called “complete data”. The notation of “incomplete data” includes the conventional sense of missing data, but it also applies to situations where the complete data represents what would be available from some hypothetical experiment. In the latter case, the complete data may contain some variables that are never observable in a data sense [50]. Within this framework, let \mathbf{X} denote “complete data”, related to \mathbf{R} by

$$P(\mathbf{X}) = P(\mathbf{x}_1, \mathbf{x}_2, \dots, \mathbf{x}_K) = \mathbf{R}, \quad (3.2)$$

where $\mathbf{P}(\cdot)$ is a many-to-one transformation related to observed (incomplete) data \mathbf{R} . $\mathbf{P}(\cdot)$ can be any non-invertible transformation. Hence, there are many possibilities to specify complete data \mathbf{X} that generate the observed data \mathbf{R} . If the probability density function of \mathbf{X} is $f_{\mathbf{X}}(\mathbf{x}; \mathbf{b})$ and $f_{\mathbf{X}|\mathbf{R}=\mathbf{r}}(\mathbf{x}; \mathbf{b})$ is the conditional probability density of \mathbf{X} given $\mathbf{R} = \mathbf{r}$

$$f_{\mathbf{X}}(\mathbf{x}; \mathbf{b}) = f_{\mathbf{X}|\mathbf{R}=\mathbf{r}}(\mathbf{x}; \mathbf{b}) \cdot f_{\mathbf{R}}(\mathbf{r}; \mathbf{b}) \quad \forall P(\mathbf{X}) = \mathbf{R}. \quad (3.3)$$

By taking the logarithm of (3.3) we end up with

$$\log f_{\mathbf{R}}(\mathbf{r}; \mathbf{b}) = \log f_{\mathbf{X}}(\mathbf{x}; \mathbf{b}) - \log f_{\mathbf{X}|\mathbf{R}=\mathbf{r}}(\mathbf{x}; \mathbf{b}). \quad (3.4)$$

We apply conditional expectation to both sides of (3.4) given $\mathbf{R} = \mathbf{r}$ at a parameter value $\hat{\mathbf{b}}$

$$\log f_{\mathbf{R}}(\mathbf{r}; \mathbf{b}) = E \left\{ \log f_{\mathbf{X}}(\mathbf{x}; \mathbf{b}) \mid \mathbf{R} = \mathbf{r}; \hat{\mathbf{b}} \right\} - E \left\{ \log f_{\mathbf{X}|\mathbf{R}=\mathbf{r}}(\mathbf{x}; \mathbf{b}) \mid \mathbf{R} = \mathbf{r}; \hat{\mathbf{b}} \right\}. \quad (3.5)$$

Let's define $L(\mathbf{b}) = \log f_{\mathbf{R}}(\mathbf{r}; \mathbf{b})$, $U(\mathbf{b}, \hat{\mathbf{b}}) = E \left\{ \log f_{\mathbf{X}}(\mathbf{x}; \mathbf{b}) \mid \mathbf{R} = \mathbf{r}; \hat{\mathbf{b}} \right\}$ and $V(\mathbf{b}, \hat{\mathbf{b}}) = E \left\{ \log f_{\mathbf{X}|\mathbf{R}=\mathbf{r}}(\mathbf{x}; \mathbf{b}) \mid \mathbf{R} = \mathbf{r}; \hat{\mathbf{b}} \right\}$.

With these definitions, equation (3.5) can be re-written as

$$L(\mathbf{b}) = U(\mathbf{b}, \hat{\mathbf{b}}) - V(\mathbf{b}, \hat{\mathbf{b}}). \quad (3.6)$$

We want to maximize $L(\mathbf{b})$, the log-likelihood of the observed data. According to Jensen's inequality $V(\mathbf{b}, \hat{\mathbf{b}}) \leq V(\hat{\mathbf{b}}, \hat{\mathbf{b}})$. Therefore, if $U(\mathbf{b}, \hat{\mathbf{b}}) \geq U(\hat{\mathbf{b}}, \hat{\mathbf{b}})$ then $L(\mathbf{b}) \geq L(\hat{\mathbf{b}})$.

From this we can form the EM algorithm. It starts with an arbitrary initial value $\hat{\mathbf{b}}^{(0)}$ and estimates the new parameter iteratively. Hence, given an initial estimate $\hat{\mathbf{b}}^{(0)}$, the n th estimate of the EM algorithm is described by

- E-step: compute $U(\mathbf{b}; \hat{\mathbf{b}}^{(n)})$
- M-step: $\hat{\mathbf{b}}^{(n+1)} = \arg \max_{\mathbf{b} \in \Lambda} U(\mathbf{b}; \hat{\mathbf{b}}^{(n)})$

where $\hat{\mathbf{b}}$ is an estimate of \mathbf{b} .

It can be shown that, in each iteration, the EM algorithm estimates monotonically increase in likelihood, and $\hat{\mathbf{b}}^{(n)}$ converges to a local maximum. The ability of the EM algorithm to find the global maximum of (3.1) generally depends on the initialization $\hat{\mathbf{b}}^{(0)}$ [17]. Furthermore, the choice of complete data may critically affect the complexity and the rate of convergence of the algorithm. Inappropriate selection of a complete data may result in a useless algorithm [17].

3.2.3 EM Solution to MLE in Gaussian Linear Systems

Let us consider a linear system model

$$\mathbf{r} = \mathbf{H}\mathbf{b} + \mathbf{n} \quad (3.7)$$

where the matrix \mathbf{H} is a known matrix, \mathbf{b} is a parameter vector that has to be estimated, vector \mathbf{r} is observed data and \mathbf{n} is a white Gaussian random vector with zero mean and variance σ^2 . It is apparent that the MLE of \mathbf{b} is found by minimizing

$$J(\mathbf{b}) = \|\mathbf{r} - \mathbf{H}\mathbf{b}\|^2 \quad (3.8)$$

where $\|\cdot\|^2$ denotes the squared Euclidean distance.

Searching for an appropriate \mathbf{b} that minimize $J(\mathbf{b})$ in (3.8) is an extensive complex task. As it is mentioned, the EM algorithm is an iterative algorithm to solve the MLE with less complexity. It has the desirable property of increasing the likelihood at each iteration. In order to apply the EM algorithm, a set of complete data should be defined. There is not any single method to choose the complete data. For the linear system in (3.7) let's consider a set of complete data \mathbf{x}_k 's defined as

$$\mathbf{x}_k = \mathbf{H}_k \mathbf{b}_k + \mathbf{n}_k \quad k = 1, \dots, K \quad (3.9)$$

It is obvious that

$$\mathbf{r} = \sum_{k=1}^K \mathbf{x}_k \quad (3.10)$$

Since \mathbf{n}_k 's with variances σ_k^2 's are IID we can easily write

$$\log f_{\mathbf{X}}(\mathbf{x}; \mathbf{b}) = g(\mathbf{x}) + \sum_{k=1}^K \frac{1}{\sigma_k^2} \|\mathbf{x}_k - \mathbf{H}_k \mathbf{b}_k\|^2 \quad (3.11)$$

where $g(\mathbf{x})$ is a function of \mathbf{x} and does not depend on \mathbf{b}_k 's. From previous section we write the conditional expectations as

$$U(\mathbf{b}, \hat{\mathbf{b}}) = E \left\{ \log f_{\mathbf{X}}(\mathbf{x}; \mathbf{b}) \mid \mathbf{R} = \mathbf{r}; \hat{\mathbf{b}} \right\} \quad (3.12)$$

Using the standard result for conditional expectations of joint random vectors [44], we have

$$\begin{aligned}\hat{\mathbf{x}}_k &= E(\mathbf{x}_k | \mathbf{R} = \mathbf{r}; \hat{\mathbf{b}}) \\ &= E(\mathbf{x}_k | \hat{\mathbf{b}}) + \mathbf{C}_{\mathbf{x}_k \mathbf{r}} \mathbf{C}_{\mathbf{r} \mathbf{r}}^{-1} (\mathbf{r} - E(\mathbf{r} | \hat{\mathbf{b}}))\end{aligned}\quad (3.13)$$

where $\mathbf{C}_{\mathbf{x}_k \mathbf{r}}$ and $\mathbf{C}_{\mathbf{r} \mathbf{r}}^{-1}$ are the covariance matrices given by

$$\mathbf{C}_{\mathbf{x}_k \mathbf{r}} = E\left(\left(\mathbf{x}_k - E(\mathbf{x}_k | \hat{\mathbf{b}})\right)^\dagger (\mathbf{r} - E(\mathbf{r} | \hat{\mathbf{b}})) | \hat{\mathbf{b}}\right) \quad (3.14)$$

$$\mathbf{C}_{\mathbf{r} \mathbf{r}} = E\left(\left(\mathbf{r} - E(\mathbf{r} | \hat{\mathbf{b}})\right)^2 | \hat{\mathbf{b}}\right) \quad (3.15)$$

It is easy to see that

$$E(\mathbf{x}_k | \hat{\mathbf{b}}) = \mathbf{H}_k \hat{\mathbf{b}}_k \quad (3.16)$$

$$E(\mathbf{r} | \hat{\mathbf{b}}) = \mathbf{H} \hat{\mathbf{b}} \quad (3.17)$$

$$\mathbf{C}_{\mathbf{x}_k \mathbf{r}} = \sigma_k^2 \mathbf{I} \quad (3.18)$$

$$\mathbf{C}_{\mathbf{r} \mathbf{r}} = \sigma^2 \mathbf{I} \quad (3.19)$$

Substituting (3.16)-(3.19) in (3.13) results in

$$\hat{\mathbf{x}}_k = \mathbf{H}_k \hat{\mathbf{b}}_k + \frac{\sigma_k^2}{\sigma^2} (\mathbf{r} - \mathbf{H} \hat{\mathbf{b}}) \quad (3.20)$$

By defining $\beta_k = \frac{\sigma_k^2}{\sigma^2}$, the E- and M-steps for the linear system in (3.7) with the complete data of (3.9) are

- E-step: calculating $\hat{\mathbf{x}}_k$ knowing the $\hat{\mathbf{b}}_k^{(n)}$

$$\hat{\mathbf{x}}_k = \mathbf{H}_k \hat{\mathbf{b}}_k^{(n)} + \beta_k \left(\mathbf{r} - \sum_{k=1}^K \mathbf{H}_k \mathbf{b}_k^{(n)} \right) \quad (3.21)$$

- M-step: calculating $\hat{\mathbf{b}}_k^{(n+1)}$

$$\hat{\mathbf{b}}_k^{(n+1)} = \arg \min_{\mathbf{b}_k} \|\hat{\mathbf{x}}_k - \mathbf{H}_k \mathbf{b}_k\|^2 \quad (3.22)$$

Hence, as it is seen, one of the most important features of the EM algorithm is that it decouples the original MLE into K separate MLEs. From Eq. (3.10), it is seen that the parameters β_k 's must satisfy the constraint

$$\sum_{k=1}^K \beta_k = 1 \quad \beta_k \geq 0 \quad (3.23)$$

The β_k 's can be used to control the rate of convergence of the algorithm and possibly to avoid the convergence to an unwanted stationary point of the algorithm [17]. As it was mentioned in the previous section the ability of the algorithm to find the global maximum generally depends on the initial values, $\hat{\mathbf{b}}_k^{(0)}$'s, [17].

3.3 WCDMA Systems and its Extension (HSDPA)

Third generation (3G) systems are intended to provide a global mobility with wide range of services including telephony, paging, messaging, multimedia, Internet and broadband data. In the standardization forums, Wideband CDMA (WCDMA) technology was selected for 3G air interface. In this section, a WCDMA system is briefly introduced.

In general, for radio systems there are two resources, frequency and time. Division by frequency, so that each pair of communicators is allocated part of the spectrum for all of the time, results in Frequency Division Multiple Access (FDMA). Division by time, so that each pair of communicators is allocated all (or at least a large part) of the spectrum for part of the time results in Time Division Multiple Access (TDMA). In Code Division Multiple Access (CDMA), every user is allocated the entire spectrum all the time. CDMA uses codes to identify connections and it uses unique spreading codes to spread the baseband data before transmission. The rate of a spreading

code is referred to as chip rate. Figure 3.1 demonstrates three main multiple access schemes.

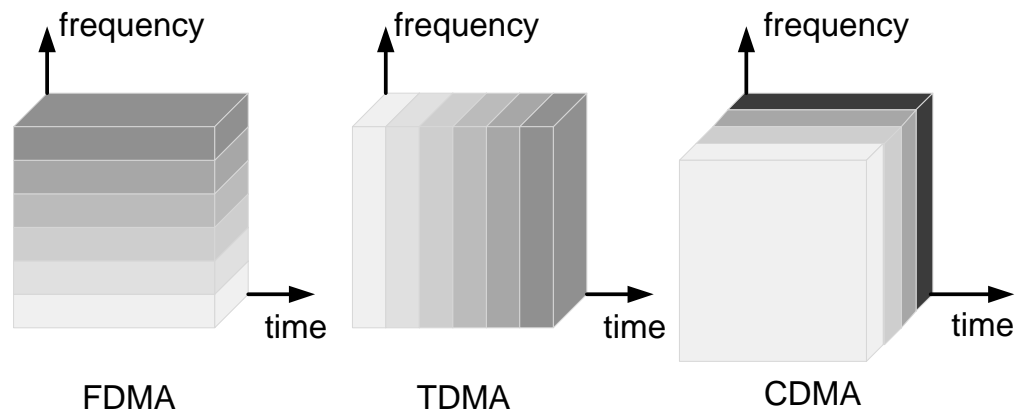


Figure 3.1: Multiple access schemes

WCDMA system is a Direct-Sequence CDMA (DS-SS-CDMA) system where user data is multiplied with quasi-random bits derived from WCDMA Spreading codes. In other words, user information bits are spread over a wide bandwidth by multiplying the user data with quasi-random bits (called chips) derived from CDMA spreading codes. WCDMA system supports very high bit rates of up to 2 Mb/s using a variable spreading factor and multicode connections. The chip rate of 3.84 Mcps leads to a carrier bandwidth of approximately 5MHz [32].

WCDMA applies a two-layered code structure consisting of orthogonal spreading codes and pseudo-random scrambling codes. Spreading is performed using channelization codes, which transform every data symbol into a number of chips, thus increasing the bandwidth of the signal. Orthogonality between the different spreading factors

can be achieved by the Orthogonal Variable Spreading Factor (OVSF) codes [32] whose construction is as follows

$$\begin{aligned} \mathbf{S}_1 &= 1, \\ \mathbf{S}_{2^n} &= \begin{bmatrix} \mathbf{S}_{2^{n-1}} & \mathbf{S}_{2^{n-1}} \\ \mathbf{S}_{2^{n-1}} & -\mathbf{S}_{2^{n-1}} \end{bmatrix}, \quad n = 1, 2, \dots \end{aligned} \quad (3.24)$$

in which each column of the matrix \mathbf{S} represents a code. OVSF codes are sometimes called Walsh or Walsh-Hadamard codes.

In a WCDMA system scrambling is used for cell separation in the downlink and user separation in the uplink. Scrambling is done on top of spreading, so it does not change the signal bandwidth but only makes signals from different sources separable from each other. Scrambling codes are pseudo-noise (PN) codes. The modulation scheme used in WCDMA system is QPSK.

In the third-Generation Partnership Project (3GPP) standardization for UMTS, a high-speed packet transmission technology called High-Speed Downlink Packet Access (HSDPA) is under development [1]. HSDPA provides peak throughput higher than 2 Mb/s (up to 7 Mb/s) in the downlink. The high peak data rate is achieved by using link adaptation and fast physical layer retransmission with soft combining. With HSDPA, two of the most fundamental features of WCDMA, variable spreading factor and fast power control, are disabled and replaced by means of adaptive modulation and coding (AMC), extensive multicode operation and a fast and spectrally efficient retransmission strategy [32]. The user data rate in HSDPA (downlink direction) may reach up to 7 Mb/s using 16-QAM modulation with 15 codes of spreading factor 16. It also supports the QPSK modulation. The assumed constellations for both QPSK and 16-QAM in HSDPA systems are shown in Fig. 3.2

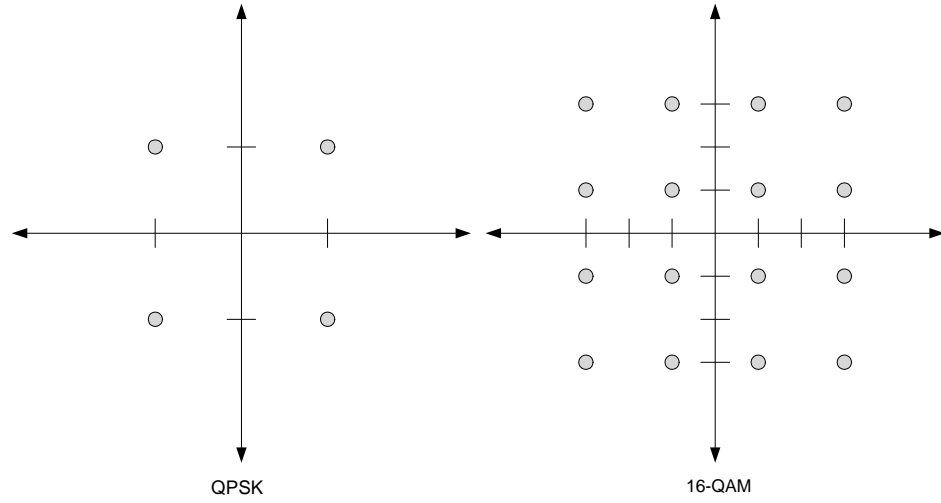


Figure 3.2: QPSK and 16-QAM constellations in the HSDPA system.

3.4 Conventional Receivers for WCDMA System

In this section, we review the optimum and some sub-optimum receivers for single-antenna and space-time block-coded WCDMA systems. We consider downlink scenarios for such systems with K users, QPSK or 16-QAM modulation, and multipath fading channels.

3.4.1 Single Antenna

The received signal, \mathbf{r} , for a SISO system can be written as

$$\mathbf{r} = \mathbf{HCSb} + \mathbf{n} \quad (3.25)$$

where \mathbf{H} is the channel matrix, \mathbf{C} is the scrambling code matrix, \mathbf{S} is the spreading code matrix for all users, \mathbf{b} is a vector of users' symbols and \mathbf{n} is an AWGN vector.

Maximum Likelihood Detection (MLD)

The optimum detector for (3.25) chooses \mathbf{b} to maximize the log-likelihood function, and it sets the vector \mathbf{b} as [44]

$$\begin{aligned}\hat{\mathbf{b}}_{MLD} &= \arg \min_{\mathbf{b}} \|\mathbf{r} - \mathbf{HCSb}\|^2 \\ &= \arg \max_{\mathbf{b}} \left(2\text{Re} \left(\mathbf{b}^\dagger \mathbf{S}^\dagger \mathbf{C}^\dagger \mathbf{H}^\dagger \mathbf{r} \right) - \mathbf{b}^\dagger \mathbf{S}^\dagger \mathbf{C}^\dagger \mathbf{H}^\dagger \mathbf{HCSb} \right)\end{aligned}\quad (3.26)$$

This is a very complex detector. Therefore, we introduce simpler receivers in the following.

Matched Filter

As it was mentioned in the previous section, the ML detector is a very computationally complex receiver. Hence, one could implement a RAKE receiver based on a matched filter which is less complex. This means that we can easily filter the received signal in (3.25) with the matched filter $(\mathbf{HCS})^\dagger$. The output of the matched filter is given by

$$\mathbf{Z}_{\text{SISO}} = \mathbf{S}^\dagger \mathbf{C}^\dagger \mathbf{H}^\dagger \mathbf{r}. \quad (3.27)$$

Parallel Interference Cancellation (PIC)

In PIC [71], we start with an initial estimate (usually it is the output of the matched filter), we regenerate the multiple user interference (MUI) and subtracts the MUI from the received signal in multiple stages. That is why we call PIC receiver as multi-stage receiver.

Mathematically, we can present PIC as follows. First we calculate the cross-correlation matrix in (3.25)

$$\mathbf{R}_{\text{SISO}} = \mathbf{S}^\dagger \mathbf{C}^\dagger \mathbf{H}^\dagger \mathbf{HCS} \quad (3.28)$$

Then, the output of PIC at the i -th stage is given by

$$\hat{\mathbf{b}}_{pic}^{(i)} = \text{dec} \left(\mathbf{Z}_{\text{SISO}} - \mathbf{U}_{\text{SISO}} \hat{\mathbf{b}}_{pic}^{(i-1)} \right) \quad (3.29)$$

where $\text{dec}(\cdot)$ denotes the decision function which depends on the modulation scheme, and \mathbf{Z}_{SISO} is the output of the matched filter. In (3.29), $\mathbf{U}_{\text{SISO}} = \mathbf{R}_{\text{SISO}} - \text{diag}(\mathbf{R}_{\text{SISO}})$ is the cross-correlation matrix minus its diagonal elements. In other word, in PIC the tentative decisions obtained from the previous stages are used to estimate and subtract the MUI. The initial value can be set as

$$\hat{\mathbf{b}}_{pic}^{(0)} = \text{dec}(\mathbf{Z}_{\text{SISO}}) \quad (3.30)$$

3.4.2 Space-Time Block Coded WCDMA

Space-time block coding was introduced in Chapter 1. Alamouti has introduced a simple transmit diversity scheme with two transmit antennas in frequency flat fading channels [3]. As it was mentioned and shown in the previous chapter, when it comes to a multipath fading channel, decoupling and detecting the transmitted symbols is not as straightforward as it is in a flat fading channel. In this section, we introduce a new modeling for an STBC WCDMA system in multipath fading channels in order to represent the received signal in more appropriate linear form. We consider a downlink scenario for such a system with K users, two transmit antennas, one receive antenna, QPSK/16-QAM modulation and multipath fading channels. The extension to two receive antennas is straightforward. The structure of the assumed STBC WCDMA is illustrated in Fig. 3.3. The received signal model can be written as

$$\mathbf{r} = \mathbf{H}_1 \mathbf{C} \mathbf{S} \mathbf{b}_1 + \mathbf{H}_2 \mathbf{C} \mathbf{S} \mathbf{b}_2 + \mathbf{n}, \quad (3.31)$$

where \mathbf{H}_1 and \mathbf{H}_2 are the channel matrices from transmit antennas 1 and 2 to the receive antenna, respectively. In (3.31), \mathbf{C} is the scrambling code matrix, \mathbf{S} is the spreading code matrix for all users, \mathbf{n} is an AWGN vector and \mathbf{b}_1 and \mathbf{b}_2 are the

STBC users' symbol vectors from transmit antennas 1 and 2, respectively, defined as follows

$$\mathbf{b}_1 = \begin{bmatrix} s^{(1)}(1) & s^{(2)}(1) & \dots & s^{(K)}(1) & -s^{(1)}(2)^* & \dots & -s^{(K)}(2)^* & \dots \end{bmatrix}^T \quad (3.32)$$

$$\mathbf{b}_2 = \begin{bmatrix} s^{(1)}(2) & s^{(2)}(2) & \dots & s^{(K)}(2) & s^{(1)}(1)^* & s^{(2)}(1)^* & \dots & s^{(K)}(1)^* & \dots \end{bmatrix}^T$$

where $s^{(i)}(j)$ is the j th symbol of the i th user.

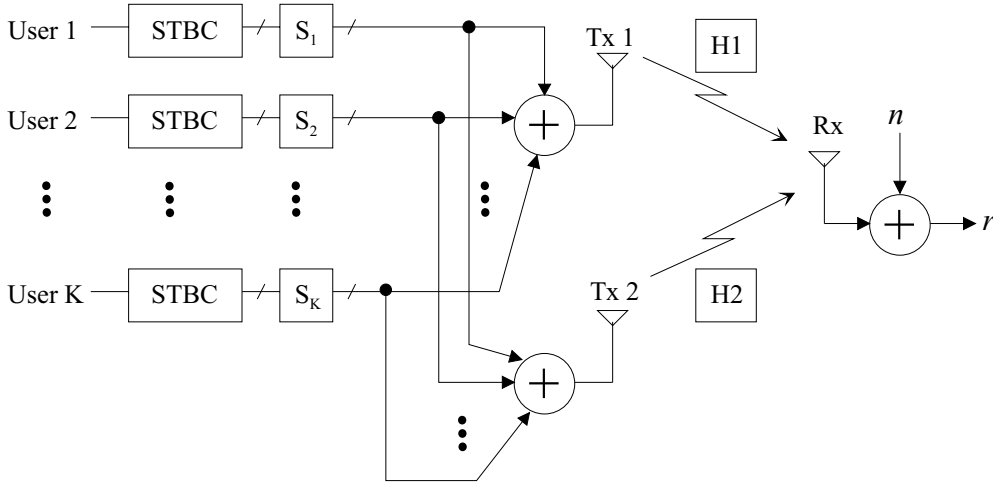


Figure 3.3: Block diagram of the downlink of a STBC-WCDMA system.

Furthermore, we can write equation (3.31) as

$$\mathbf{r} = (\mathbf{H}_1 \mathbf{C} \mathbf{T}_1 + \mathbf{H}_2 \mathbf{C} \mathbf{T}_2) \mathbf{b} + \mathbf{n}, \quad (3.33)$$

where \mathbf{T}_1 and \mathbf{T}_2 are the transformation matrices defined as

$$\begin{cases} \mathbf{b}_1 = \mathbf{T}_1 \mathbf{b} \\ \mathbf{b}_2 = \mathbf{T}_2 \mathbf{b} \end{cases} \quad (3.34)$$

Vector \mathbf{b} is a real vector which includes real and imaginary parts of symbols, separately: $\mathbf{b} = [s_{Re}^{(1)}(1) \ s_{Im}^{(1)}(1) \ s_{Re}^{(2)}(1) \ s_{Im}^{(2)}(1) \ \dots \ s_{Re}^{(K)}(1) \ s_{Im}^{(K)}(1) \ s_{Re}^{(1)}(2) \ s_{Im}^{(1)}(2) \ s_{Re}^{(2)}(2)$

$s_{Im}^{(2)}(2) \cdots]^T$ in which $s_{Re}^{(i)}(j)$ and $s_{Im}^{(i)}(j)$ are the real and imaginary parts of the j th symbol of the i th user, respectively.

If, for example, STB encoding is performed on a two symbol block of user 1, \mathbf{b}_1 , \mathbf{b}_2 , \mathbf{b} , \mathbf{T}_1 , and \mathbf{T}_2 are given by

$$\mathbf{b}_1 = \begin{bmatrix} s^{(1)}(1) \\ -s^{(1)}(2)^* \end{bmatrix}, \mathbf{b}_2 = \begin{bmatrix} s^{(1)}(2) \\ s^{(1)}(1)^* \end{bmatrix}, \mathbf{b} = \begin{bmatrix} s_{Re}^{(1)}(1) \\ s_{Im}^{(1)}(1) \\ s_{Re}^{(1)}(2) \\ s_{Im}^{(1)}(2) \end{bmatrix}, \quad (3.35)$$

$$\mathbf{T}_1 = \begin{bmatrix} 1 & j & 0 & 0 \\ 0 & 0 & -1 & j \end{bmatrix}, \mathbf{T}_2 = \begin{bmatrix} 0 & 0 & 1 & j \\ 1 & j & 0 & 0 \end{bmatrix}$$

Let us define \mathbf{G} as

$$\mathbf{G} = \mathbf{H}_1 \mathbf{C} \mathbf{S} \mathbf{T}_1 + \mathbf{H}_2 \mathbf{C} \mathbf{S} \mathbf{T}_2, \quad (3.36)$$

then we can write

$$\mathbf{r} = \mathbf{G} \mathbf{b} + \mathbf{n}. \quad (3.37)$$

Equation (3.37) is a linear equation of users' symbols and it is in a more proper way for detecting the symbols.

Maximum Likelihood Detection (MLD)

As in single-antenna case, the optimal detector for (3.37) chooses \mathbf{b} to maximize the log-likelihood function, and it sets the vector \mathbf{b} as

$$\hat{\mathbf{b}}_{MLD} = \arg \max_{\mathbf{b}} \left[2\text{Re} \left(\mathbf{b}^T \mathbf{G}^\dagger \mathbf{r} \right) - \mathbf{b}^T \mathbf{G}^\dagger \mathbf{G} \mathbf{b} \right]. \quad (3.38)$$

Matched Filter

The output of the matched filter for the STBC WCDMA system presented in Eq. (3.37) is given by

$$\mathbf{Z} = \mathbf{G}^\dagger \mathbf{r}. \quad (3.39)$$

Parallel Interference Cancellation (PIC)

As for the PIC solution for this case, first, the cross-correlation matrix of (3.37) is calculated as

$$\mathbf{R} = \mathbf{G}^\dagger \mathbf{G} \quad (3.40)$$

Then, the output of PIC at the i -th stage is given by

$$\hat{\mathbf{b}}_{pic}^{(i)} = \text{dec} \left(\mathbf{Z} - \mathbf{U} \hat{\mathbf{b}}_{pic}^{(i-1)} \right) \quad (3.41)$$

where \mathbf{Z} is the output of the matched filter. In (3.41), $\mathbf{U} = \mathbf{R} - \text{diag}(\mathbf{R})$ is the cross-correlation matrix minus its diagonal elements. The initial value can be set as

$$\hat{\mathbf{b}}_{pic}^{(0)} = \text{dec}(\mathbf{Z}) \quad (3.42)$$

3.5 EM Algorithm Based Receiver for WCDMA System

3.5.1 Single Antenna

In order to use the EM algorithm, first the complete data should be specified. Let us consider the complete data \mathbf{x}_k 's as

$$\mathbf{x}_k = \mathbf{H}_k \mathbf{C}_k \mathbf{S}_k \mathbf{b}_k + \mathbf{n}_k \quad k = 1, \dots, K \quad (3.43)$$

This equation is similar to Eq. (3.9). Hence, we can easily derive the E- and M-steps as

- E-step: calculating $\hat{\mathbf{x}}_k$

$$\hat{\mathbf{x}}_k = \mathbf{H}_k \mathbf{C}_k \mathbf{S}_k \hat{\mathbf{b}}_k^{(n)} + \beta_k \left(\mathbf{r} - \sum_{k=1}^K \mathbf{H}_k \mathbf{C}_k \mathbf{S}_k \mathbf{b}_k^{(n)} \right) \quad (3.44)$$

- M-step: calculating $\hat{\mathbf{b}}_k^{(n+1)}$

$$\hat{\mathbf{b}}_k^{(n+1)} = \arg \min_{\mathbf{b}_k} \|\hat{\mathbf{x}}_k - \mathbf{H}_k \mathbf{C}_k \mathbf{S}_k \mathbf{b}_k\|^2 \quad (3.45)$$

Expanding (3.45) results in

$$\hat{\mathbf{b}}_k^{(n+1)} = \arg \max_{\mathbf{b}_k} \left(2\text{Re} \left(\mathbf{b}_k^\dagger \mathbf{S}_k^\dagger \mathbf{C}_k^\dagger \mathbf{H}_k^\dagger \hat{\mathbf{x}}_k \right) - \mathbf{b}_k^\dagger \mathbf{S}_k^\dagger \mathbf{C}_k^\dagger \mathbf{H}_k^\dagger \mathbf{H}_k \mathbf{C}_k \mathbf{S}_k \mathbf{b}_k \right). \quad (3.46)$$

Equation (3.46) provides us an iterative equation to detect the symbols of the users. In case of QPSK modulation this equation has the following simple form

$$\hat{\mathbf{b}}_k^{(n+1)} = \text{csign} \left(\mathbf{S}_k^\dagger \mathbf{C}_k^\dagger \mathbf{H}_k^\dagger \hat{\mathbf{x}}_k \right) \quad (3.47)$$

where $\text{csign}(a + jb) = \text{sign}(a) + j\text{sign}(b)$. By choosing an appropriate initial value and parameter β_k , the algorithm will converge to the local maximum value of the log-likelihood function. A good choice for $\hat{\mathbf{b}}^{(0)}$ is to use the output of the matched filter. Parameter β_k has a critical role in the EM algorithm. By setting $\beta_k = 0$ we see that (3.46) loses its iteration and reduces to a matched filter receiver, and by assuming $\beta_k = 1$, (3.46) is exactly a PIC detector. Here, β_k 's are initially set experimentally for best performance. There are some suggestions regarding how to choose the β_k 's in [5, 6] for a CDMA system.

3.5.2 Space-Time Block Coded WCDMA

In order to apply the EM algorithm we first define a complete data set \mathbf{x}_k as

$$\mathbf{x}_k = \mathbf{G}_k \mathbf{b}_k + \mathbf{n}_k \quad k = 1, \dots, K \quad (3.48)$$

where \mathbf{b}_k is a real vector of symbols of the k th user (\mathbf{b}_k is defined the same way as the \mathbf{b} vector but includes only symbols of the k th user). In (3.48), \mathbf{n}_k 's are AWGN which are obtained by arbitrarily decomposing the total noise \mathbf{n} into the K components so

that $\sum_{k=1}^K \mathbf{n}_k = \mathbf{n}$. If the covariance matrices of \mathbf{n}_k and \mathbf{n} are \mathbf{Q}_k and \mathbf{Q} , respectively, then $\mathbf{Q}_k = \beta_k \mathbf{Q}$ in which β_k 's are arbitrary real valued scalars satisfying

$$\sum_{k=1}^K \beta_k = 1 \quad \beta_k \geq 0 \quad (3.49)$$

In (3.48), \mathbf{G}_k is defined by

$$\mathbf{G}_k = \mathbf{H}_1 \mathbf{C} \mathbf{S}_k \tilde{\mathbf{T}}_1 + \mathbf{H}_2 \mathbf{C} \mathbf{S}_k \tilde{\mathbf{T}}_2, \quad (3.50)$$

where \mathbf{S}_k is the k th user's spreading code matrix, and $\tilde{\mathbf{T}}_1$ and $\tilde{\mathbf{T}}_2$ are new transformation matrices. We can easily see that $\tilde{\mathbf{T}}_1$ and $\tilde{\mathbf{T}}_2$ are block-diagonal matrices as follows

$$\tilde{\mathbf{T}}_1 = \begin{bmatrix} \mathbf{A}_1 & \mathbf{0} & \mathbf{0} & \cdots \\ \mathbf{0} & \mathbf{A}_1 & \mathbf{0} & \cdots \\ \mathbf{0} & \mathbf{0} & \mathbf{A}_1 & \\ \vdots & \vdots & & \ddots \end{bmatrix}, \quad (3.51)$$

$$\tilde{\mathbf{T}}_2 = \begin{bmatrix} \mathbf{A}_2 & \mathbf{0} & \mathbf{0} & \cdots \\ \mathbf{0} & \mathbf{A}_2 & \mathbf{0} & \cdots \\ \mathbf{0} & \mathbf{0} & \mathbf{A}_2 & \\ \vdots & \vdots & & \ddots \end{bmatrix}$$

where $\mathbf{A}_1 = \begin{bmatrix} 1 & j & 0 & 0 \\ 0 & 0 & -1 & -j \end{bmatrix}$, $\mathbf{A}_2 = \begin{bmatrix} 0 & 0 & 1 & j \\ 1 & -j & 0 & 0 \end{bmatrix}$, $j = \sqrt{-1}$ and $\mathbf{0}$ is a 2×4 matrix with zero elements.

The relation between the complete data \mathbf{x}_k and incomplete data \mathbf{r} is given by

$$\mathbf{r} = \sum_{k=1}^K \mathbf{x}_k = \sum_{k=1}^K (\mathbf{G}_k \mathbf{b}_k + \mathbf{n}_k) = \sum_{k=1}^K \mathbf{G}_k \mathbf{b}_k + \mathbf{n}. \quad (3.52)$$

Using (3.52) the problem at hand is similar to the signal model treated in 3.2.3. Hence, we can conclude that the E- and M-steps as

$$\text{E-step:} \quad \hat{\mathbf{x}}_k = \mathbf{G}_k \hat{\mathbf{b}}_k^{(n)} + \beta_k \left[\mathbf{r} - \sum_{i=1}^K \mathbf{G}_i \hat{\mathbf{b}}_i^{(n)} \right] \quad (3.53)$$

Tap	Delay (μs)	Power (dB)
1	0.0	0.0
2	0.26	-2.80
3	0.78	-5.97
4	1.042	-11.43
5	1.30	-10.91
6	2.34	-9.35

Table 3.1: Delay and power profile of the ITU pedestrian B channel

Tap	Delay (μs)	Power (dB)
1	0.0	0.0
2	0.260417	-1.92
3	0.520833	-7.31
4	0.781250	-10.39
5	1.041667	-10.89

Table 3.2: Delay and power profile of the ITU vehicular A channel

$$\text{M-step: } \hat{\mathbf{b}}_k^{(n+1)} = \arg \min_{\mathbf{b}_k} \|\hat{\mathbf{x}}_k - \mathbf{G}_k \mathbf{b}_k\|^2 \quad (3.54)$$

By expanding (3.54) we come up to

$$\hat{\mathbf{b}}_k^{(n+1)} = \arg \max_{\mathbf{b}_k} \left[2\text{Re} \left(\mathbf{b}_k^T \mathbf{G}_k^\dagger \hat{\mathbf{x}}_k \right) - \mathbf{b}_k^T \mathbf{G}_k^\dagger \mathbf{G}_k \mathbf{b}_k \right]. \quad (3.55)$$

In case of QPSK modulation this equation has the following form

$$\hat{\mathbf{b}}_k^{(n+1)} = \text{csign} \left(\mathbf{G}_k^\dagger \hat{\mathbf{x}}_k \right) \quad (3.56)$$

By choosing the appropriate initial value and parameter β_k , the algorithm will converge to the local maximum value of the log-likelihood function. A good choice for $\hat{\mathbf{b}}^{(0)}$ is to use the output of the matched filter. Similar to the SISO case, if we set $\beta_k = 0$, Eq. (3.55) loses its iteration and reduces to a matched filter receiver, and by assuming $\beta_k = 1$, Eq. (3.55) is a PIC detector.

3.6 Simulation Results

In this section, we provide computer simulation results to illustrate the performance of the proposed iterative receivers for an STBC WCDMA system. We simulate two downlink scenarios

- 1) the base station is equipped with two transmit antennas and mobile stations have one receive antenna

2) the base station is equipped with two transmit antennas and mobile stations have two receive antennas.

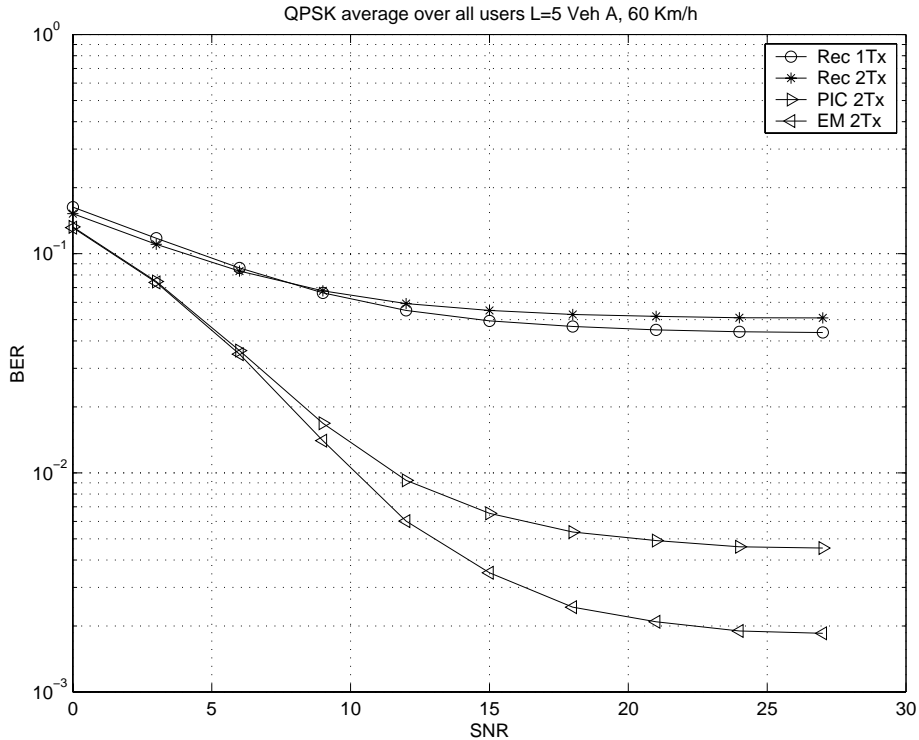


Figure 3.4: BER versus SNR in Veh. A channel, 2-Tx and 1-Rx antennas.

It is assumed that the channel responses are perfectly known and fading is uncorrelated between the transmit-receive antenna pairs. Furthermore, the base station transmits QPSK/16-QAM symbols with equal powers. From the interference cancellation point of view, the equal-power setup is the worst case scenario. The signature waveforms are derived from Walsh sequences of length 16 and the number of users is $K = 15$ (almost fully loaded system). We assume that the total radiated power from two transmit antennas is equal to that of the single transmit antenna. In both PIC and EM receivers, three-stage detectors with a RAKE receiver as the first stage have been used. The best value for parameter β_k in EM was obtained experimentally

as stated in the previous section. We found the best values for β_k 's as $\beta_k = 0.8$ and $\beta_k = 0.9$ for one-receive and two-receive antenna scenarios, respectively.

The simulations were done for the ITU pedestrian B and vehicular A channel models. These channel models have been summarized in Tables 3.1 and 3.2.

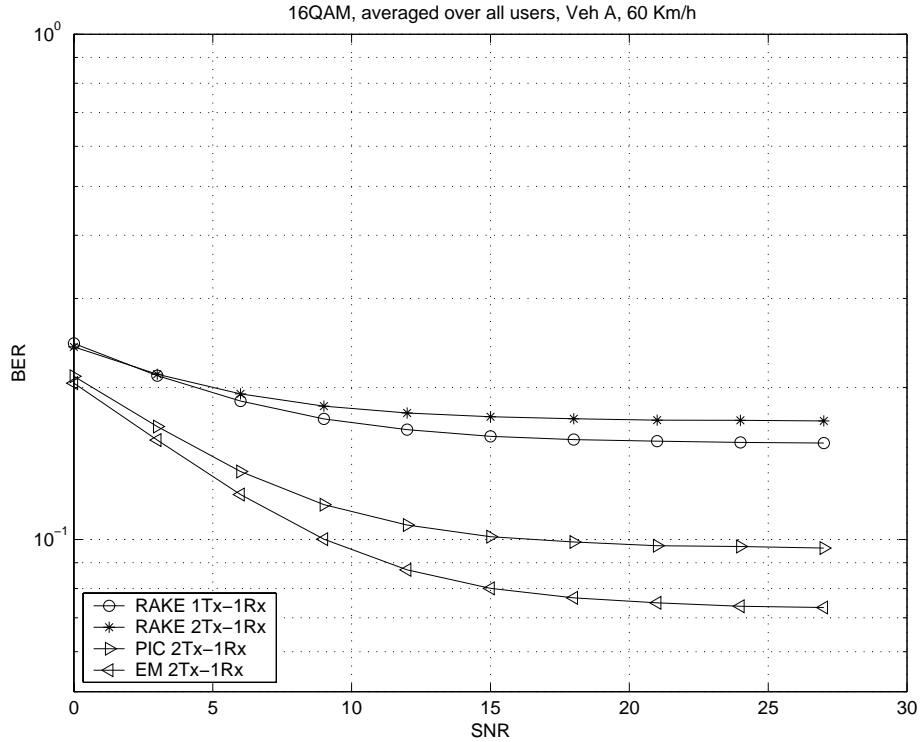


Figure 3.5: BER versus SNR in Veh. A channel, 2-Tx and 1-Rx antennas.

Fig. 3.4 shows the simulation results for the first downlink scenario and the case with ITU vehicular (Veh.) A channels (60 km/h) and QPSK modulation. From the figure we can see an improvement for EM-based MUD compared to the PIC detector; while, PIC itself provides some performance gains over the RAKE receiver. We also notice that the two-transmit antenna RAKE receiver does not necessarily have a better performance than that of a single-transmit antenna in Veh. A channels. Fig. 3.5 includes the simulation results with the same condition as in the previous figure

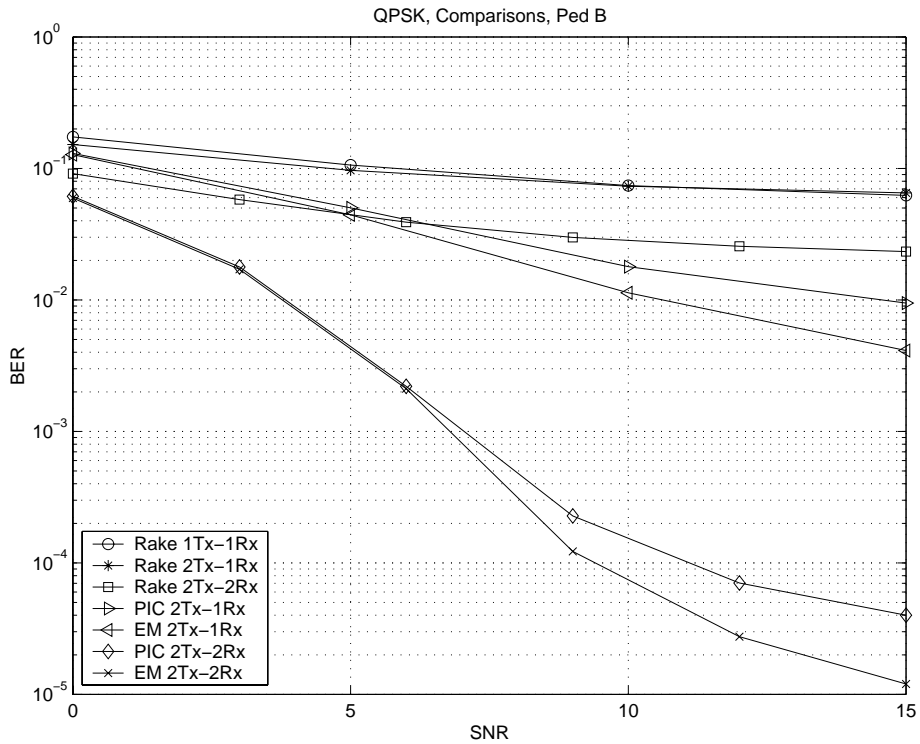


Figure 3.6: BER versus SNR in Ped. B channel (3 km/h).

except that the modulation is 16QAM. In case of 16QAM, we see the high BER for all proposed receivers. However, we notice some improvement using PIC and EM algorithms.

Figs. 3.6 and 3.7 illustrate the performance results for both downlink scenarios for ITU pedestrian B channels (3 km/h), and QPSK and 16QAM modulations, respectively. These results confirm the performance advantage of EM-based receiver over RAKE and PIC receivers. Substantial improvement is seen in the performance of EM and PIC receivers by using two receive antennas. We observe that in Fig. 3.7 when $SNR = 5$ (dB) the performance of the RAKE receiver for two receive antennas is equal to that of the EM receiver for one receive antenna. This is an important point from a cellular handset design point of view.

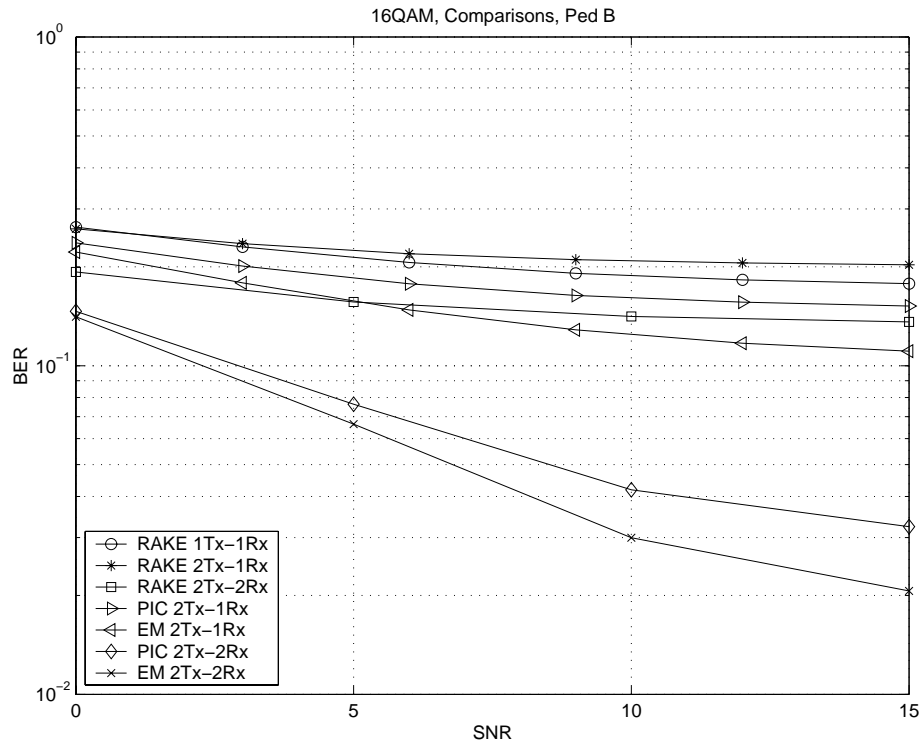


Figure 3.7: BER versus SNR in Ped. B channel (3 km/h).

3.7 Summary

In order to provide higher capacities for future wireless systems, a MIMO system is used. It is also very probable that multiuser detection algorithms will be used to mitigate the effects of interferences, particularly MAI.

In this chapter, we presented the EM algorithm and receivers based on it for both SISO and STBC WCDMA systems. We generated a real linear model for an STBC WCDMA system over multipath fading channels using transformation matrices. We compared the performance of the EM-based receiver to that of PIC and RAKE receivers in different ITU channels. Our analysis and numerical results have shown that

the EM-based receiver provides substantial performance gains over PIC and conventional detectors. In addition, the EM-based receiver is controlled by a parameter, whose value can be suitably chosen so as to cause the receiver to function either as a PIC receiver or as a conventional receiver. Appropriate values of the parameter have been obtained by simulations.

Chapter 4

Multi-Carrier CDMA

4.1 Introduction

Multicarrier technologies are emerging as a considerable force to support the needs of next generations wireless communication systems [4]. Among multicarrier schemes OFDM has gained a lot of attention lately [9]. In OFDM, a single high-speed data stream is transmitted over a number of lower rate subcarriers which makes the system robust against multipath fading and intersymbol interference, because the symbol duration increases for the lower-rate parallel subcarriers.

In the previous chapter we briefly introduced the CDMA technique. The attempt to combine the benefits of CDMA and OFDM gave birth to the idea of MC-CDMA in early 90's. Different variations of combination of CDMA and OFDM are known under acronyms MC-CDMA [7, 16, 80], MC-DS-CDMA (multi-carrier direct sequence CDMA) [12], and MT-CDMA (multitone CDMA) [70]. In this chapter, the MC-CDMA technique is studied. The MC-CDMA system we consider in this thesis is the one where a signal is spread and then converted into parallel data streams each is transmitted over a different subcarriers [7, 16, 26, 75, 80].

Although it is believed that a type of OFDM or MC-CDMA will be the choice

for next generations of mobile systems, there are some barriers that need to be conquered. If a MC-CDMA signal is transmitted through a frequency selective multipath fading channel, all subcarriers have different amplitude levels and phase shifts. This results in loss of orthogonality among users. Furthermore, at high mobile speeds the orthogonality of subcarriers is lost due to Doppler spreads which cause intercarrier interference (ICI). Therefore, we need advanced receivers to overcome such problems.

In this chapter, we first give an overview of an OFDM system. Then the system model for the proposed SISO MC-CDMA is explained. The channel estimation based on least squares (LS) algorithm and used in the receiver architecture is described. Then we explain the proposed receivers, which are based on the MRC, MMSE, PIC and EM algorithms. The Doppler effects on the performance of the proposed receiver algorithms are studied. We perform the complete complexity analysis for all receiver blocks of an SISO MC-CDMA system. Due to the benefit of using a MIMO system as was explained in Chapter 2 and also the simplicity of decoding for space-time block coding technique, we study the STBC MC-CDMA system. We propose the same receiver algorithms used in SISO MC-CDMA in the STBC MC-CDMA. Numerical results for both cases SISO and STBC are provided. We also study the effects of frequency interleaving on the performance of the proposed receiver algorithms.

4.2 OFDM

The main idea behind multicarrier modulation is to combine multiple low data rate carriers by a transmitter to form a composite high data rate transmission. In a parallel transmission system several sequential streams of data are transmitted simultaneously. In a classical parallel transmission system, the available spectrum is divided into several non-overlapping frequency subchannels. Each subchannel is modulated with a separate symbol and, then, the subchannels are frequency multiplexed.

The main advantage of the parallel approach is that it increases the symbol time

by modulating the symbols into narrow subchannels. Therefore, fading is spread out over many symbols. This randomizes burst errors caused by fading, so that not all adjacent symbols are completely destroyed.

Such parallel data transmission techniques have been previously used during the early 1960's in several high frequency military communication systems such as the KINEPLEX, ANDEFT and KATHRYN ([9] and references therein).

When there is a sufficient bandwidth available for data transmission, a classical parallel system can be used where the entire bandwidth available is divided into narrow subchannels and data can be modulated into each of these subchannels. In such a system there is usually sufficient guard space between adjacent subchannels to isolate them at the receiver using conventional filters. A much more efficient use of the bandwidth is possible if the spectra of individual subchannels are permitted to overlap. By allowing the subcarrier tones to be separated by the reciprocal of the symbol duration, independent separation of the frequency multiplexed tones is possible. This ensures that the spectra of individual subchannels are zeros at other subcarrier frequencies. This is the fundamental concept of OFDM. Fig. 4.1 shows the basic OFDM system [9]. The N serial data elements are spaced by $\Delta t = 1/f_s$ where f_s is the symbol rate. These N serial data elements modulate N subcarrier frequencies, which are then frequency division multiplexed. The symbol interval T has been increased to $N\Delta t$, which provides robustness to the delay spread impairments. The subcarrier frequencies are spaced by multiples of $1/T$ so that the subchannels are orthogonal over a symbol duration (in the absence of channel distortion) [9].

The main objections of the system in Fig 4.1 are the complexity, the possibility of severe mutual interference among the subchannels, and the accurate cut-off frequencies for filters. The complexity can be greatly reduced using the Discrete Fourier Transform (DFT) to implement the modulation process. The DFT can in turn be implemented using a Fast Fourier Transform (FFT) algorithm particularly when N , the number of subcarriers, is large. Fig 4.2 demonstrates an OFDM system implemented

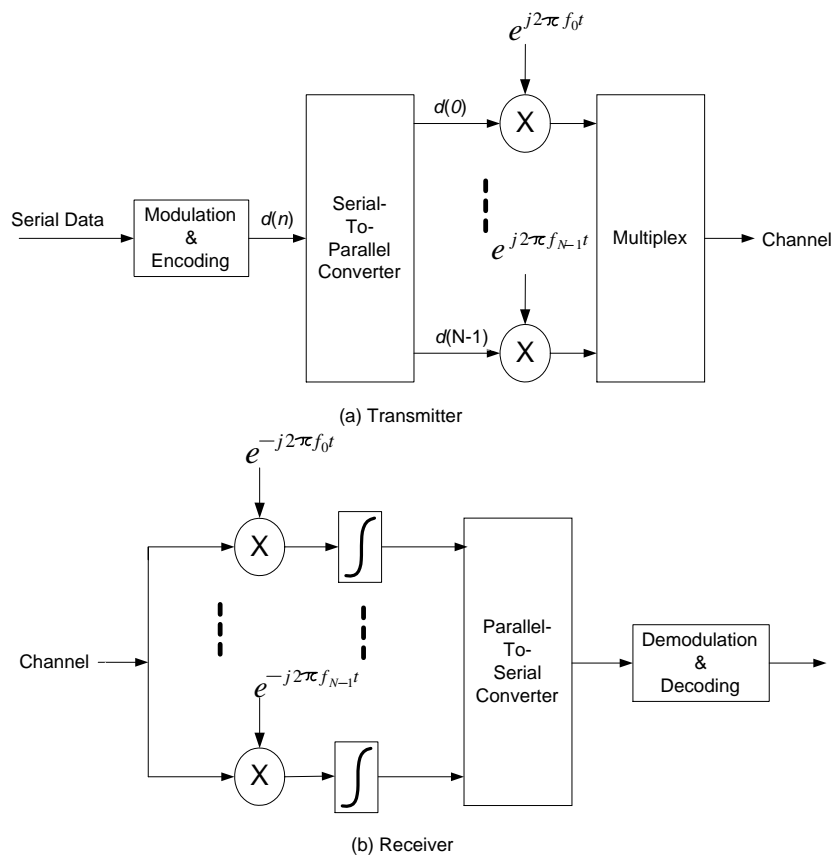


Figure 4.1: Basic OFDM System.

using FFT [9].

4.2.1 Cyclic Prefix

One of the important developments of the OFDM system was due to Peled and Ruiz in 1980 [57], who introduced the concept of the cyclic prefix (CP). A CP is a cyclic extension of the OFDM symbol. This effectively simulates a channel performing circular convolution and if it is larger than the maximum delay spread it ensures orthogonality of subcarriers over multipath fading channels. Adding cyclic prefix

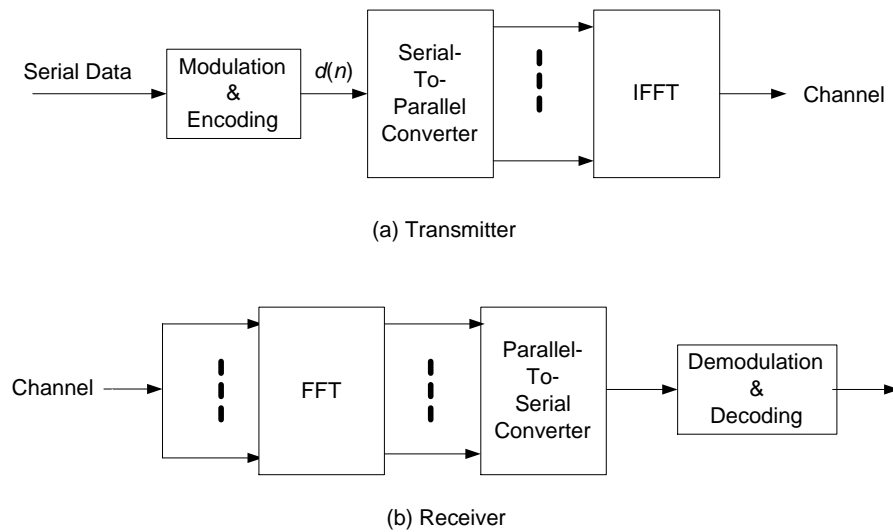


Figure 4.2: OFDM System Implemented using IFFT/FFT.

results in an increased chip rate (larger bandwidth) and introduces an energy loss proportional to the length of the CP.

4.2.2 Zero Padding

It is also proposed to replace the generally non-zero CP by zero padding (ZP) [53]. Specifically, in each block of the transmission, zero symbols are appended after the IFFT operation. If the number of zero symbols equals the CP length, then zero-padded OFDM (ZP-OFDM) and cyclic prefix OFDM (CP-OFDM) transmissions have the same spectral efficiency. The advantage of using ZP is avoiding bandwidth and energy consumptions. However, the price paid is a somewhat increased receiver complexity [53].

4.3 SISO MC-CDMA System Model

OFDM scheme was introduced in the previous section and CDMA was explained in chapter 3. The combination of OFDM and CDMA introduces the MC-CDMA. The baseband model for MC-CDMA system is shown in Figure 4.3. The modulated data symbols are spread by means of Walsh-Hadamard codes and summed up together. The chip sequences are interleaved. The interleaving module performs block interleaving operation over the spread signal. Pilot symbols are inserted uniformly into the interleaved signal. These pilot symbols are used for channel estimation purposes as it is explained in Section 4.4. After pilot insertion, the signal is scrambled and sent to the inverse discrete Fourier transform (IDFT) block. A cyclic prefix (CP) of length equal to at least the channel memory is inserted in each output block that comes from IDFT to prevent interblock interference (IBI). The transmitted signal goes through the multipath fading channel. At the receiver, the cyclic prefix is removed first, then the signal is passed through a discrete Fourier transform (DFT) block. The output of the DFT block is further de-scrambled and de-interleaved for channel estimation and information data detection purposes.

Now, let us consider a MC-CDMA downlink transmission with K users. Each user transmits $N_s - 1$ symbols over different frequency bins. If the spreading code length, the number of subcarriers and the number of pilots are assumed to be N , M , and N , respectively, then for each transmitted block we have $M = N \cdot N_s$. The received signal after DFT can be expressed in matrix notation as

$$\mathbf{r} = \mathbf{F}\mathbf{H}\mathbf{F}^{-1}\mathbf{C}\mathbf{S}\mathbf{b} + \mathbf{n} \quad (4.1)$$

where \mathbf{b} is users' symbols vector, \mathbf{S} is the spreading code matrix for all users, \mathbf{C} is the scrambling code matrix, \mathbf{H} is the channel matrix, \mathbf{F} and \mathbf{F}^{-1} are the DFT and IDFT matrices, respectively. The standard M -dimensional IDFT matrix has the form

$$\mathbf{F}^{-1}(p, q) = 1/\sqrt{M}e^{j(2\pi/M)pq} \quad 0 \leq p, q \leq M - 1. \quad (4.2)$$

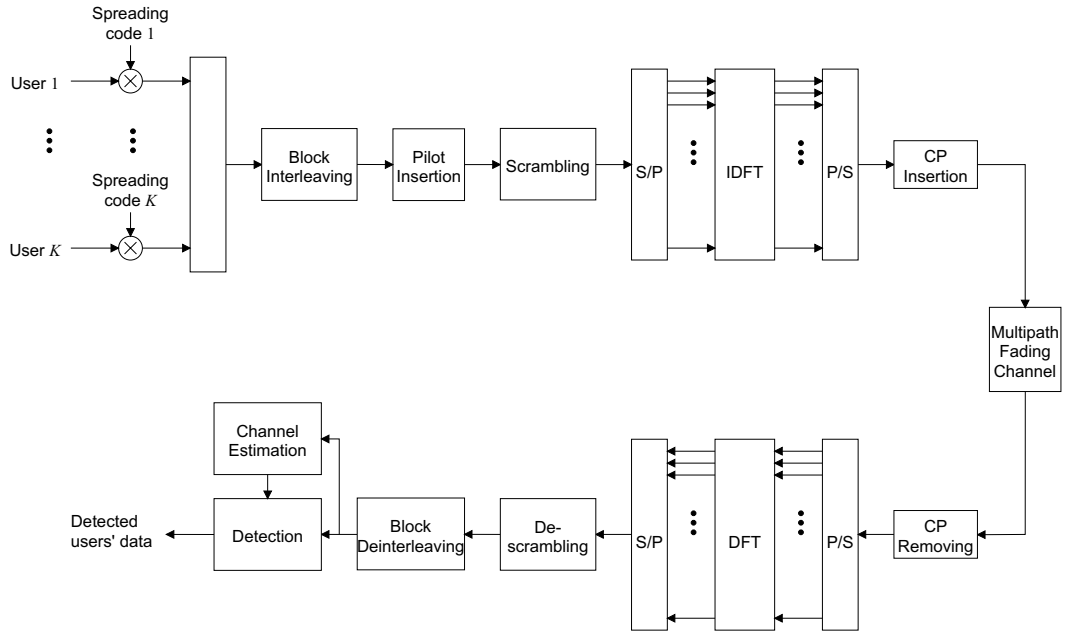


Figure 4.3: Baseband model for the MC-CDMA system.

We assume that a cyclic prefix of length equal to the channel memory is inserted in each input block to eliminate interblock interference. The cyclic prefix serves as a guard interval between blocks when we have channel time variation within a transmission block. However, when the channel impulse response is time invariant over the block \mathbf{H} becomes a block-circulant matrix.

We can write (4.1) in a compact form as

$$\mathbf{r} = \mathbf{GCSb} + \mathbf{n} \quad (4.3)$$

and

$$\mathbf{r} = \mathbf{Ub} + \mathbf{n} \quad (4.4)$$

where $\mathbf{G} = \mathbf{FHF}^{-1}$ and $\mathbf{U} = \mathbf{GCS}$.

4.4 Channel Estimation

In this section, the channel estimator is derived in the MC-CDMA system. We apply the least squares (LS) channel estimation algorithm presented in [33]. As proposed in [33], we use the comb-type pilot arrangement where pilot signals are uniformly distributed within each MC-CDMA block. In other words, pilot signals are equispaced in each transmitted block. Since only some subcarriers contain the pilot signal, the channel response of non-pilot subcarriers will be estimated by interpolating neighboring pilot sub-channels.

For comb-type pilot subcarrier arrangement, the N_p pilot symbols $b_p(i), i = 0, 1, \dots, N_p - 1$ are uniformly (equispaced) inserted into \mathbf{b} . This means that the first subcarrier of each group of $L = M/N_p$ is used to transmit the pilot signal. The transmitted MC-CDMA on the m th subcarrier is

$$b(m) = b(iL + l) = \begin{cases} b_p(i), & l = 0, \\ \text{Users's data}, & l = 1, 2, \dots, L - 1 \end{cases} \quad (4.5)$$

where $m = 0, 1, \dots, M - 1$. The pilot symbols can be either equal complex values or randomly generated data. Now, we assume that the received pilot symbols are collected in the vector \mathbf{r}_p and if the pilot symbols are denoted by \mathbf{b}_p , the estimate of pilot signals by using least square criterion is given by

$$\mathbf{h}_p = \left[\frac{r_p(0)}{b_p(0)} \quad \frac{r_p(1)}{b_p(1)} \quad \dots \quad \frac{r_p(N_p-1)}{b_p(N_p-1)} \right]^T \quad (4.6)$$

After the estimation of the channel responses of the pilot tones, the channel responses of data tones can be interpolated according to the adjacent pilot tones. In our studies, we have used the linear interpolation algorithm. In linear interpolation, two successive pilot signals are used to determine the channel response for data subcarriers that are located in between the pilots. After the interpolation we have the estimated channel vector \mathbf{H}_p with a total length of M (number of subcarriers). Therefore, the

estimated \mathbf{G} after channel estimation in (4.3) is a diagonal matrix with \mathbf{H}_p vector as diagonal elements

$$\hat{\mathbf{G}} = \text{diag}(\mathbf{H}_p). \quad (4.7)$$

And the estimated \mathbf{U} in (4.4) is simply $\hat{\mathbf{U}} = \hat{\mathbf{G}}\mathbf{C}\mathbf{S}$.

4.5 Multiuser Detection for SISO MC-CDMA

Given the estimated channel and $\hat{\mathbf{U}}$ in (4.4), we can employ the following detection schemes.

4.5.1 Maximum Ratio Combining (MRC)

The simplest detection scheme is the MRC detector based on the conventional matched filter. The output of the MRC receiver is given as

$$\mathbf{y}_{MRC} = \hat{\mathbf{U}}^\dagger \mathbf{r}. \quad (4.8)$$

The MRC scheme is not the optimal solution. Detected symbols for QPSK modulation are simply

$$\hat{\mathbf{b}}_{MRC} = \text{csign}(\mathbf{y}_{MRC}) \quad (4.9)$$

where *csign* is defined as $\text{csign}(a + jb) = \text{sign}(a) + j\text{sign}(b)$.

4.5.2 Minimum Mean Square Error (MMSE)

The MMSE detector is a Bayesian approach to parameter estimation [44]. The output of the MMSE detector is given by

$$\mathbf{y}_{MMSE} = \hat{\mathbf{U}}^\dagger \left(\hat{\mathbf{U}}\hat{\mathbf{U}}^\dagger + \sigma^2\mathbf{I}_M \right)^{-1} \mathbf{r} \quad (4.10)$$

where \mathbf{I}_M is an $M \times M$ identity matrix. The MMSE detector requires the knowledge of the noise power σ^2 . Although in (4.10) we are dealing with matrix inversion, the implementation of the MMSE receiver in MC-CDMA is not that complex since we need to invert a diagonal matrix. The detected symbols for QPSK modulation are

$$\hat{\mathbf{b}}_{MMSE} = csign(\mathbf{y}_{MMSE}). \quad (4.11)$$

4.5.3 EM-based Detection and PIC

The Expectation-Maximization algorithm was introduced in the previous chapter. It basically provides an iterative approach to maximum likelihood-based parameter estimation when direct maximization of the likelihood function may not be feasible. In order to apply the EM algorithm we first define a complete data set \mathbf{x}_k as

$$\mathbf{x}_k = \mathbf{U}_k \mathbf{b}_k + \mathbf{n}_k \quad k = 1, \dots, K \quad (4.12)$$

where \mathbf{b}_k is a vector of the k th user's symbols, \mathbf{n}_k 's are white Gaussian noise which are obtained by arbitrarily decomposing the total noise \mathbf{n} into the K components, so that $\sum_{k=1}^K \mathbf{n}_k = \mathbf{n}$. If the covariance matrices of \mathbf{n}_k and \mathbf{n} are \mathbf{Q}_k and \mathbf{Q} , respectively, then $\mathbf{Q}_k = \beta_k \mathbf{Q}$ in which β_k 's are arbitrary real valued scalars satisfying

$$\sum_{k=1}^K \beta_k = 1 \quad \beta_k \geq 0 \quad (4.13)$$

The relation between the complete data \mathbf{x}_k and incomplete data \mathbf{r} is given by

$$\mathbf{r} = \sum_{k=1}^K \mathbf{x}_k = \sum_{k=1}^K (\mathbf{U}_k \mathbf{b}_k + \mathbf{n}_k) = \sum_{k=1}^K \mathbf{U}_k \mathbf{b}_k + \mathbf{n}. \quad (4.14)$$

With this and based on the formulation presented in the previous chapter, the E- and M-steps are

$$\text{E-step:} \quad \hat{\mathbf{x}}_k = \mathbf{U}_k \hat{\mathbf{b}}_k^{(n)} + \beta_k \left[\mathbf{r} - \sum_{i=1}^K \mathbf{U}_i \hat{\mathbf{b}}_i^{(n)} \right] \quad (4.15)$$

$$\text{M-step:} \quad \hat{\mathbf{b}}_k^{(n+1)} = \arg \min_{\mathbf{b}_k} \|\hat{\mathbf{x}}_k - \mathbf{U}_k \mathbf{b}_k\|^2 \quad (4.16)$$

where $\|\cdot\|^2$ denotes the squared Euclidean distance. For QPSK modulation the solution is

$$\hat{\mathbf{b}}_k^{(n+1)} = csign(\mathbf{U}_k^\dagger \hat{\mathbf{x}}_k). \quad (4.17)$$

This equation provides an iterative method to detect symbols of the users. By choosing an appropriate initial value and parameter β_k 's, the algorithm converges to a stationary point of the log-likelihood function where each iteration cycle increases the likelihood. One of the choices for the initial estimate $\hat{\mathbf{b}}_k^{(0)}$ is to use the output of the MRC receiver which is not necessarily a good alternative due to the poor performance of the MRC receiver. Since in the MC-CDMA the MMSE solution is not that complex and has much better performance than that of MRC, a better choice for initial values is to use the output of the MMSE receiver. Parameter β_k has a critical role in the EM-based algorithm. By setting $\beta_k = 0$ we see that (4.17) loses its iteration and reduces to a MRC or MMSE receiver (depending on the chosen receiver for the initial value), and by assuming $\beta_k = 1$, (4.17) is exactly a PIC detector [71]. In our study, β_k 's are initially found by experiments for the best performance.

4.6 Simulation Results for SISO MC-CDMA System

In this section, we provide computer simulation results to illustrate the performance of the proposed channel estimation and signal detection algorithms for SISO MC-CDMA. The simulation results for an OFDM system is also provided. The performance is measured as uncoded bit error rate (BER) versus signal to noise ratio (SNR). A downlink scenario is assumed where a base station transmits QPSK symbols with equal powers. The signature waveforms are derived from Walsh sequences of length 32 and the number of users is $K = 32$ (a fully-loaded system). The total number of subcarriers and pilots are 512 and 32, respectively. Pilots are uniformly inserted into

transmitted blocks as it was explained in Section 4.4. In both PIC and EM receivers, three-stage detectors with a MMSE receiver as the first stage have been used. The best value for parameter β_k in EM was obtained by experiments as stated in the previous section. We found the best values for β_k 's as $\beta_k = 0.8$. Simulations were done for the ITU pedestrian B and vehicular A channel models. The delay and power profiles for these channels have been summarized in Tables 3.1 and 3.2. Fig. 4.4

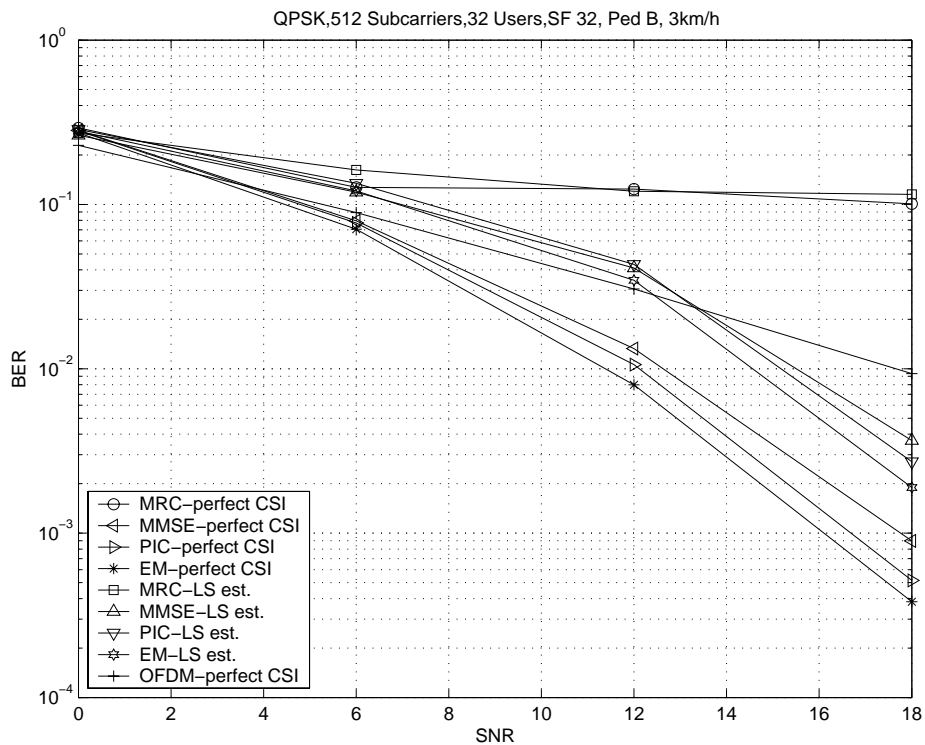


Figure 4.4: BER versus SNR, Ped. B channels.

shows the simulation results for the case with ITU pedestrian B channel (3 km/h). This figure includes the performance results of the detection algorithms for the case when perfect channel state information (CSI) exists at the receiver as well as for the case when channels are estimated at the receiver using the proposed algorithm. As it is expected and seen from the figure, in general, channel estimation degrades the

performance of detection algorithms compared to the case when perfect CSI exists at the receiver. The MMSE algorithm improves significantly the performance of the receiver compared to that of the MRC receiver. We can further improve the performance of the MMSE receiver by using PIC and EM-based detector as it is seen from the same figure. For an OFDM system we have implemented an MMSE receiver. The superiority of a MC-CDMA system compared to an OFDM system is seen in terms of improvement in BER. The degradation in performance of the receiver in the MC-CDMA system due to the channel estimator is noticeable when MMSE, PIC, and EM are implemented.

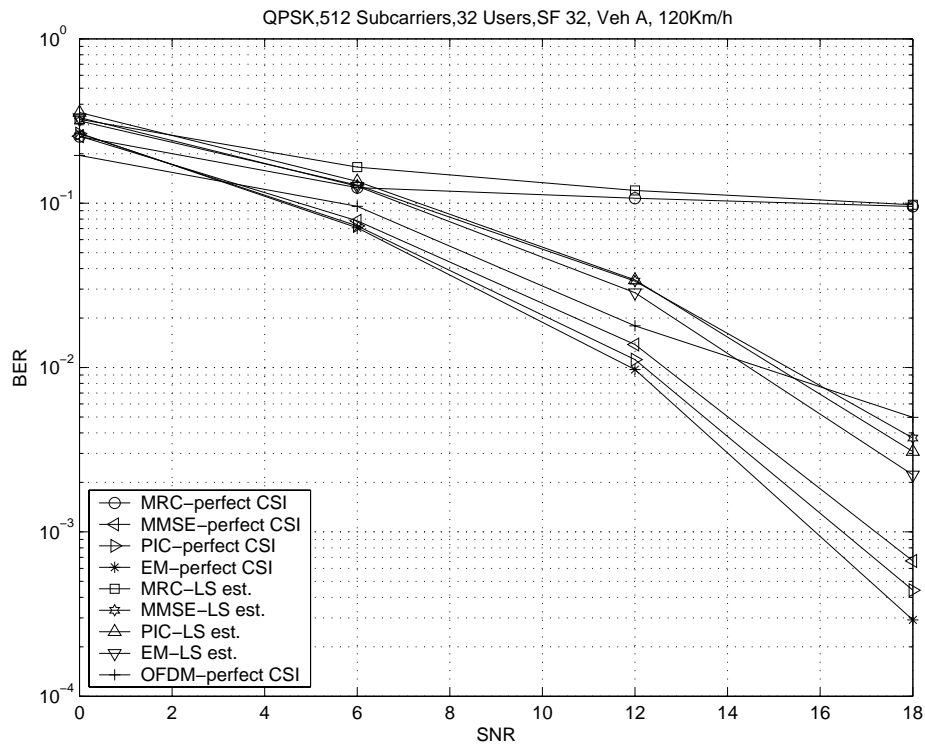


Figure 4.5: BER versus SNR, Veh. A channel.

Fig. 4.5 illustrates the performance results for ITU vehicular A channels (120 km/h). These results confirm the performance advantage of advanced receivers such

as MMSE, PIC and EM-based receivers. As can be seen, in this scenario, with MMSE receiver we achieve much better performance than that with MRC. Further improvements can be gained by using PIC and EM detectors.

4.7 Doppler Effects

In OFDM/MC-CDMA systems, each waveform is located around a particular subcarrier frequency and the bandwidth is small enough so that each waveform experiences frequency flat fading when the received signal passes through a moderately frequency selective channel. Inverse FFT is implemented for transmitting information bits in order to maintain the orthogonality of the signal waveforms. However, OFDM/MC-CDMA reception over channels with Doppler spread and corresponding time variations corrupts the orthogonality of the OFDM/MC-CDMA subcarrier waveform. In other words, Inter-Carrier Interference (ICI) occurs since signal components from one subcarrier cause interference to neighboring subcarriers. In this section, we briefly address the performance of the MC-CDMA system with Doppler effects. The performance of our channel estimation and signal detection algorithms (MRC, MMSE, PIC and EM) are examined in fast-fading channels.

Doppler shift is the frequency shift of the received signal due to its relative motion. It is proportional to the speed of the mobile terminal. The Doppler shift in a multipath propagation environment spreads the bandwidth of the multipath waves within the range of $f_c \pm f_D$, where f_D is the maximum Doppler shift given by

$$f_D = \frac{vf_c}{c} \quad (4.18)$$

where c is the speed of light.

In Figure 4.6, we have considered three different scenarios in downlink for a SISO MC-CDMA system. All these scenarios have the same channel model (Vehicular A), but with different speeds for the mobile users. In these simulation scenarios, CSI are

not known at the receiver and LS channel estimation is used in the receiver. A speed of 30 km/h is considered low mobility; 120 km/h high mobility, and 500 km/h very high mobility. These speeds at $f_c = 2.5 \times 10^9$ Hz are equal to the maximum Doppler shifts of

- velocity = 30 km/h $\Rightarrow f_D = (\text{velocity}) \cdot f_c / 3.6 / 3 \times 10^8 = 69$ Hz,
- velocity = 120 km/h $\Rightarrow f_D = (\text{velocity}) \cdot f_c / 3.6 / 3 \times 10^8 = 278$ Hz,
- velocity = 500 km/h $\Rightarrow f_D = (\text{velocity}) \cdot f_c / 3.6 / 3 \times 10^8 = 1157$ Hz.

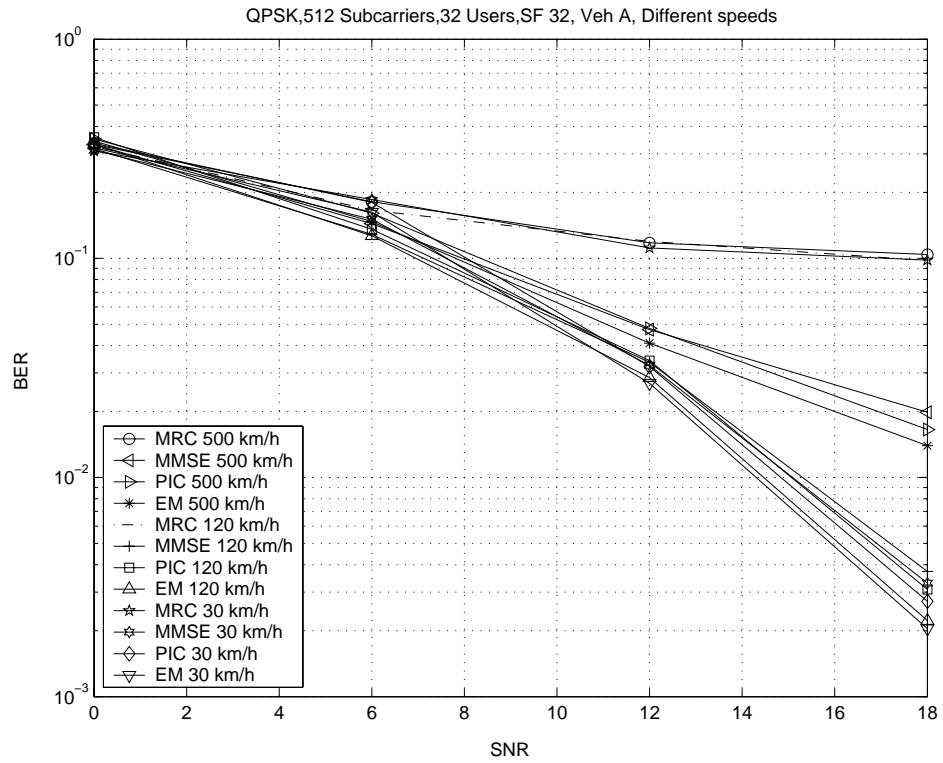


Figure 4.6: Doppler effects, Veh. A channels.

The system bandwidth in our simulation is 5 MHz and the number of subcarriers is 512. Therefore, the carrier spacing is 9767 Hz. From the Fig. 4.6, it is seen

that MRC has basically the same performance for all speeds. As for the advanced algorithms (MMSE, PIC and EM), degradation in the performance of the receivers is observed by increasing the speed of the mobile users. As a matter of fact, for speeds of 30 and 120 km/h, we see minor degradation in performance gains. This is due to the fact that the corresponding Doppler shifts of these speeds are small compare to the carrier spacing. As soon as the Doppler shift is comparable to carrier spacing we see significant drop in the performance of the advanced algorithm.

4.8 Complexity Analysis for the SISO MC-CDMA

This section provides computational complexity analysis for various MC-CDMA receiver structures studied in the previous sections.

4.8.1 Background and Assumptions

Complexity is estimated by the required number of real-valued Addition-Equivalent-Operations (AEOs) and the number of real-valued multiplication operations (MULTs). For a more tangible result, the operation counts are scaled to operations per second. Table 4.1 shows how the high-level operations are mapped to the used complexity measures. In calculating the complexity of the algorithms, system parameters are assumed as they are presented in Table 4.2. In addition to the assumed system parameters in Table 4.2, the following assumptions are considered

- two's complement number representation
- noise variance known at the receiver
- channel estimates are available
- division and multiplication operations are equally complex
- QPSK modulation is used

Table 4.1: The used mapping from higher-level operations to the two used complexity measures

High-level operation C : Complex number R : Real number	Real AOE's	Real MULT's
$\{R\} + \{R\}$	1	0
$\{R\} \times \{R\}$	0	1
$\{R\} \times \{\pm 1\}$	1	0
$\{R\} \times \{\pm 1 \pm j\}$	2	0
$\{R\}/\{R\}$	0	1
$\{C\} + \{C\}$	2	0
$\{C\} \times \{C\}$	2	4
$\{C\} \times \{\text{constant } C\}$	3	3
$\{C\} \times \{R\}$	0	2
$\{C\} \times \{\pm 1 \pm j\}$	6	0
$\{C\} \times \{\pm 1\}$	2	0
$\{C\}/\{R\}$	0	2
$\{C\}^*$	1	0
$ \{C\} ^2$	1	2
$\{C\}/\{C\}$	4	8
$\{C\}/\{\pm 1 \pm j\}$	4	0
$\{\pm 1\}/\{\pm 1 \pm j\}$	1	0

4.8.2 Complexity of LS Channel Estimation

The channel estimation algorithm was explained in Section 4.4. We assume the pilot symbols are complex numbers with the format of $\{\pm 1 \pm j\}$ and we consider linear interpolation as it is explained in the channel estimation section. The linear interpolation process is shown in Fig 4.7. Based on these assumptions the complexity of the LS channel estimation is presented in Table 4.3.

4.8.3 Complexity of Common Parts

The complexity of the receiver parts that are commonly used in different receiver structure is presented here. The operation counts for Decimation-In-Frequency FFT

Table 4.2: System Parameters

N : Number of subcarriers (FFT size)	512
P : Number of pilots	32
SF : Spreading factor	32
K : Number of users	32
Bandwidth	5 MHz
OFDM symbol rate	$5/512$ MHz = 9.77 KHz
M : Number of PIC and EM iterations	2

Table 4.3: The operation counts for the LS channel estimation

High-level operation	No. of high-level operations per symbol	Mapped to Real AOE's	Mapped to Real MULTs	AOE MIPS	MULT MIPS
$\{C\}/\{\pm 1 \pm j\}$	$P = 32$	128	0	1	0
Linear interpolation $\{C\} + \{C\}$	$N = 512$	1024	0	10	0
TOTAL		1152	0	11	0

are summarized in Table 4.4. The de-interleaving has certainly a non-zero complexity, but it does not contain any AEOs or multiplication operations in the data path and thus its complexity measure in this analysis is considered to be zero.

Table 4.4: The operation counts for the Decimation-In-Frequency (DIF) FFT

High-level operation	No. of high-level operations per symbol	Mapped to Real AOE's	Mapped to Real MULTs	AOE MIPS	MULT MIPS
$\{C\} + \{C\}$	$N \log_2 N$ = 4608	9216	0	90	0
$\{C\} \times \{\text{constant } C\}$	$\frac{N}{2} ((\log_2 N) - 1)$ = 2048	6144	6144	60	60
TOTAL		15360	6144	150	60

The de-scrambling operation counts are included in Table 4.5. The de-spreading operation is assumed to be done independently for each code, i.e., the Walsh-Hadamard

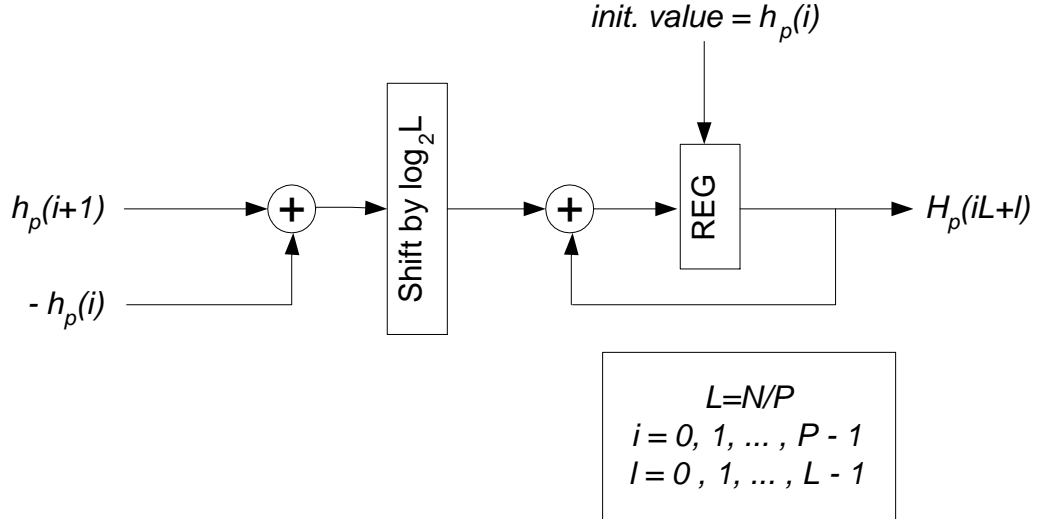


Figure 4.7: Linear interpolation for channel estimation.

transform is not performed simultaneously for the whole set of codes. The operation counts for de-spreading are summarized in Table 4.6.

Table 4.5: The operation counts for the de-scrambling operation

High-level operation	No. of high-level operations per symbol	Mapped to Real AOE	Mapped to Real MULT	AOE MIPS	MULT MIPS
$\{C\} \times \{\pm 1 \pm j\}$	$N = 512$	3072	0	30	0
TOTAL		3072	0	30	0

4.8.4 Complexity of MRC

The MRC receiver was described in Section 4.5.1. In MRC, the operation $R_n \hat{H}_n^*$ is performed on each element of the received complex vector, where \hat{H}_n is the estimated channel coefficient for subcarrier n . The resulting complexity measures are provided

Table 4.6: The operation counts for the de-spreading operation

High-level operation	No. of high-level operations per symbol	Mapped to Real AOE	Mapped to Real MULTs	AOE MIPS	MULT MIPS
$\{C\} \times \{\pm 1\}$	$KN = 16384$	32768	0	320	0
$\{C\} + \{C\}$	$(SF - 1)K \left(\frac{N}{SF}\right) = 15872$	31744	0	310	0
TOTAL		64512	0	630	0

in Table 4.7.

Table 4.7: The operation counts for the MRC

High-level operation	No. of high-level operations per symbol	Mapped to Real AOE	Mapped to Real MULTs	AOE MIPS	MULT MIPS
$\{C\}^*$	$N = 512$	512	0	5	0
$\{C\} \times \{C\}$	$N = 512$	1024	2048	10	20
TOTAL		1536	2048	15	20

4.8.5 Complexity of MMSE

The MMSE receiver was covered in Section 4.5.2. In MMSE, the following operation is performed to each frequency-domain complex symbol R_n

$$\frac{R_n \hat{H}_n^*}{\hat{H}_n^* \hat{H}_n + \sigma^2}$$

where \hat{H}_n is the estimated channel coefficient for subcarrier n and σ^2 is the noise variance. The complexity measures are provided in Table 4.8.

4.8.6 Complexity of PIC

The PIC algorithm for MC-CDMA was explained in Section 4.5.3. The initial estimates for the PIC receiver are assumed to be obtained from the MRC receiver.

Table 4.8: The operation counts for the MMSE

High-level operation	No. of high-level operations per symbol	Mapped to Real AOE	Mapped to Real MULTs	AOE MIPS	MULT MIPS
$\{C\}^*$	$N = 512$	512	0	5	0
$\{C\} \times \{C\}$	$N = 512$	1024	2048	10	20
$\{C\}/\{R\}$	$N = 512$	0	1024	0	10
$ \{C\} ^2$	$N = 512$	512	1024	5	10
$\{R\} + \{R\}$	$N = 512$	512	0	5	0
TOTAL		2560	4096	25	40

Thus, the needed MRC operations are included into the complexity measures. Two PIC-iterations are assumed on top of the initial estimates. Using the same notation as in [26], one PIC-iteration is as follows

$$\hat{\mathbf{b}}_k^{(m+1)} = \text{csign} \left(\hat{\mathbf{U}}_k^\dagger \left(\hat{\mathbf{U}}_k \hat{\mathbf{b}}_k^{(m)} + \left(\mathbf{r} - \sum_{k'=1}^K \hat{\mathbf{U}}_{k'} \hat{\mathbf{b}}_{k'}^{(m)} \right) \right) \right)$$

where $\hat{\mathbf{U}} = \hat{\mathbf{G}}\mathbf{C}\mathbf{S}$.

Further algebraic manipulations leads to

$$\begin{aligned} \hat{\mathbf{b}}_k^{(m+1)} &= \text{csign} \left(\mathbf{S}_k^\dagger \mathbf{C}^\dagger \hat{\mathbf{G}}^\dagger \left(\hat{\mathbf{G}}\mathbf{C}\mathbf{S}_k \hat{\mathbf{b}}_k^{(m)} + \left(\mathbf{r} - \sum_{k'=1}^K \hat{\mathbf{G}}\mathbf{C}\mathbf{S}_{k'} \hat{\mathbf{b}}_{k'}^{(m)} \right) \right) \right) \\ &= \text{csign} \left(\mathbf{S}_k^\dagger \hat{\mathbf{G}}^\dagger \hat{\mathbf{G}}\mathbf{S}_k \hat{\mathbf{b}}_k^{(m)} + \mathbf{S}_k^\dagger \mathbf{C}^\dagger \hat{\mathbf{G}}^\dagger \mathbf{r} - \sum_{k'=1}^K \mathbf{S}_k^\dagger \hat{\mathbf{G}}^\dagger \hat{\mathbf{G}}\mathbf{S}_{k'} \hat{\mathbf{b}}_{k'}^{(m)} \right) \\ &= \text{csign} \left(\mathbf{S}_k^\dagger \left(\mathbf{D}\mathbf{S}_k \hat{\mathbf{b}}_k^{(m)} + \mathbf{C}^\dagger \hat{\mathbf{G}}^\dagger \mathbf{r} - \sum_{k'=1}^K \mathbf{D}\mathbf{S}_{k'} \hat{\mathbf{b}}_{k'}^{(m)} \right) \right) \end{aligned}$$

where \mathbf{D} is a real diagonal matrix, whose elements are the power of the frequency-domain channel estimates. For instance, for the n 'th subcarrier, the diagonal element is computed as

$$D(n, n) = H_n^* H_n = |H_n|^2 \Leftrightarrow N \times |\{C\}|^2 \text{ per one OFDM - symbol}$$

The computation of \mathbf{D} is not repeated for each PIC-iteration. The term $\mathbf{C}^\dagger \hat{\mathbf{G}}^\dagger \mathbf{r}$ has already been computed while computing the initial MRC-estimates. So, it does

not add any additional computational complexity. The multiplication by \mathbf{S}_k^\dagger performs the de-spreading operation and its complexity is taken from Table 4.6. Part of the complexity stems from computing the code-specific terms

$$\mathbf{D}\mathbf{S}_k \hat{\mathbf{b}}_k^{(m)} \Leftrightarrow N \text{ times } \{R\} \times \{\pm 1 \pm j\} \text{ and } \{\pm 1\} \times \{\pm 1 \pm j\} \text{ per OFDM - symbol}$$

The sum over all k results in $N(K-1)(\{C\} + \{C\})$ -operations. Finally, there are two complex additions per each code and each subcarrier.

Summarizing all the above considerations results in the operation counts for PIC in Table 4.9.

Table 4.9: The operation counts for the PIC with 2 iterations

High-level operation	No. of high-level operations per symbol	Mapped to Real AOE's	Mapped to Real MULT's	AOE MIPS	MULT MIPS
MRC init estimates	see Table 4.7	2560	4096	25	40
$ \{C\} ^2$	$N = 512$	512	1024	5	10
$\{R\} \times \{\pm 1 \pm j\}$	$2N = 1024$ (2-iter. PIC)	2048	0	20	0
$\{\pm 1\} \times \{\pm 1 \pm j\}$	$2N = 1024$ (2-iter. PIC)	1024	0	10	0
$\{C\} + \{C\}$	$2N(K-1)$ $= 31744$	63488	0	620	0
$\{C\} + \{C\}$	$22NK = 32768$	65536	0	640	0
De-spreading	$2 \times$ Table 4.6	129024	0	1260	0
TOTAL		263168	3072	2570	50

4.8.7 Complexity of EM

The EM algorithm based receiver was described in Section 4.5.3. The complexity calculation of EM receiver is similar to that of the PIC receiver except that in the EM algorithm there is an extra multiplication due to the parameter β_k . Therefore, the complexity of the EM algorithm can be summarized as presented in Table 4.10.

Table 4.10: The operation counts for the EM with 2 iterations

High-level operation	No. of high-level operations per symbol	Mapped to Real AOE's	Mapped to Real MULTs	AOE MIPS	MULT MIPS
MRC init estimates	see Table 4.7	2560	4096	25	40
$\{C\}^2$	$N = 512$	512	1024	5	10
$\{R\} \times \{\pm 1 \pm j\}$	$2N = 1024$ (2-iter. PIC)	2048	0	20	0
$\{\pm 1\} \times \{\pm 1 \pm j\}$	$2N = 1024$ (2-iter. PIC)	1024	0	10	0
$\{C\} + \{C\}$	$2N(K - 1)$ $= 31744$	63488	0	620	0
$\{C\} + \{C\}$	$22NK = 32768$	65536	0	640	0
De-spreading	$2 \times$ Table 4.6	129024	0	1260	0
$\{C\} \times \{R\}$	$2N = 1024$	0	2048	0	20
TOTAL		263168	5120	2570	70

4.9 Space-Time Block-Coded MC-CDMA System Model

The orthogonal space-time block coding was explained in Section 2.4.1. As it was described in the same section, Alamouti discovered a simple scheme for transmit diversity based on the space-time block coding [3, 63].

We consider an STBC MC-CDMA. The block diagram for an STBC MC-CDMA system is illustrated in Fig. 4.8. A downlink scenario for an STBC MC-CDMA system with K users, two transmit antennas, one receive antenna and multipath fading channels is considered. The extension to two receive antennas is straightforward. Each user transmits N_s symbols over different frequency bins. If the spreading code length and the number of subcarriers are M and N , respectively, then for each transmitted block we have $M = N \cdot N_s$. It is assumed that the fading processes associated with different transmitter-receiver antenna pairs are uncorrelated. Let us define \mathbf{H}_{11} and \mathbf{H}_{12} as channel matrices from transmit antennas 1 and 2, respectively, to receive

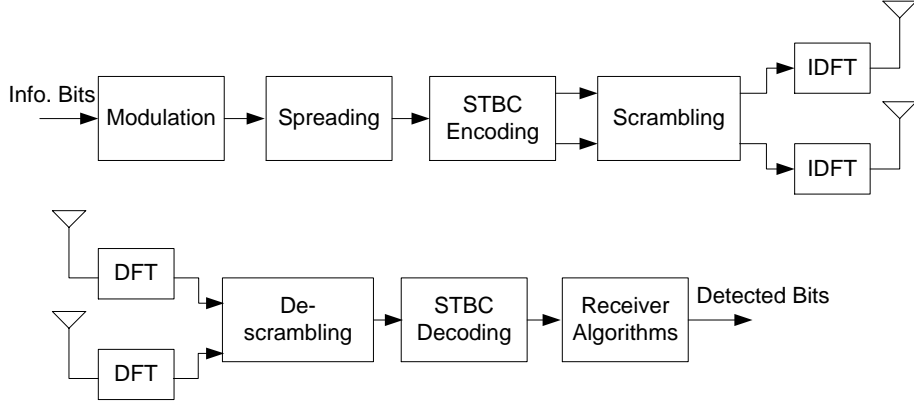


Figure 4.8: Transmitter and receiver structure for an STBC MC-CDMA system.

antenna. The received signal after DFT can be expressed in a matrix notation as [37]

$$\mathbf{r} = \begin{bmatrix} \mathbf{F}\mathbf{H}_{11}\mathbf{F}^{-1}\mathbf{C}\mathbf{S} & \mathbf{F}\mathbf{H}_{12}\mathbf{F}^{-1}\mathbf{C}\mathbf{S} \\ -(\mathbf{F}\mathbf{H}_{12}\mathbf{F}^{-1}\mathbf{C}\mathbf{S})^* & (\mathbf{F}\mathbf{H}_{11}\mathbf{F}^{-1}\mathbf{C}\mathbf{S})^* \end{bmatrix} \mathbf{b} + \mathbf{n} \quad (4.19)$$

where $\mathbf{b} \in \mathbb{C}^{2 \cdot N_s \cdot K \times 1}$ is users' symbols vector, $\mathbf{S} \in \mathbb{R}^{N \cdot N_s \times N_s \cdot K}$ is the spreading code matrix for all users, $\mathbf{C} \in \mathbb{C}^{N \cdot N_s \times N \cdot N_s}$ is the scrambling code matrix, $\mathbf{n} \in \mathbb{C}^{M \times 1}$ is a complex additive white Gaussian noise (AWGN), $\mathbf{F} \in \mathbb{C}^{M \times M}$ and $\mathbf{F}^{-1} \in \mathbb{C}^{M \times M}$ are the DFT and IDFT matrices, respectively. The standard M -dimensional IDFT matrix has the form presented in (4.2).

We can further simplify the above equation to

$$\mathbf{r} = \mathbf{U}\mathbf{b} + \mathbf{n} \quad (4.20)$$

where $\mathbf{U} = \begin{bmatrix} \mathbf{F}\mathbf{H}_{11}\mathbf{F}^{-1}\mathbf{C}\mathbf{S} & \mathbf{F}\mathbf{H}_{12}\mathbf{F}^{-1}\mathbf{C}\mathbf{S} \\ -(\mathbf{F}\mathbf{H}_{12}\mathbf{F}^{-1}\mathbf{C}\mathbf{S})^* & (\mathbf{F}\mathbf{H}_{11}\mathbf{F}^{-1}\mathbf{C}\mathbf{S})^* \end{bmatrix}$.

We also assume that a cyclic prefix of length equal to the delay spread of the channel is inserted in each input block to eliminate interblock interference. When the

channel impulse response is time invariant over the transmission block, $\mathbf{H}_{11} \in C^{M \times M}$ and $\mathbf{H}_{12} \in C^{M \times M}$ become block-circulant matrices.

Considering the linear model for STBC MC-CDMA in (4.20) we can simply implement the same receiver algorithm used in the SISO case. They include MRC, MMSE, PIC and finally EM-based algorithm [37].

4.10 Simulation Results for STBC MC-CDMA System

In this section, we provide simulation results to illustrate the performance of the proposed receivers for an STBC MC-CDMA system in terms of raw bit error rate (BER) versus signal-to-noise (SNR). We simulate two downlink scenarios

- 1) the base station is equipped with two transmit antennas and mobile stations have one receive antenna
- 2) the base station is equipped with two transmit antennas and mobile stations have two receive antennas.

It is assumed that the channel responses are perfectly known at the receiver and fading is uncorrelated between the transmit-receive antenna pairs. Furthermore, the base station transmits QPSK symbols with equal powers. The signature waveforms are derived from Walsh sequences of length 32 and the number of users is $K = 32$ (a fully-loaded system), the bandwidth is 5 MHz and the carrier frequency is 2.56 GHz. The number of subcarriers is 512 which are equally spaced in a 5 MHz bandwidth. Long scrambling codes are used. We assumed that the total radiated power from two transmit antennas is equal to that of a single transmit antenna. In both the PIC and EM receivers, three-stage detectors with a MRC receiver as the first stage have been used. The best value for the parameter β_k in the EM algorithm was obtained by experiments. We found the best values for β_k 's as $\beta_k = 0.8$ for both one-receive

and two-receive antenna scenarios.

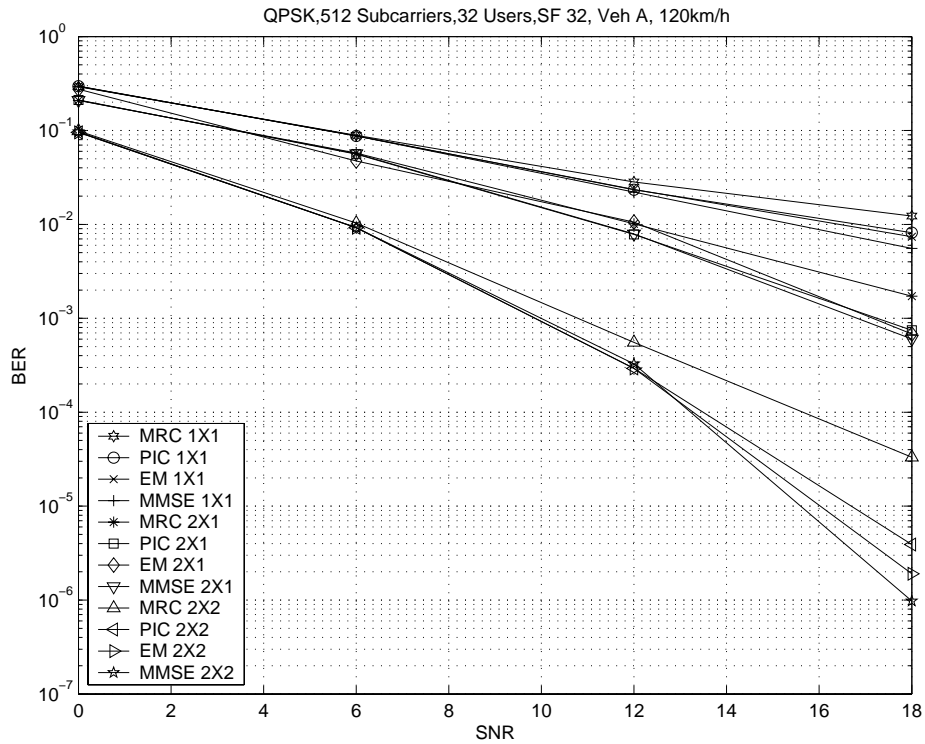


Figure 4.9: Raw BER vs. SNR in Vehicular A channel.

Fig. 4.9 shows the simulation results for both downlink scenarios in the vehicular A channel. As it is observed, by increasing the number of antenna we achieve more performance gain as expected. From the figure we can recognize three different groups. Group one includes the performance results for single-transmit single receive antenna case, group two is two-transmit one-receive antenna and finally, group three is for the two-transmit two-receive antenna case. The performance of the receiver algorithms within each group is consistent, that is, the MMSE receiver has the best performance behavior and the MRC has the worst. Starting with MRC outputs as the initial value for the PIC algorithm, results get improved to the extent shown in the figure after two iterations for the PIC algorithm. The EM-based algorithm can improve MRC

outputs a bit better than the PIC algorithm with the same number of iterations. This improvement due to the EM algorithm is more noticeable especially in high SNR. It is obvious if we start with a better initial value than MRC outputs for the PIC and EM (e.g., outputs of the MMSE receiver), we achieve better performance gains. However, the complexity of the receiver increases surely.

Fig. 4.10 shows the simulation results for both downlink scenarios in the pedestrian B channel. Similar results in the vehicular A channel case are observed.

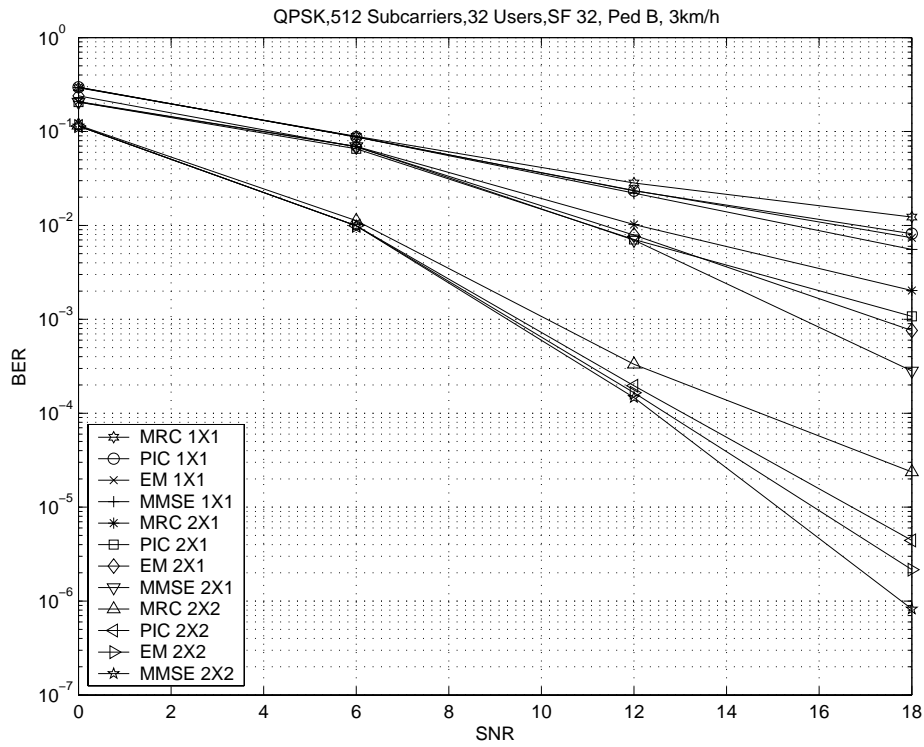


Figure 4.10: Raw BER vs. SNR in Pedestrian B channel

4.11 Effects of Frequency Interleaving

In this section, we present the effect of the frequency interleaver in both SISO and STBC MC-CDMA systems. In Figure 4.11 we see the effect of the frequency interleaver on the MRC, MMSE, PIC and EM algorithms in a SISO MC-CDMA system when the modulation is QPSK and the channel is vehicular A (120 km/h). As we can see, there is a big degradation in the performance of the MRC receiver when the frequency interleaver is applied while for the other receivers (MMSE, EM, and PIC) we get rather good gain by applying the frequency interleaver. For the PIC and EM receivers, three stages of iteration with MMSE outputs as the first stage are considered. In Fig. 4.12, effects of the frequency interleaving are shown in an

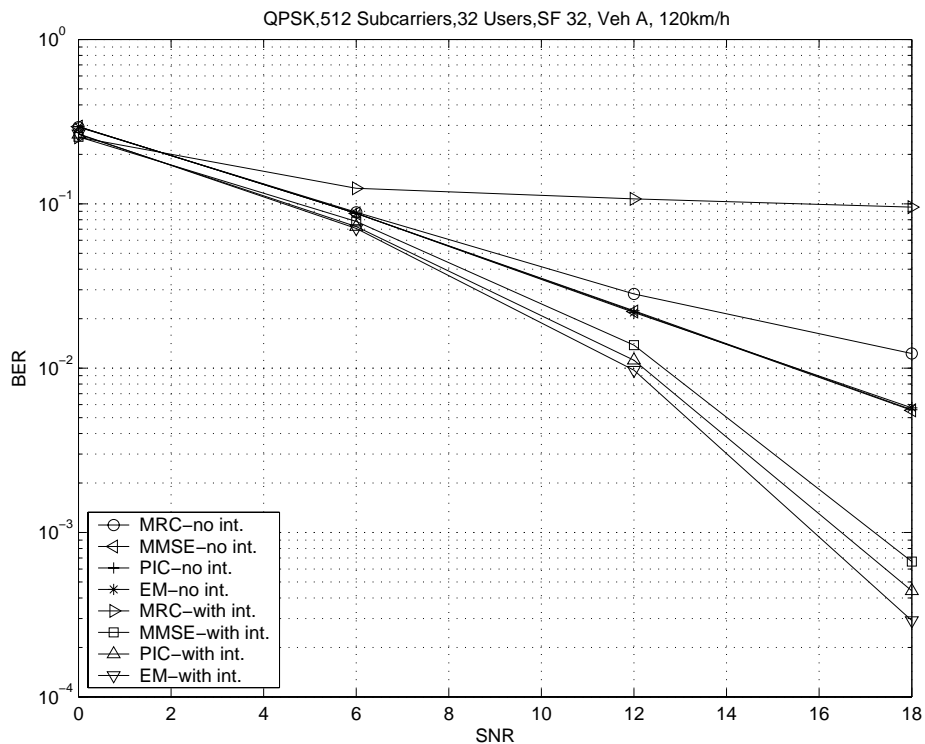


Figure 4.11: Effects of frequency interleaving in a MC-CDMA system.

STBC MC-CDMA system with QPSK and in the vehicular A channel. The MRC and MMSE receivers are considered. We observe from the figure that, interleaving degrades the performance of the MRC algorithm while it improves the MMSE output. The conclusion is that when advanced receivers, such as the MMSE, PIC, and EM

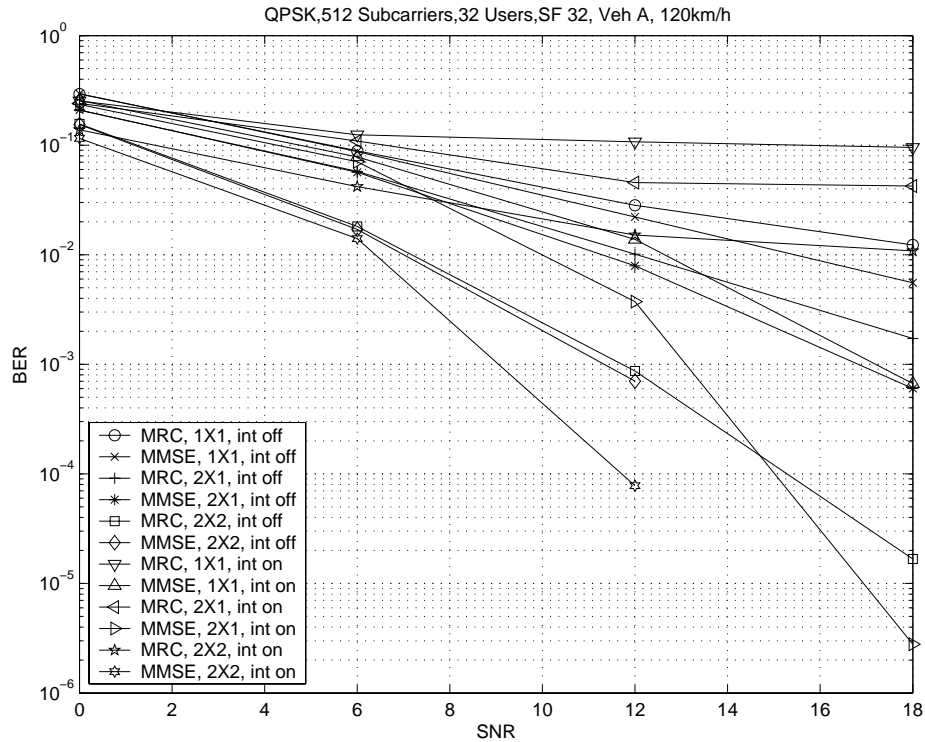


Figure 4.12: Effects of frequency interleaving in an STBC MC-CDMA system.

are implemented, frequency interleaving improves further their performances whereas in the case of a simple receiver, such as the MRC, it degrades its performance.

4.12 Summary

In order to provide a high peak data throughput for future mobile communication systems, multiple antennas and multicarrier techniques are likely to be used. It

is also very probable that advanced receivers will be used to mitigate the effect of interference.

In this chapter, we presented the LS channel estimation and signal detection algorithms including the MRC, MMSE, PIC and EM-based detectors in the SISO and STBC MC-CDMA systems over multipath fading channels. In the SISO MC-CDMA, our results showed that the MMSE receiver provides a huge performance gain over an MRC receiver in terms of BER. Since the implementation of the MMSE receiver in the MC-CDMA system is not complex, we can use some advanced detectors (such as the PIC or EM) to further improve the performance of the receiver. We provided the complete complexity analysis for the baseband part of a SISO MC-CDMA system with our proposed receiver algorithms. The effects of Doppler shifts on the performance of our proposed receiver algorithms were studied. If the Doppler shift is comparable to the frequency spacing of the system then we face high degradation in the performance of the proposed receiver algorithm.

In the STBC MC-CDMA system, we compared the performance of the proposed receivers in two downlink scenarios. In one scenario we assume two transmit and one receive antennas and in another scenario two transmit and two receive antennas. The results of these two scenarios were compared with the SISO case. We see that by increasing the number of antennas the achieved gain is increased and a high gain is achieved when two transmit and two receive antennas are used. This shows the advantage of using multiple antennas. In all cases and scenarios, our PIC and EM-based algorithms show better results than those of the MRC receiver if we take the MRC output as initial values for those algorithms. However, with two iterations in the PIC and EM algorithms, we cannot achieve the same performance gain as that in an MMSE receiver. According to our numerical results, the MMSE receiver has the best performance in terms of BER versus SNR. If MMSE results are used as initial values for the PIC and EM algorithms, then we can possibly further improve the results achieved from it. However, this increases the complexity of the PIC and

EM-based receivers.

We also studied the effects of the frequency interleaver on the performance of the proposed receiver algorithms. Frequency interleaving substantially improves the performance of the MMSE, PIC, and EM-based receivers and highly degrades the performance of the simple receiver such as the MRC receiver.

Chapter 5

Conclusions and Future Research

5.1 Conclusions

In the first part of this work, we considered MIMO and space-time coding concepts. We discussed the information theoretic aspects of multiple antenna systems. The space-time block coding was considered due to its simplicity. Then, the problems of using space-time block coding in multipath fading channels and in a system with more than two transmit antennas were addressed. It was seen with simulation that the performance of a 2×1 space-time block coded system in a multipath fading channel is not necessarily better than that of a SISO system. By implementing an additional receive antenna in a space-time block coded system, the performance of the system will be dramatically improved. We considered time-reversal space-time block coding in order to overcome the problem of multipath fading channels. Since there exists no orthogonal space-time block code for more than two transmit antennas derived from complex signals, the non-orthogonal or semi-orthogonal space-time block code was introduced. When it comes to non-orthogonal STB coding, one is facing the interference from the codes themselves. If the channel is multipath fading the situation is even worse due to interference caused by the delay spread of

the channel. We introduced the novel time-reversal non-orthogonal space-time block code for a multipath fading channel. This novel transmission scheme greatly improves the performance of non-orthogonal space-time block codes.

In the second part of this thesis, we considered the WCDMA system, which is an accepted technology for the air-interface of 3G systems. Since space-time block coding is part of the standard of 3G systems, we gave the system model for a space-time block coded WCDMA system. In a real scenario, when we are dealing with multipath channels, MAI is a main element to decrease the performance of the system. Therefore, we need multiuser detection. We went through some conventional receivers and finally we introduced our novel EM-based algorithm for tackling the problem of MAI in a space-time block coded WCDMA system when channels are multipath fading. It was shown that the EM-based receiver can be downscaled to a conventional RAKE receiver or can be transformed to a PIC receiver by adjusting a scalar parameter. Performance of the EM-based multiuser detection was shown to be better than both RAKE and PIC. Then, the EM-based algorithm was used in the WCDMA system extension, HSDPA, when the modulation order is higher (16QAM). We showed that even in that system, we gain better performance compared to RAKE and PIC.

In the third part, the combination of OFDM and CDMA systems, i.e., MC-CDMA, was considered. As it was mentioned in the introduction, a multicarrier scheme is most likely going to be the air-interface of the B3G or 4G systems. We first considered a SISO MC-CDMA system in a multipath fading channel. A pilot-based channel estimation and different receiver algorithms including MRC, MMSE, PIC and EM-based were introduced for this system. The complexity analysis for different parts of SISO MC-CDMA were provided. Then, we introduced the STBC MC-CDMA in a multipath fading channel and we examined the performance of the different receiver algorithms for this system. The conclusion is that the MC-CDMA scheme can be a highly potential method for future wireless communication systems but it has its own challenges, some of which were addressed in the third part of this thesis.

5.2 Future Research

Since future wireless communications systems become faster and ubiquitous, there is a cogent need for key innovations at the algorithmic level. Specifically, signal processing techniques are crucial to future wideband wireless communications.

In this dissertation, we review the multiple antenna concept. There are still many open questions. From the information theory point of view, the capacity of MIMO for time-varying fading ISI channels is completely unknown. The capacity of a MIMO system is also unknown when the channel is fast time-varying fading and the CSI is not known at the transmitter. The proposed time-reversal algorithm in this work and in general, most of the MIMO techniques herein and elsewhere are considered in a single user system. In many practical systems, multiple users share the same channel, at the same time and frequency band, resulting in MAI at the receiver. Therefore, there are a number of unanswered questions about the performance of these techniques in multiuser scenarios.

To have a high spectral efficiency, future wireless communications should be able to utilize advances in receiver algorithms such as multiuser detection, interference cancellation, and iterative detection and decoding strategies. There has been great interests in finding suboptimum detectors with acceptable complexity and marginal performance degradation compared with the optimum detector. However, still the big challenge ahead is to develop better multiuser detection and interference cancellation approaches that will greatly increase the performance of the existing methods without greatly increased complexity.

As it was mentioned throughout this thesis, one of the major challenges for the design of a wideband wireless communication system is the multipath propagation that results in time-varying high channel time dispersion and frequency selectivity. Frequently proposed candidates in such situations are multicarrier schemes such as OFDM and the combination of OFDM and CDMA or DS-SS-CDMA (MC-SS-CDMA).

OFDM and MC-CDMA convert a frequency-selective channel into a parallel collection of frequency flat subchannels. The main challenges are solutions for high speed mobile usage that causes large Doppler shifts and increasing the efficiency of the system for the broad value range of relevant parameters, e.g., data rate and delay spread.

Bibliography

- [1] 3GPP, “UTRA high speed downlink packet access (HSDPA) - overall description,” *www.3gpp.org*, no. TS 25.308, Mar. 2002.
- [2] —, “Physical channels and mapping of transport channels onto physical channels (FDD),” *www.3gpp.org*, no. TS 25.211 v6.3.0., Dec. 2004.
- [3] S. Alamouti, “A simple transmitter diversity scheme for wireless communications,” *IEEE Journal on Selected Areas in Communications*, vol. 16, no. 8, pp. 1451–1458, Oct. 1998.
- [4] J. A. Bingham, “Multicarrier modulation for data transmission: An idea whose time has come,” *IEEE Communications Magazine*, pp. 5–14, May 1990.
- [5] M. J. Borran and B. Aazhang, “EM-based multiuser detection in fast fading multipath environments,” *EURASIP Journal on Applied Signal Processing*, no. 8, pp. 787–796, 2002.
- [6] M. J. Borran and M. Nasiri-Kenari, “An efficient detection technique for synchronous CDMA communication systems based on the expectation maximization algorithm,” *IEEE Transactions on Vehicular Technology*, vol. 49, no. 5, pp. 1663–1668, Sept. 2000.

- [7] A. Chouly, A. Brajal, and S. Jourdan, “Orthogonal multicarrier techniques applied to direct sequence spread spectrum CDMA systems,” in *Proc. GLOBECOM 1993*, Houston, USA, Nov. 1993, pp. 1723–1728.
- [8] C. Chuah, D. Tse, J. Kahn, and R. Valenzuela, “Capacity scaling in MIMO wireless systems under correlated fading,” *IEEE Transactions on Information Theory*, vol. 48, no. 3, pp. 637–650, Mar. 2002.
- [9] L. J. Cimini, “Analysis and simulation of a digital mobile channel using orthogonal frequency division multiplexing,” *IEEE Transactions on Communications*, vol. 33, no. 4, pp. 665–675, July 1985.
- [10] T. M. Cover and J. A. Thomas, *Elements of Information Theory*. Wiley, 1991.
- [11] D. C. Cox and R. P. Leck, “Distribution of multipath delay spread and average excess delay for 910MHz urban mobile radio paths,” *IEEE Transactions on Antennas and Propagation*, pp. 206–213, Mar. 1975.
- [12] V. M. DaSilva and E. S. Sousa, “Performance of orthogonal CDMA codes for quasi-synchronous communication systems,” in *Proc. ICUPC 1993*, vol. 2, Ottawa, ON, Canada, Oct. 1993, pp. 995–999.
- [13] A. P. Dempster, N. M. Laird, and D. B. Rubin, “Maximum-likelihood from incomplete data via the EM algorithm,” *Journal of the Royal Statistical Society*, vol. 39, pp. 1–38, 1977.
- [14] S. Diggavi, N. Al-Dhahir, and A. R. Calderbank, “Algebraic properties of space-time block codes in intersymbol interference multiple-access channels,” *IEEE Transactions on Information Theory*, vol. 49, no. 10, pp. 2403–2414, Oct. 2003.
- [15] ETSI, “Digital video broadcasting (DVB); framing structure, channel coding and modulation for digital terrestrial television (DVB-T),” *www.etsi.org*, no. ETSI EN 300 744 v1.4.1., Jan. 2001.

- [16] K. Fazel and L. Papke, "On the performance of convolutionally-coded CDMA/OFDM for mobile communication system," in *Proc. PIMRC 1993*, Yokohama, Japan, Sept. 1993, pp. 468–472.
- [17] M. Feder and E. Weinstein, "Parameter estimation of superimposed signals using the EM algorithm," *IEEE Transactions on Acoustics, Speech, and Signal Processing*, vol. 36, no. 4, pp. 477–489, Apr. 1988.
- [18] J. A. Fessler and A. O. Hero, "Complete-data spaces and generalized EM algorithms," in *Proc. ICASSP'93*, vol. 4, Minneapolis, USA, Apr. 1993, pp. 1–4.
- [19] G. J. Foschini and M. J. Gans, "On limits of wireless communications in a fading environment when using multiple antennas," *Wireless Personal Communications*, vol. 6, no. 3, pp. 311–335, Mar. 1998.
- [20] H. E. Gamal and M. O. Damen, "Universal space-time coding," *IEEE Transactions on Information Theory*, vol. 49, pp. 1097–1119, May 2003.
- [21] G. Ganesan and P. Stoica, "Space-time diversity using orthogonal and amicable orthogonal designs," in *Proc. IEEE ICASSP'00*, vol. 5, Istanbul, Turkey, June 2000, pp. 2561–2564.
- [22] D. Gesbert, M. Shafi, D. Shiu, P. J. Smith, and A. Naguib, "From theory to practice: An overview of MIMO space-time coded wireless systems," *IEEE Journal on Selected Areas in Communications*, vol. 21, no. 3, pp. 281–302, Apr. 2003.
- [23] K. S. Gilhousen, I. M. Jacobs, R. Padovani, A. Viterbi, L. A. Weaver, and C. Wheatly, "On the capacity of a cellular CDMA system," *IEEE Transactions on Vehicular Technology*, vol. 40, no. 2, pp. 303–312, May 1991.
- [24] J. Ha, A. N. Mody, J. H. Sung, J. R. Barry, S. W. McLaughlin, and G. L. Stuber, "LDPC coded OFDM with Alamouti/SVD diversity technique," *Journal of Wireless Personal Communications*, vol. 23, no. 1, pp. 183–194, Oct. 2002.

- [25] M. Haardt *et al.*, “Space-time signal processing and MIMO systems,” *White Paper, Research Focus MOBIKOM*, available at <http://www-emt.tu-ilmenau.de/WWWdocuments/downloads/reports/WG8-WhitePaper.pdf>, Feb. 2004.
- [26] S. Hara and R. Prasad, “Overview of multicarrier CDMA,” *IEEE Communications Magazine*, pp. 126–133, Dec. 1997.
- [27] B. Hassibi and B. Hochwald, “High-rate codes that are linear in space and time,” *IEEE Transactions on Information Theory*, vol. 48, no. 7, pp. 1804–1824, July 2002.
- [28] A. O. Hero and J. A. Fessler, “Asymptotic convergence properties of EM-type algorithms,” Communications and Signal Processing Lab, Dept. of EECS, Univ. of Michigan, <http://www.eecs.umich.edu/systems/TechReportList.html>, Ann Arbor, MI, USA, Tech. Rep. 282, Apr. 1993.
- [29] B. Hochwald and T. Marzetta, “Unitary space-time modulation for multiple-antenna communications in rayleigh flat fading,” *IEEE Transactions on Information Theory*, vol. 46, no. 3, pp. 543–565, Mar. 2000.
- [30] B. M. Hochwald, T. L. Marzetta, and C. B. Papadias, “A novel space-time spreading scheme for wireless CDMA systems,” in *Proc. 37th Annual Allerton Conf. on Commun. Control, and Computing*, Monticello, IL, USA, Sept. 1999, pp. 1284–1293.
- [31] B. M. Hochwald and W. Sweldens, “Differential unitary space-time modulation,” *IEEE Transactions on Communications*, vol. 48, pp. 2041–2052, Dec. 2000.
- [32] H. Holma and A. Toskala, *WCDMA for UMTS: Radio Access for Third Generation Mobile Communications*, 3rd ed. John Wiley & Sons, 2004.

- [33] M. H. Hsieh and C. H. Wei, "Channel estimation for OFDM systems based on comb-typed pilot arrangement in frequency selective fading channels," *IEEE Transactions on Consumer Electronics*, vol. 44, no. 1, pp. 217–225, Feb. 1998.
- [34] IEEE, "IEEE 802 LAN/MAN standards committee website," <http://grouper.ieee.org/groups/802/index.html>.
- [35] S. Iraji and J. Lilleberg, "EM-based multiuser detection and parallel interference cancellation for space-time block coded WCDMA employing 16-QAM over multipath fading channels," in *Proc. IEEE PIMRC'02*, vol. 2, Lisboa, Portugal, Sept. 2002, pp. 688–692.
- [36] —, "Performance of EM-based multiuser detection for space-time block coded WCDMA over multipath fading channels," in *Proc. IEEE ISSSTA'02*, vol. 3, Prague, Czech, Sept. 2002, pp. 707–711.
- [37] —, "Interference cancellation for space-time block-coded MC-CDMA systems over multipath fading channels," in *Proc. IEEE VTC-FALL'03*, vol. 2, Orlando, FL, USA, Oct. 2003, pp. 1104–1108.
- [38] —, "Multiuser detection for space-time block-coded WCDMA systems based on expectation-maximization algorithm," *Submitted to EURASIP Journal on Applied Signal Processing*, Oct. 2004.
- [39] S. Iraji, T. Sipilä, and J. Lilleberg, "Channel estimation and signal detection for MC-CDMA in multipath fading channels," in *Proc. IEEE PIMRC'03*, vol. 3, Beijing, China, Sept. 2003, pp. 2286–2290.
- [40] S. Iraji, O. Tirkkonen, and A. Hottinen, "Non-orthogonal space-time block code for multipath channel," *Accepted to International Journal of Wireless Information Networks*, Jan. 2005.

- [41] S. Iraji, O. Tirkkonen, A. Hottinen, and K. Kuchi, "Non-orthogonal space-time block code for multipath channel," in *Proc. IEEE PIMRC'04*, vol. 4, Barcelona, Spain, Sept. 2004, pp. 2303–2307.
- [42] H. Jafarkhani, "A quasi-orthogonal space-time block code," *IEEE Transactions on Communications*, vol. 49, pp. 1–4, Jan. 2001.
- [43] W. C. Jakes, *Microwave Mobile Communications*. Wiley-IEEE Press, 1994.
- [44] S. M. Kay, *Fundamentals of Statistical Signal Processing: Estimation Theory*. Prentice-Hall, 1993.
- [45] E. Lindskog and A. Paulraj, "A transmit diversity scheme for channels with intersymbol interference," in *Proc. IEEE ICC'00*, vol. 1, New Orleans, USA, June 18–22, 2000, pp. 307–311.
- [46] S. Loyka and A. Kouki, "New compound upper bound on MIMO channel capacity," *IEEE Communications Letters*, vol. 6, no. 3, pp. 96–98, Mar. 2002.
- [47] X. Ma and G. B. Giannakis, "Complex field coded MIMO systems: performance, rate, and trade-offs," *Journal of Wireless Communications and Mobile Computing*, pp. 693–717, Nov. 2002.
- [48] T. Marzetta and B. Hochwald, "Capacity of a mobile multiple-antenna communication link in rayleigh flat fading," *IEEE Transactions on Information Theory*, vol. 45, no. 1, pp. 139–157, Jan. 1999.
- [49] MBOA, "MultiBand OFDM Alliance website," <http://www.multibandofdm.org/>.
- [50] G. J. McLachlan and T. Krishnan, *The EM Algorithm and Extensions*. John Wiley & Sons, 1997.
- [51] L. Milstein, "Wideband code division multiple access," *IEEE Journal on Selected Areas in Communications*, vol. 18, no. 8, pp. 1344–1354, Aug. 2000.

- [52] T. K. Moon, "The expectation-maximization algorithm," *IEEE Signal Processing Magazine*, pp. 47–60, Nov. 1996.
- [53] B. Muquet, Z. Wang, G. B. Giannakis, M. de Courville, and P. Duhamel, "Cyclic prefixing or zero padding for wireless multicarrier transmissions?" *IEEE Transactions on Communications*, vol. 50, no. 12, pp. 2136–2148, Dec. 2002.
- [54] A. Naguib, "On the matched filter bound of transmit diversity techniques," in *Proc. IEEE ICC'01*, vol. 2, Helsinki, Finland, June 11–14, 2001, pp. 596–603.
- [55] O. Oyman, R. Nabar, H. Bölcskei, and A. Paulraj, "Tight lower bounds on the ergodic capacity of rayleigh fading MIMO channels," in *Proc. IEEE GLOBECOM'02*, vol. 2, Taipei, Taiwan, Nov. 2002, pp. 1172–1176.
- [56] A. Paulraj and C. B. Papadias, "Space-time processing for wireless communications," *IEEE Signal Processing Magazine*, vol. 14, pp. 49–83, Nov. 1997.
- [57] A. Peled and A. Ruiz, "Frequency domain data transmission using reduced computational complexity algorithms," in *Proc. ICASSP 1980*, vol. 5, Denver, Colorado, USA, Apr. 1980, pp. 964–967.
- [58] J. G. Proakis, *Digital Communications*, 3rd ed. McGraw-Hill, 1995.
- [59] T. Rappaport, *Wireless Communications*, 1st ed. Prentice Hall, 1996.
- [60] N. Seshadri and J. Winters, "Two schemes for improving the performance of frequency-division duplex (FDD) transmission systems using transmitter antenna diversity," *Int. Journal Wireless Information Networks*, vol. 1, pp. 49–60, Jan. 1994.
- [61] C. E. Shannon, "A mathematical theory of communication," *Bell Sys. tech. J.*, vol. 27, pp. 623–656, Oct. 1948.

- [62] G. L. Stuber, J. R. Barry, S. W. McLaughlin, Y. Li, M. A. Ingram, and T. G. Pratt, "Broadband MIMO-OFDM wireless communications," *Proceedings of the IEEE*, vol. 92, no. 2, pp. 271–294, Feb. 2004.
- [63] V. Tarokh, H. Jafarkhani, and A. R. Calderbank, "Space-time block codes from orthogonal designs," *IEEE Transactions on Information Theory*, vol. 45, pp. 1456–1467, July 1999.
- [64] ———, "Space-time block coding for wireless communications: performance results," *IEEE Journal on Selected Areas in Communications*, vol. 17, pp. 451–460, Mar. 1999.
- [65] V. Tarokh, N. Seshadri, and A. R. Calderbank, "Space-time codes for high data rate wireless communication: Performance criterion and code construction," *IEEE Transactions on Information Theory*, vol. 44, pp. 744–765, Mar. 1998.
- [66] E. Telatar, "Capacity of multi-antenna gaussian channels," *European Transactions on Telecommunications*, vol. 10, no. 6, pp. 585–695, Nov./Dec. 1999.
- [67] O. Tirkkonen, "Optimizing space-time block codes by constellation rotations," in *Proc. Finnish Wireless Comm. Workshop*, Tampere, Finland, Oct. 2001, pp. 59–60.
- [68] O. Tirkkonen, A. Boariu, and A. Hottinen, "Minimal non-orthogonal rate 1 space-time block code for 3+ tx antenna," in *Proc. IEEE ISSSTA'00*, vol. 2, New Jersey, USA, Sept. 6–8, 2000, pp. 429–432.
- [69] O. Tirkkonen and A. Hottinen, "Complex space-time block codes for four Tx antennas," in *Proc. IEEE GLOBECOM'00*, vol. 2, San Fransisco, USA, Nov./Dec. 2000, pp. 1005–1009.

- [70] L. Vandendorpe, "Multitone direct sequence CDMA system in an indoor wireless environment," in *Proc. IFSCVT 1993*, Oct. 1993, pp. 4.1.1–4.1.8.
- [71] M. K. Varanasi and B. Aazhang, "Multistage detection in asynchronous code-division multiple-access systems," *IEEE Transactions on Communications*, vol. 38, pp. 509–519, Apr. 1990.
- [72] S. Verdu, *Multuser Detection*. Cambridge University Press, 1998.
- [73] A. M. Viterbi and J. Viterbi, "Erlang capacity of a power controlled CDMA system," *IEEE Journal on Selected Areas in Communications*, vol. 11, no. 6, pp. 892–900, Aug. 1993.
- [74] B. Vucetic and J. Yuan, *Space-Time Coding*. Wiley, 2003.
- [75] Z. Wang and G. Giannakis, "Wireless multicarrier communications," *IEEE Signal Processing Magazine*, pp. 29–48, May 2000.
- [76] WiMax, "WiMAX forum website," <http://www.wimaxforum.org/home>.
- [77] J. Winters, "Smart antennas for wireless systems," *IEEE Personal Communications Magazine*, vol. 5, no. 1, pp. 23–27, Feb. 1998.
- [78] A. Wittneben, "A new bandwidth efficient transmit antenna modulation diversity scheme for linear digital modulation," in *Proc. IEEE ICC'93*, vol. 3, Geneva, Switzerland, 1993, pp. 1630–1634.
- [79] P. W. Wolniansky, G. J. Foschini, G. D. Golden, and R. A. Valenzuela, "V-BLAST: An architecture for realizing very high data rates over the rich-scattering channel," in *Proc. ISSSE'98*, Pisa, Italy, Sept./Oct. 1998, pp. 295–300.
- [80] N. Yee, J. P. Linnatz, and G. Fettweis, "Multicarrier CDMA in indoor wireless radio networks," in *Proc. PIMRC 1993*, Yokohama, Japan, Sept. 1993, pp. 109–113.

- [81] S. Zhou and G. Giannakis, "Space-time coding with maximum diversity gains over frequency-selective fading channels," *IEEE Signal Processing Letters*, vol. 8, no. 10, pp. 269–272, Oct. 2001.

Tampereen teknillinen yliopisto
PL 527
33101 Tampere

Tampere University of Technology
P.O. Box 527
FIN-33101 Tampere, Finland